Karlsruhe Institute of Technology

European Windstorms in a Warmer Climate - a Nudged Storyline Approach

Master's Thesis of

Jana Knandel

At the KIT
Institute for Meteorology and Climate Research

First examiner:	Prof. Joaquim Pinto
Second examiner:	Prof. Andreas Fink
First advisor:	Dr. Patrick Ludwig

03. February 2025 – 02. February 2026

European Windstorms in a Warmer Climate
- a Nudged Storyline Approach (Master's Thesis)

I declare that I have developed and written the enclosed thesis completely by myself. I have not used any other than the aids that I have mentioned. I have marked all parts of the thesis that I have included from referenced literature, either in their original wording or paraphrasing their contents. I have followed the by-laws to implement scientific integrity at KIT.

Pfinztal, 02. February 2026

. . . . . .

(Jana Knandel)

Abstract

Windstorms are among the most dangerous natural hazards affecting Europe. They are responsible for large damages and high economic costs, with individual extreme events exceeding 10 billion euros of economic loss. With ongoing climate change, the question arises how the characteristics of European windstorms may change in a warming world. Due to high case to case variability and the interaction of many dynamical and thermodynamical factors, there is still low confidence in the changes of properties like wind and precipitation associated with European windstorms. It is necessary to bridge the gap between idealized simulations and large ensembles of global climate modeling. One possibility to do so could be to apply the so called nudged storyline approach to European windstorms. The examples presented in this thesis try to answer the question whether this approach is able to provide new insights into future windstorms.

This study focuses on three windstorms, Kyrill in 2007, Christian in 2013 and Thomas in 2017. First, limited area ICON simulations of these storms are performed with a resolution of 12 km by using ERA5 reanalysis data as forcing data. For windstorm Kyrill, additionally, a nested simulation over Germany with a resolution of 3 km is conducted. It is shown that the storms are well represented by the ICON model. Next, nudged storyline simulations, performed with the earth system model of the Alfred-Wegener Institute (AWI-CM1), are used to asses the impact of climate change. The nudging is applied by forcing of the upper level vorticity and divergence with ERA5 reanalysis data, to constrain the large scale circulations at the upper levels. By downscaling the global AWI simulations with ICON, a resolution of 12 km is achieved. For windstorm Kyrill a further nesting step is performed, to a resolution of 3 km over Germany. Those storyline simulations are conducted for the present climate and for 2 and 3 K warming levels.

The comparison of the present storyline simulations (1.4 K global warming) to the ERA5 simulations shows that the nudged storyline simulations are generally able to reproduce the windstorms in a way that a comparison to the historic events is meaningful. In the high resolution (3 km) simulations of windstorm Kyrill even the convective cells with high gusts and strong precipitation are represented. For windstorms Kyrill and Thomas, an increase in storm intensity is found for both warming levels. Considering the distributions of strong gusts and precipitation, it can be shown that the distributions shift towards higher values, and in the case of precipitation, show stronger local variability for future climate conditions. Windstorm Christian is an example, where the approach reaches its limitations, as the storm is not present in the 2 K warming level simulation and only weak system develops in the 3 K warming level run. Therefore, it can be concluded that for future studies stronger nudging should be applied to be able to represent more storms and get better comparability.

Nevertheless, this thesis shows clearly that the nudged storyline approach has the potential to provide new insights, on how windstorms will develop in a warmer climate, especially on the changes of properties, like wind and precipitation, where there is still quite low confidence.

Zusammenfassung

Windstürme gehören zu den gefährlichsten Naturereignissen in Europa. Sie verursachen große Schäden und hohe wirtschaftliche Verluste, wobei einzelne Extremereignisse zu Schadenssummen von mehr als 10 Milliarden Euro führen. Angesichts des fortschreitenden Klimawandels stellt sich die Frage, wie sich europäische Windstürme und deren Charakteristika in einer wärmeren Welt verändern. Aufgrund der hohen Fall-zu-Fall Variabilität und der Wechselwirkung vieler dynamischer und thermodynamischer Faktoren, herrscht nach wie vor große Unsicherheit darüber, wie sich Eigenschaften von Windstürmen, wie Wind oder Niederschlag, ändern werden. Es ist notwendig, die Lücke zwischen idealisierten Simulationen und großen Ensembles aus globalen Klimasimulationen zu schließen. Eine Möglichkeit dafür könnte die Anwendung des sogenannte Nudged-Storylines-Approaches für europäische Windstürme sein. Mit Hilfe der in dieser Arbeit vorgestellten Beispiele soll die Frage beantwortet werden, ob dieser Ansatz neue Erkenntnisse über zukünftige Windstürme liefern kann.

Diese Studie konzentriert sich auf drei Windstürme, Kyrill im Jahr 2007, Christian (2013) und Thomas (2017). Zuerst werden für diese drei Stürme limited area ICON Simulationen mit einer Auflösung von 12 km durchgeführt. Dabei werden ERA5 Reanalyse Daten als Antriebsdaten verwendet. Für Windsturm Kyrill wird zusätzlich eine Simulation über Deutschland mit einer höheren Auflösung von 3 km durchgeführt. Es wird gezeigt, dass die Stürme im ICON Modell gut dargestellt werden können. Anschließend werden mit dem Erd-System-Modell des Alfred-Wegener-Institutes erstellte Nudged-Storyline-Simulationen verwendet, um die Auswirkungen des Klimawandels zu analysieren. Um die großräumigen Zirkulationen in den oberen Schichten durch Nudging festzuschreiben, werden Wirbelstärke und Divergenz in den oberen Schichten mit ERA5-Reanalyse-Daten forciert. Indem die globalen AWI Simulationen mit ICON herunterskaliert werden, wird eine Auflösung von 12 km erreicht. Für Windsturm Kyrill wird ein weiterer Schritt gemacht, um eine Auflösung von 3 km über Deutschland zu erhalten. Solche Storyline-Simulationen werden für das heutige Klima und einen Erwärmungsgrad von 2 und 3 K erstellt.

Der Vergleich der Storyline-Simulationen im heutigen Klima mit den ERA5 Simulationen zeigt, dass die Nudged-Storyline-Simulationen im allgemeinen in der Lage sind, Windstürme so zu reproduzieren, dass ein Vergleich mit den historischen Ereignissen aussagekräftig ist. In den höher aufgelösten Simulationen (3 km) von Windsturm Kyrill sind sogar die konvektiven Zellen, die mit hohen Windböen und starkem Niederschlag einhergehen, gut sichtbar. Im Fall von Kyrill und Thomas wird eine Zunahme der Sturmintensität für beide Erwärmungsgrade festgestellt. Die Verteilungen von Windböen und Niederschlag zeigen eine Verschiebung hin zu höheren Werten für beide Erwärmungsgrade, sowie, beim Niederschlag, eine erhöhte

lokale Variabilität für zukünftige klimatische Bedingungen. Windsturm Christian ist ein Beispiel, bei dem der Nudged-Storyline-Ansatz seine Grenzen erreicht. Der Sturm ist in der Simulation mit einem Erwärmungsgrad von 2 K nicht repräsentiert und bei einem Erwärumgsgrad von 3 K entwickelt sich nur ein deutlich abgeschwächtes System. Daraus wird geschlossen, dass stärkeres Nudging benötigt wird, um mehr Stürme gut repräsentieren zu können und eine höhere Vergleichbarkeit zu gewährleisten. Trotz allem zeigt diese Thesis deutlich, dass der Nudged-Storyline-Ansatz das Potential hat neue Erkenntnisse darüber zu liefern, wie sich Windstürme und deren Eigenschaften, wie Wind und Niederschlag, deren Änderungen bislang noch unsicher sind, in einem wärmeren Klima entwickeln werden.

Contents

List of Figures

List of Tables

1. Introduction

European windstorms include strong winds, heavy precipitation and storm surges. Therefore, they are one of the main sources of damage due to natural hazards in Europe and are frequently responsible for significant economic losses (Fink et al., 2009, Moemken et al., 2024). These losses emerge from various factors, such as damage to personal belongings, including houses or cars, or losses affecting certain industry sectors. One of these sectors is the insurance industry. In Figure 1.1, the losses for the insurance sector from windstorm events causing an insured loss of more than a billion euros between 2010 and 20255 are shown. Another industry often affected is the forestry sector. Windstorm Kyrill (2007) led to 25 million downed trees only in North Rhine-Westphalia, which corresponds to 1.5 billion euros of economic loss for the industry (Wald und Holz NRW, 2021). Furthermore, infrastructure, like streets, railways or power supply lines, gets damaged during European windstorms. For instance during storm Eowyn in 2025, 120 trees fell over railway tracks (H. Lennon and L. Piper, 2025). These damages often cause disruptions in transport or power supply, affecting the lives of millions of people. Unfortunately, European windstorms not only lead to loss of money or damage to personal belongings, but are also often responsible for fatalities. The ten costliest storms between 1987 and 2010 alone were responsible for nearly 500 fatalities (see Figure 1.2), caused by trees falling on cars, flying debris and other storm related accidents.

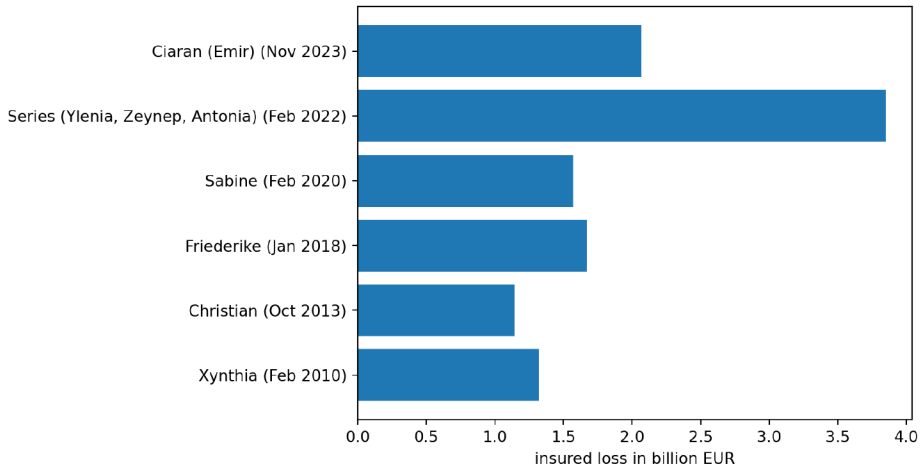

Figure 1.1.: Insured loss through windstorm events between 2010 and 2025 according to PERILS (2026), events with more than 1 billion euro of insured loss are considered

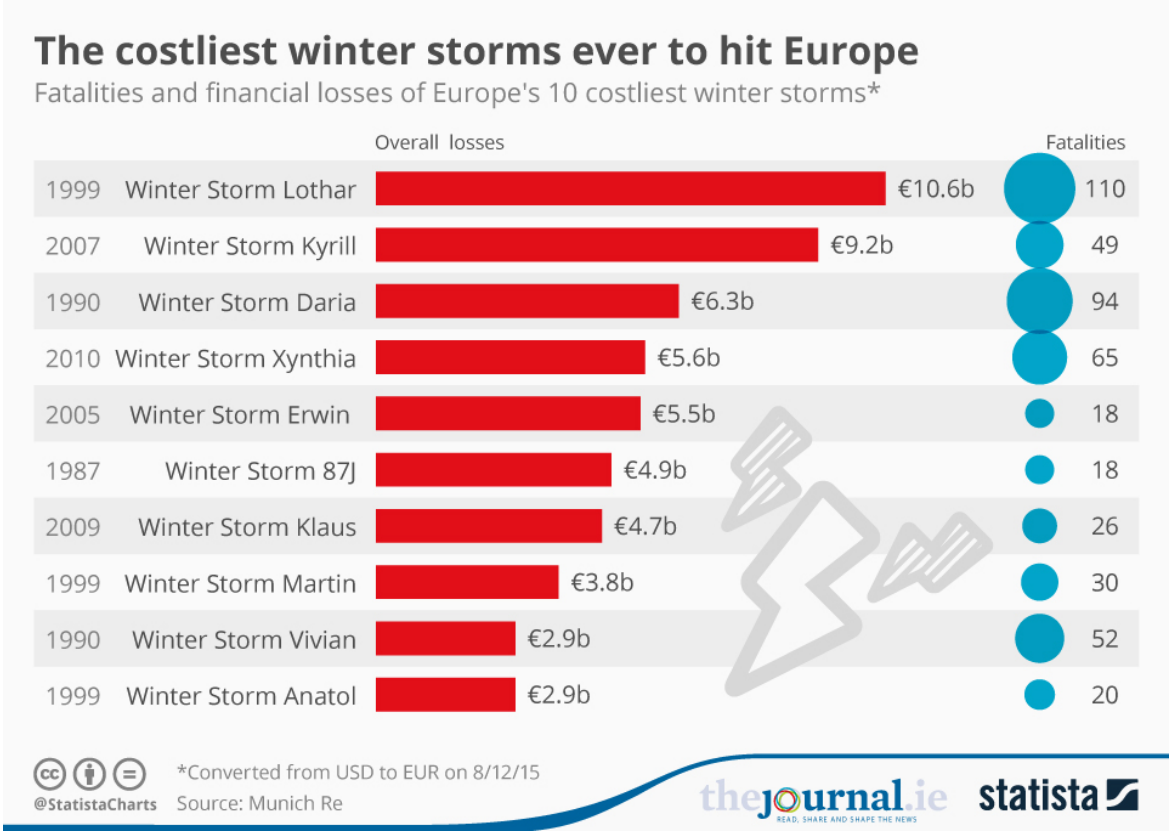

Figure 1.2.: Fatalities and Economic losses of the ten costliest European windstorms from 1990 to 2015

Overall, European windstorms are responsible for large economic losses associated with natural hazards. This number is projected to increase with climate change. The synthesis paper on tropical and extratropical storm damage by Ranson et al. (2014) found an average increase in damage of 8 % per degree of warming for European windstorms, assuming no adaptations to climate change. This increase could be reduced by adapting to changing climate risks, for instance through forest management (Gardiner, 2013) and the improvement of buildings, like the angling of roofs (European Commission. Joint Research Centre., 2020). To do so, reliable information is necessary that is easily accessible to municipalities and policymakers.

Today, there is only low confidence in how the key properties of European windstorms, which are the main factors for damage, such as wind and precipitation, may change in a future climate (Catto et al., 2019). There is quite high confidence in the changes of properties influencing extratropical cyclone (ETC) development, such as the upper and lower level horizontal temperature gradient or the increase of latent heating. However, the changes projected in these variables often have counteracting influences on European windstorms. Therefore, the changes in European windstorms themselves are difficult to quantify. Additionally, the occurrence of European windstorms, especially those with high intensities, is subject to large decadal variability (Cusack, 2022). Often, individual extreme

windstorms are responsible for many times more damage compared to an average European windstorm. Windstorm Kyrill in 2007 is one such example, leading to an economic loss of 7.6 billion Euros (Moemken et al., 2024), as well as the series of three severe storms in December 1999, namely Anatol, Lothar and Martin, which led to more than 20 billion Euros of economic loss in Europe (Fink et al., 2009). Such extreme events at the tail of the distribution are very rare. Thus, it is difficult to assess the possible changes in the intensity of these high impact events.

In the traditional approach, large ensembles with global climate models are performed over timescales of several decades, to get statistical insights into the changes of European windstorms (Ulbrich et al., 2009). Therefore, much computational effort is needed to get a high enough sample size to analyze rare extreme events (Shepherd et al., 2018). Additionally, these simulations have a relatively low resolution of around 100 km (Intergovernmental Panel On Climate Change [Ipcc], 2023) and need to be further downscaled to examine local changes and assess small scale processes.

Besides the high amount of computational power needed, the statistical results of simulations like this are quite difficult to communicate to the public, especially concerning the limits and uncertainties of the results (Parker, 2010). Even if this communication succeeds, it often does not lead to substantial adaptation measures (Shepherd et al., 2018). This is partially due to the so called availability bias (Kahneman, 2024), which means that people tend to underestimate the risks of events that are outside of what they have experienced. This is the reason why adaptation measures are often set in place after the occurrence of an extreme event, even if experts beforehand tried to communicate the need for them. This gap between lived experience and projected changes can be reduced by referring to events that people actually have experienced. An approach to do so is the so called storyline approach. Storylines aim to provide "qualitative understanding rather than quantitative precision" (Shepherd et al., 2018) and are therefore not predictions, but tales of how a future climate could look. This makes them potentially more accessible for the public. Furthermore, by looking at the changes of historic events, the damage delt during those events is known. Therefore, the changes in the properties responsible for the damage, like precipitation or wind, can be translated very easily into changes in damage. This can lead to better risk assessment and damage projections.

I addition to providing more accessible results, this approach brings several scientific advantages. A storyline is defined as "a physically self-consistent unfolding of past events, or of plausible future events or pathways" by Shepherd et al. (2018). Therefore, certain historical events are reproduced in a given climate state, mostly the future. To do so, less computational effort is necessary, as only the event itself has to be simulated. Furthermore, as the large scale dynamics are fixed, fewer ensemble members are necessary to make reliable statements. This reduction of computational effort enables the use of much higher resolutions, helping to better understand local changes and small scale processes. As described above, extreme events are difficult to assess with traditional large ensemble GCM simulations. The storyline approach is especially useful to look deeper into extreme events, such as extreme windstorms, and how climate change could impact them. Those extreme events are usually remembered by most people in the affected regions. Therefore, they build

an ideal basis for communicating the risks of further extreme events to those responsible for climate change adaptations.

The large decadal variability of the occurrence of severe European windstorms is associated with large scale processes and atmospheric circulations like the North Atlantic Oscillation (NAO), whose variability is not yet very well understood. This and the counteracting effects of changes in latent heating and large scale temperature gradients lead to difficulties in making reliable statements about the future frequency of extreme European windstorms (Catto et al., 2019). By applying the storyline approach, these uncertainties can be left aside, as the large scale dynamics are forced to follow the historic period. This allows focusing on the changes in properties like precipitation and wind. Apart from the precipitation intensity, which is very likely to increase, statements on the changes in these key properties can only be made with low confidence yet (Catto et al., 2019). By using global climate model ensembles, many different factors interact and it is challenging to disentangle the processes. Therefore, idealized simulations are used to get a better process understanding without having to deal with all interactions (Reed et al., 2025). This leads to a good understanding of the changes in some properties, such as the increase in precipitation and latent heating. However, idealized models, due to their simplifications, are not able to assess the feedback of these changes on storm intensity. The storyline approach could help to fill this gap by determining the large scale structures. This simplifies the problem by avoiding the uncertainties of changes in the large scale dynamics, similar to the idea of idealized studies. Unlike idealized studies, however, storyline simulations are still capable to simulate the complicated feedback processes in the storm.

Klimiuk et al. (2025) used the storyline approach to investigate extreme heatwaves. However, unlike heatwaves, which are associated with large scale stationary blocking, European windstorms are much more sensitive to small changes in the large scale. This could make the application of this approach to European windstorms more challenging. Therefore, case studies are conducted, using the nudged storyline approach to analyze the future changes of three European windstorms. The main questions that this thesis aims to answer are:

1 Is the nudged storyline approach applicable for European windstorms? Is it able to provide new insights?

2a Is it possible to reproduce European windstorms with nudged storyline simulations?

2b How will the analyzed storms change in the future climate?

To answer these questions, regional climate simulations are performed with the ICON model, using ERA5 reanalysis data, to verify the ability of the limited area mode of the ICON model to represent European windstorms. The observations of the considered storms, together with the ERA5 simulations, are then compared to the nudged storyline simulations of the storms in the present climate state, to make sure that the historic events could be rebuilt in the storyline simulations. The second step is to compare the present storyline simulations to two future storyline simulations at the warming levels of approximately 2 and 3 K for each storm, leading to the second research question: How do the characteristics of the considered storms change in a warmer climate?

Following the introduction, the thesis introduces some basics on Climate Modeling and the storyline approach in chapter 2. In chapter 3 the current state, as well as the expected changes of European windstorms are addressed. Chapter 4 explains the methodology of this thesis. The first part of the second research question is assessed in chapter 5 and the second part in chapter 6. The thesis is concluded by chapter 7, discussing the results of the previous chapters and providing concluding answers to the research questions. Furthermore, in this chapter an outlook is given on how future studies, using the nudged storyline approach, could look like.

2. Climate Modeling

Weather and climate models build the basis of most current meteorological and climate research. The idea of such models is to represent the physical processes of the climate system by a set of equations in certain time steps over a predefined spatial grid. The first models used by climate researchers were one-dimensional Energy Balance Models, which considered only the outgoing and incoming energy of the earth. Despite their simplicity, they were still able to provide information on the earths sensitivity to changes in solar radiation (Brasseur et al., 2023). Later, general circulation models were developed, which are much more complex. General circulation models consist of a three-dimensional grid, as the necessary equations can only be solved numerically, and are able to represent the horizontal and vertical exchange between the gridcells. For each gridcell and timestep a set of primitive equations is calculated, involving the three dimensional momentum conservation, mass and energy conservation, as well as the ideal gas law. Depending on the spatial resolution of the grid, not all processes can be simulated directly. Therefore small scale processes have to be parametrized. This means that the statistical impacts of the subgrid-scale processes on the grid scale are directly incorporated into the equations of the simulation as parameters. In many cases, convective processes are an example for parametrized processes, because they are sub-scale compared to the resolution. The components of a general circulation model involve the atmosphere and the ocean as well as a coupling, allowing the exchange between those two components. Today so called earth system models are used for climate modeling. They have an increased horizontal and vertical resolution and feature many additional components of the climate system, such as aerosols, land ice or dynamical vegetation and have an increased horizontal and vertical resolution.

With the help of these earth system models, simulations of the future climate can be performed. These simulations provide important insights into the changes coming along with climate change. However, the expected changes strongly depend on the future emission pathways, as the warming is directly related to greenhouse gas emissions via the climate sensitivity. Therefore, assumptions about future emissions have to be made. To achieve better comparability and a scientific basis for these assumptions, the shared socio-economic pathways (SSPs) were defined (O'Neill et al., 2014). Out of these, a standard group of five scenarios was chosen, covering the whole range from strong mitigation of emissions to nearly no action (see Figure 2.1). The scenarios are named as SSPX-Y, with the scenario number X and the radiative forcing Y. One of those scenarios, namely SSP3-7.0, was considered in this thesis.

Typical simulations with global climate models (GCMs) have low resolutions, as the simulations are performed over the entire globe for several decades. Hence, they are effective at

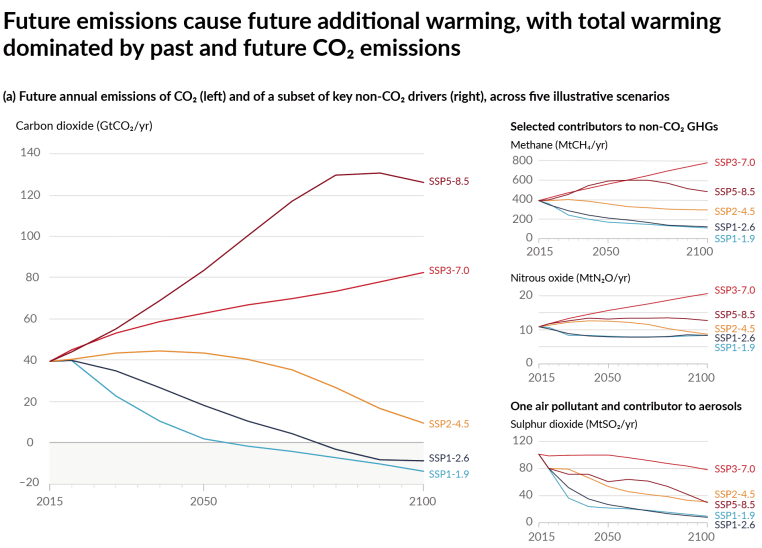

Figure 2.1.: Emission Pathways for the five main SSP scenarios (Ipcc, 2023)

providing information on long term, large scale trends, such as mean changes in temperature or humidity for certain regions or changes in the large scale atmospheric circulations. However, these global models are barely able to provide information on certain extreme events and regional changes. Consequently, higher resolutions or different modeling techniques are necessary. Higher resolutions can be achieved by dynamically downscaling the results of the global climate model (Giorgi, 2019). Therefor, so called regional climate models (RCMs) are used. As they are only applied for simulating a limited area of interest, they rely on input data the boundaries of the considered domain. These boundary conditions usually come from GCMs or other RCMs that cover a larger region, and are imposed on the RCMs via nudging. To do so, a nudging zone at the upper and lateral boundaries is defined. Inside this nudging zone, for certain variables, a term is added to force them towards the boundary data. This nudging term is multiplied by a nudging coefficient that decreases through the nudging zone, such that the strongest nudging at the outer boundary is smoothly decreased towards the inner boundary, where the nudging is set to zero and the model can evolve freely. Another technique to avoid some of the downsides of global climate modeling is to use different modeling approaches. Two of them are presented below.

2.1. Storyline and Pseudo-Global Warming Approach

2.1.1. Nudged Storyline Approach

The definition of a storyline according to Shepherd et al. (2018) is "a physically self-consistent unfolding of past events, or of plausible future events or pathways". So the idea of the storyline approach is to rebuild certain historic events in a different climate state, mostly the future climate. Instead of statistic results through large GCM ensembles, the storyline

approach aims to give a better understanding of processes by looking at individual events. By reproducing events in different climate states, their changes can be directly assessed.

If a normal GCM simulation is started at a certain initial state it evolves freely from a certain inital state (see Figure 2.2). Therefore, to reproduce historic events, so called nudging has to be imposed, to force the GCM to follow the large scale structures of a historic period. In this thesis, global climate model simulations including spectral nudging are used. Spectral nudging, refers to the use of wave instead of grid space. Small wavenumbers correspond to large scale structures. This allows to only apply the nudging on large scale structures, up to a certain wavenumber, while all smaller structures, with higher wavenumbers can evolve freely (Huang et al., 2021). It is vital to find the right nudging strength. With weak nudging the dynamics are able to develop quite freely, such that possible changes in the dynamics might be investigated. On the other hand this can lead to an historic event not being represented as good as it would be with stronger nudging (Klimiuk et al., 2025).

There are several advantages of the nudged storyline approach. They are very accessible for the public and decision-makers by referring to events that people have experienced. Therefore, it might be able to counteract the availability bias. The availability bias, that describes the phenomenon that people tend to underestimate the risk of certain events if they have not yet experienced something similar, even if enough information is available (Kahneman, 2024). The statistic results of GCM ensembles are often difficult to communicate. This is different with storyline simulations that can be seen as tales of a plausible future climate. However it is important to notice, that they are no predictions.

As the large scale dynamics are nudged, such that the event of interest is reproduced, storyline simulations are not able to make any statements on the probability of occurrence of the event. This weakness is important to keep in mind, especially if very rare extreme events are assessed with the nudged storyline approach, because they will likely still not occur very often in the future. It could even be possible, that the nudged storyline approach shows an increase in intensity of certain events, but changes in the large scale dynamics, that are not incorporated, show a decrease in frequency of exactly this event counteracting the effect. The weakness of not incorporating the changes in the large scale dynamics is, at the same time, an advantage of the nudged storyline approach. In general the changes in thermodynamics with climate change are better understood than the changes in the large-scale atmosphere dynamics (Shepherd et al., 2018, Shepherd, 2014). This approach allows to leave aside the changes in large scale dynamics and the associated uncertainties and to focus on the thermodynamic and small scale dynamic processes and changes. This can make it easier to assess events where many different processes interact and often different changes in large scale dynamics would lead to conflicting changes of the event. Additionally the nudged storyline approach is especially effective in considering rare extreme events. When doing so, it must be kept in mind that they might still be rare in the future and the approach cannot make any statements about their future occurrence. But the interest in assessing those extreme events is huge, as they are responsible for the majority of damage.

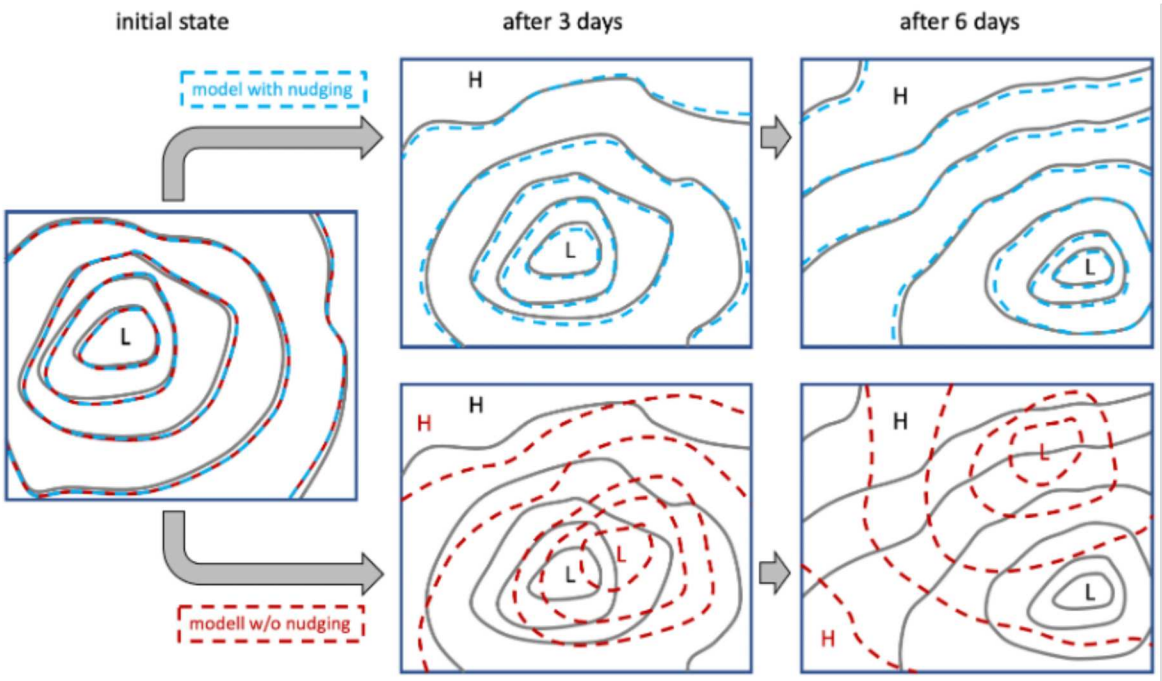

Figure 2.2.: Illustration of the idea of spectral nudging, black lines show the isobars of an hypothetical historic event, blue (red) lines exemplarily show the development of a climate simulation with (without) nudging, left side shows the initial state, mid and right show the simulated state after three and six days (courtesy of H. Gössling)

2.1.2. Pseudo Global Warming Approach

A related approach is the Pseudo-global warming (PGW) approach, which is another simulation strategy in regional climate modeling (Brogli et al., 2023). The idea is to take a regional climate simulation and then impose large scale changes, such as increased surface temperature, via the boundary conditions. Often realistic large-scale changes for a certain scenario are derived from GCM simulations.

The boundary conditions for pseudo-global warming simulations are derived by adding some change Δ to the present day boundary conditions CTRL:

$$\text{PGW} = \text{CTRL} + \Delta$$

The changes are derived from

$$\Delta = \text{SCEN} - \text{HIST}$$

with SCEN being a future climate projection and HIST a historical one, both from 30 year time periods, to get rid of internal variability (Brogli et al., 2023). To maintain the physical balance of the system, mainly the hydrostatic balance, it might be necessary to perform a pressure adjustment process as described in Brogli et al. (2023).
Compared to normal RCM simulations the PGW approach has some practical benefits. First of all it needs less computational effort, than traditional downscaling techniques. By using 30 year climate projections to calculate Δ, the interannual variability vanishes. This means that

shorter time PGW simulations are sufficient to make meaningful predictions, rather than the 30 year periods typically used in ordinary RCM simulations (Brogli et al., 2023). On the other hand, it is not possible to make statements about changes in the interannual variability with this approach. Furthermore, the PGW approach allows for a much more flexible design by only taking into account changes to specific variables, instead of a Δ achieved from a GCM Schär et al. (1996). For instance, by only applying a change on the thermodynamic variables, it is possible to disentangle the reaction of the climate system to changes in the thermodynamic and dynamic forcing. This can lead to better process understanding, as the changes in dynamics are often more uncertain, while the thermodynamic changes are better understood.

3. Extratropical Cyclones

Our earth has a big temperature gradient between the equatorial regions and the poles on both hemispheres. To maintain the internal balance of the system, heat is transported from the low altitudes towards the high latitudes, by the ocean and the atmosphere. This leads to the development of the three circulation cells (Hadley, Ferrel, Polar). Assuming geostrophic balance, due to the rotation of the earth, the pressure gradient force from south to north is balanced by the Coriolis force, leading to the westward geostrophic wind. The horizontal temperature gradient further causes a vertical shear in the geostrophic wind and consequently the thermal wind. This increase of wind with height leads to the development of strong wind bands at the borders of the three cells in a height of approximately 300 hPa in both hemispheres (Mölders and Kramm, 2014). The wind band located at 45-60 °N, called the polar jet, is associated with the so called polar front, separating warm subtropical and cold arctic air masses.

This jet stream is meandering in waves, called Rossby waves, see Figure 3.1. They are mainly caused by continental barriers, but can also be influenced by different heating of water and land masses for instance (Mölders and Kramm, 2014). These waves build so called ridges and troughs that go hand in hand with high and low pressure systems at the surface. The troughs are regions of high baroclinicity. Baroclinicity is a measure of the misalignment between temperature and pressure gradient. In a barotropic atmosphere, temperature and pressure gradients are parallel. The opposite of this is a barocline atmosphere, where the misalignment between temperature and pressure gradients leads to a vertical shear in the geostrophic wind, which causes advection (Mölders and Kramm, 2014). Therefore, high baroclinicity supports the growth of small initial perturbations into extratropical cyclones (ETCs) and plays an important role in cyclone evolution (Eady, 1949). Subsequently storm tracks are located in regions of maximum baroclinicity, e.g. in the vicinity of the jet stream (Hoskins and Valdes, 1990). The resulting low pressure systems are then rotating counter-clockwise on the Northern Hemisphere, while their anticyclonic counterparts are rotating clockwise. On the southern hemisphere the opposite is the case, cyclones rotate clockwise, while anticyclones are moving counterclockwise.

3.1. Cyclogenesis

Extratropical cyclones do not develop solely along the polar front, but also out of other frontal structures or close to orographic features. For example ETCs often develop on the

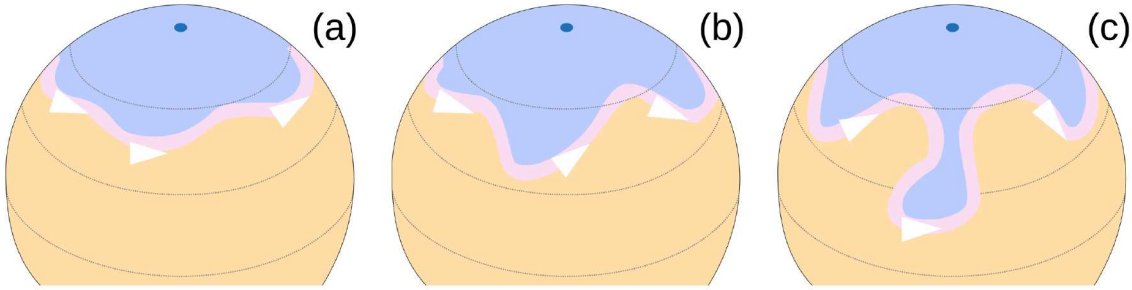

Figure 3.1.: Rossby waves of different amplitude in the jet stream on the Northern Hemisphere (the Oyster, 2014)

trailing cold fronts of existing low pressure systems as small systems. The exact process of cyclone evolution can be explained by different cyclone models. The two most frequent ones are the Norwegian Model, which was developed by researchers in Norway in the early 20th century (Henry, 1922) and the Shapiro-Keyser-model, a more recent model, which was proposed in 1990 (Shapiro and Keyser, 1990). Today it seems like both models are helpful to describe ETCs, as some systems do resemble more the Shapiro-Keyser-model, while others can be better described by the Norwegian model.

3.1.1. Norwegian Model

The development of a cyclone starts with a kink in the polar front, with a low pressure system in the middle. Cycling around this low is a warm front, as boundary of the warm air in the warm sector, which is followed by the cold front leading the cold sector. According to the Norwegian model the cold front is moving faster than the warm front, because the cold air is moving beneath the warm air of the warm sector, while the warm front has to raise over the air of the cold sector. This leads to the cold front slowly catching up with the warm front, leading to the formation of the occluded front, which grows as the cyclone ages, leading to its decay (Figure 3.2).

3.1.2. Shapiro-Keyser Model

According to this model the original kink in the polar front develops into a cyclone through a fracture at the cold front center, which leads to a separation and strengthening of the cold and the warm front. Then the cold front is moving around the low, while the warm front is bending around it. This leads to the so called T-bone-structure, which is typical for Shapiro-Keyser cyclones, as can be seen in Fig. 3.2 b III. The warm front then continues to cycle around the cyclone center, resulting in a warm air sector in the middle of the system, called warm seclusion.

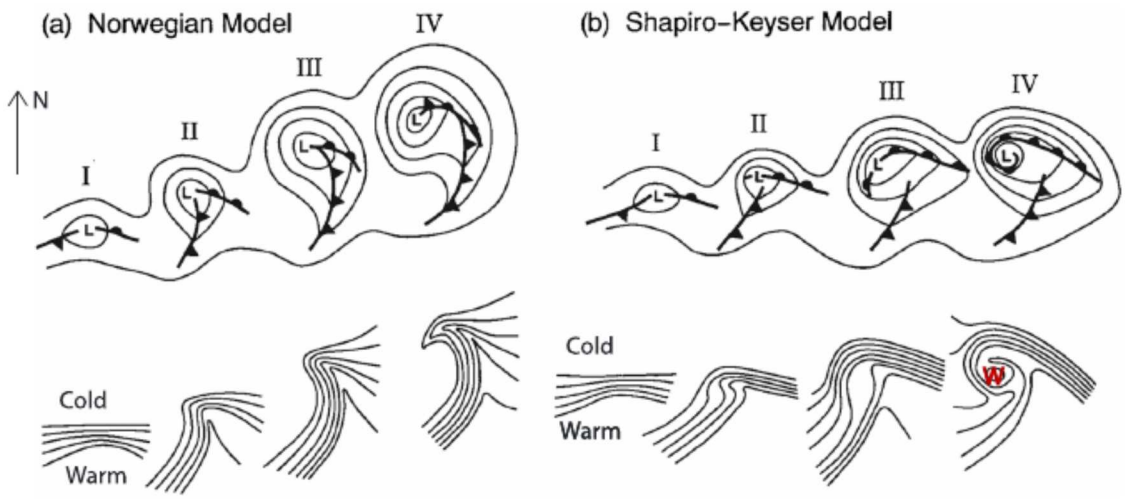

Figure 3.2.: Illustration showing the cyclone evolution in the Norwegian and the Shapiro-Keyser model (Catto, 2016), top: 850 hPa geopotential height with the cold and warm fronts, bottom: lower tropospheric potential temperature

3.2. Weather Associated with the Passage of a Cyclone

A large part of the weather in the mid-latitudes is driven by the formation and passage of cyclones and anticyclones. Following Mölders and Kramm (2014), this paragraph describes the weather sequence usually associated with the passage of a cyclone and its associated cold and warm fronts. The vicinity of the warm front goes along with increasing winds, a fall in surface pressure and increasing temperature and dew point. The warm front itself is characterized by front parallel winds and stratiform clouds caused by the adiabatic cooling of the ascending air. Often, long lasting homogeneous precipitation can be observed, as well as sometimes frontal fog, if the warm sector is cut off from the ground by the cold sector and the rain falls in colder air. The weather in the warm sector is quite stable, with decreasing winds, as well as constant pressure and temperature. The passage of a cold front is often associated with strong wind gusts and intense precipitation from convective clouds. Behind the cold front there is a significant decrease in temperature, as the weather is now determined by the cold sector.

Cyclones best described by the Norwegian model usually follow this sequence, while Shapiro-Keyser cyclones exhibit the described T-bone structure, with the warm front building the warm seclusion in the center of the cyclone. The three dimensional structure of a cyclone can be better described using the model of conveyor belts, see Figure 3.3. The warm conveyor belt is located in the warm sector and starts near the cold front, close to the surface (Eisenstein et al., 2022). It then ascends along the cold front, splitting up into two parts, one anticyclonic and one cyclonic part. Simultaneously the cold conveyor belt is a low level airstream, bending cyclonically around the center of the cyclone along the warm front or occluded front.

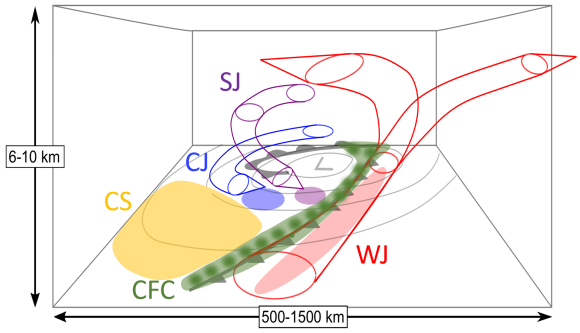

Figure 3.3.: Three dimensional structure of an ETC (Eisenstein et al., 2022), showing the cold (CJ, blue) and warm (WJ, red) conveyor belt jet and the sting jet (purple, SJ), the shaded regions show the regions of strong surface winds associated with the cold, warm and sting jet, the cold sector (CS) and the cold frontal convection (CFC)

3.3. European Windstorms

The passage of cyclones characterizes our day to day weather. But sometimes ETCs develop into destructive storms that are memorized by most people living in the affected regions, like for example windstorm Kyrill in 2007 (Fink et al., 2009) or windstorm Lothar in 1999 (Ulbrich et al., 2001). European windstorms, as assessed in this work, can be defined as ETCs with storm wind speed (>24.5 $\frac{m}{s}$) that mainly occur during winter season and can cause serious damage over large areas caused by high gust speeds and flooding through heavy precipitation or storm surges. Hence they are by definition extreme events, in contrast to ETCs that are first of all normal weather phenomena.

European windstorms regularly lead to significant socio-economic losses in the affected regions. Figure 1.2 shows the fatalities and financial losses of the ten costliest winter storms that hit Europe from 1990 to 2010. Altogether they caused nearly 500 deaths and each of them led to several billion euros of economic loss, with the costliest storm, storm Lothar in 1999, even exceeding 10 billion euros of loss and more than 100 fatalities. To prevent fatalities and damage through European windstorms, reliable forecasts are important. Therefore, it is vital to understand the development and structure of the key properties of European windstorms. Catto et al. (2019) identifies eight main features to look at (see Fig. 3.4 a), with the first four and the last one being features that influence the development of ETCs, while feature five to seven are properties characterizing them.

The first two features are the upper and lower level temperature gradient. These temperature gradients influence the storm development through their influence on the baroclinic instability of the atmosphere. As mentioned above storms develop in regions of high baroclinicity. The meridional temperature gradient between the tropics and the poles leads to a shear between temperature and pressure gradient and therefore to a region of high baroclinic instability (Mölders and Kramm, 2014). With climate change, these temperature gradients both are expected to change. Due to arctic amplification the lower level temperature gradient is projected to decrease, while the upper level temperature gradient is expected to increase due to enhanced heating in the upper level troposphere of the tropics (Ipcc, 2023).

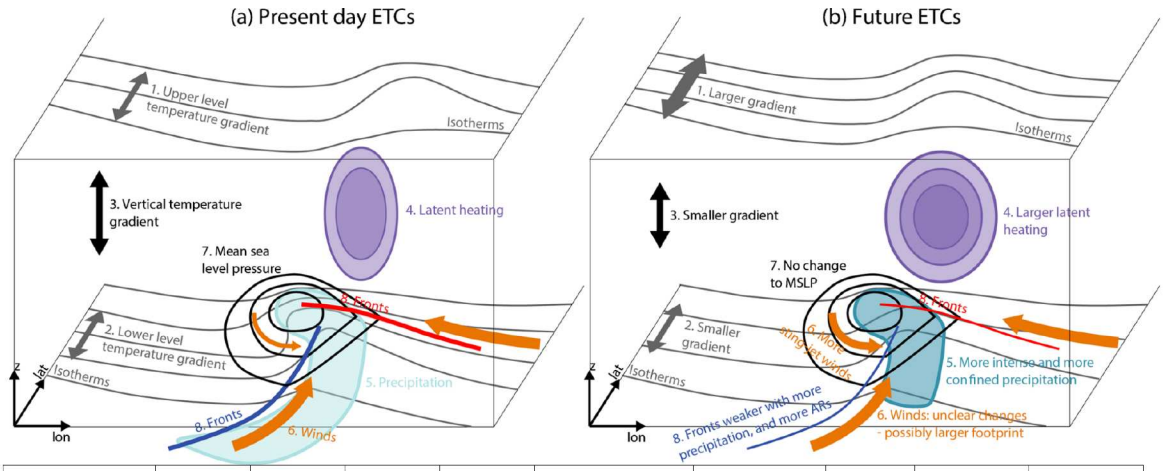

Feature	1	2	3	4	5 (intensity)	5 (extent)	6	7	8
Confidence	High	High	High	High	High	Low	Low	Medium	Low

Figure 3.4.: Schematic diagram summarizing the future changes of ETCs found by Catto et al. (2019) in their review paper, focusing on the changes of eight key features, the confidence in the identified changes is indicated in the table (Catto et al., 2019)

These changes have a counteracting influence on the baroclinic instability, which leads to difficulties in predicting how the baroclinic instability and its effect on ETCs may change.

The vertical temperature gradient (Fig. 3.4 feature 3) influences the static stability of the atmosphere. The atmosphere is considered to be stable if the equivalent potential temperature increases monotonically with height (Mölders and Kramm, 2014). In an unstable atmosphere this is not the case, hence air parcels rise, which leads to cloud formation. Such unstable conditions are generally associated with strong winds, for example through downward mixing of high momentum (Ludwig et al., 2015). The vertical temperature gradient is influenced by the horizontal temperature gradients in the upper and lower troposphere and therefore affected by their changes. Another factor that affects the vertical temperature gradient is latent heating.

Latent heating (feature 4 in 3.4) is the energy that is released through condensation of water vapor. High rates of latent heating lead to a higher amount of energy accessible for the strengthening of a cyclone. It is found to be a crucial energy source during the development of many cyclones (Fink et al., 2012, Ludwig et al., 2014). Due to enhanced atmospheric moisture content the role of latent heating is expected to increase with climate change.

Although confidence in the changes in upper and lower level temperature gradient, vertical temperature gradient and latent heating is quite high, it is difficult to assess how the changes described will change ETCs, because the effects interact with each other, in reinforcing and counteracting ways (Catto et al., 2019). All of this can lead to a changing frequency, intensity and location of ETCs, as well as a change in the key weather properties coming along with an European windstorm.

One of those properties is precipitation. Heavy precipitation is often leading to damage during the passage of an European windstorm. The precipitation is mainly located close to the cyclone center, as well as along the fronts. The warm front usually only brings light stratiform precipitation, while the highest amount of precipitation can be found along the cold front and in the cold conveyor belt. There is high confidence that the intensity of the precipitation associated with European windstorms will increase due to Clausius-Clapeyron scaling (Catto et al., 2019). Some studies found that the largest increase in precipitation will be close to the cyclone center (Pfahl et al., 2015, Tierney et al., 2018). Concerning the area affected by heavy precipitation there is less confidence. Michaelis et al. (2017) suggest that there will be a strong increase in the average area affected by heavy precipitation, which they define as more than 38 mm in 6 hours, while Catto et al. (2019) find with low confidence that the precipitation area will be more confined, see Fig 3.4 feature 6.

European windstorms are characterised by strong winds and wind gusts. There are four main regions of high winds in an European windstorm, see Figure 3.3. One of them is the cold front, where strong winds are often associated with convective cells. As the cold front is mostly stronger in cyclones following the Norwegian model, strong winds at the cold front occur more often in such cyclones. The second region is the warm jet at the surface along the warm conveyor belt, which is the largest and longest lasting one of those regions, but usually not responsible for the strongest winds (Eisenstein et al., 2022, Hewson and Neu, 2015). The third one is the wind of the cold jet, which reaches the surface at the tip of the cold conveyor belt, bended around the cyclone center. In many storms, especially Shapiro-Keyser cyclones, a wind maximum is located equatorward of the low at the end of the back bend front. This is sometimes due to the cold conveyor belt jet, which is wrapped around the center. However, in some cases this wind maximum is caused by a so called sting jet (Schultz and Browning, 2017). In general sting jets occur in earlier stages of the storm, than the wind maximum of the cold conveyor belt jet, but sometimes they appear at the same time and the wind maximum consists of two distinct air streams (Schultz and Browning, 2017). A sting jet is always associated with descent, often very rapid, from the mid-troposphere (Browning, 2004) and goes along with a distinct region, usually less than 100 km width, of very high wind speeds. Sting jets are primarily found in Shapiro-Keyser cyclones. Schultz and Browning (2017) estimate that in about 39-49% of the strongest ETCs a sting jet occurs. It is not yet totally clear how sting jets develop and where their intense downward acceleration comes from, but processes favoring the descent of air, such as dry intrusions, provide good conditions for the development of sting jets (Korosec, 2024). To summarize, nowadays the strongest gusts are observed along the fronts and sometimes around the center at the tip of the back bent front in the cold conveyor belt or during the occurrence of a sting jet. The changes of the windfield in future ETCs are quiet difficult to assess and the answer is often dependent on the exact region or property looked at. For example Li et al. (2014) expect overall no change in the maximum windspeed, but an increase over the British isles and the North Sea. The storm lifetime peak might decrease, while local extreme values could increase, as found by Chen et al. (2024). Considering the mean wind speed, only no or very small changes are expected (Chen et al., 2024, Ipcc, 2023). Additionally Martínez-Alvarado et al. (2018) found an increase in the frequency of sting jet events.

Another feature assessed by Catto et al. (2019) is the mean sea level pressure (MSLP). Often, speaking about the strength of European windstorms, refers to the minimum MSLP in the low pressure center. The drop in surface pressure is caused by ascending air. Therefore, upper-level divergence plays a crucial role in intensifying the systems. High values of upper-level divergence are often associated with a strong jet stream and can mainly be found in the area of the jet streak, the region of maximum windspeed in the jet stream. For some storms the deepening phase is very rapid. If there is a decrease in the core pressure of more than $24\frac{\sin\varphi}{\sin 60}$ hPa in 24 hours, which in the mid-latitudes corresponds approximately to more than 24 hPa, it is called explosive cyclogenesis (Catto, 2016). In figure 3.4, Catto et al. (2019) state with low confidence that in the future the core pressure of ETCs will not change, while Michaelis et al. (2017) state that studies using minimum sea level pressure as a measure of cyclone intensity mostly project an increase in extreme events. But one needs to consider that the isolated consideration of minimum core pressure might be misleading, because it is influenced by the background MSLP. Therefore, the conclusions of studies considering minimum MSLP perturbation might be more meaningful. These studies tend to find a decrease in extreme events (Michaelis et al., 2017).

The last feature considered in Figure 3.4 are the fronts. As explained above (see section 3.2) fronts play an important role in the formation of ETCs and are therefore indispensable for the development of European windstorms. Simultaneously they are themselves an important characteristic of the storm by mainly determining the weather sequence during the passage of the storm. According to Catto et al. (2014) there is a decrease in front frequency in the northern hemisphere, with a small increase over western Europe and a poleward shift of the front maxima. Additionally, in Figure 3.4 it is stated that fronts associated with ETCs will weaken with an increase in precipitation and atmospheric river frequency. This agrees with Schemm et al. (2017), a study using ERA-Interim reanalysis data from 1979-2014, which concludes that there was an increase in the number of extremely strong fronts over Europe tied to an increase in humidity.

In this thesis, the focus will be on the features directly responsible for the damage, namely precipitation and winds, as well as the MSLP as the main indicator for the intensity and track of the storms.

4. Methodology

4.1. Tools and Data

4.1.1. ICON

The ICOsahedral Non-hydrostatic model (ICON) is a modern modeling framework developed in Germany and Switzerland (Zängl et al., 2015). In contrast to other, earlier climate models, ICON has exact local mass conservation and the ability for flexible grid nesting. The model consists of two fundamental components. The model physics and a non-hydrostatic dynamical core. Those components are evaluated on different timescales. The basic time step Δt specifies the time steps of the evaluation of "fast" physical processes, having a timescale comparable or shorter than the model time step. Δt is also referred to as fast-physics timestep (Reinert et al., 2024). In the dynamical core a shorter timestep $\Delta\tau$ is used. The ratio between Δt and $\Delta\tau$ is the number of dynamic substeps N_{ds}.

The vertical ICON grid consists of terrain following layers with a higher layer density near the surface. As the name suggests, ICON has a horizontal grid that is based on an Icosahedron projected onto a sphere. Higher resolutions can be achieved by dividing the edges of the initial triangles in two steps. First, the edges are divided in n parts, then k edge bisections of the resulting triangles are performed. For a global grid, this leads to a number of

$$N = 20n^2 4^k$$

grid cells (Reinert et al., 2024) with a resolution of

$$\overline{\Delta x} = \sqrt{\frac{S_{\mathrm{earth}}}{N}} \approx \frac{5050}{n2^k}\mathrm{km} \quad ,$$

where S_{earth} is the earths surface and Δx is the edge length of a square with the same area as the mean triangular grid cell. The notation to specify the resolution is RnBk with n and k from above. With this grid structure it is possible to perform simulations in varying resolutions, for example by increasing the resolution over a certain area of interest, which is called nesting. This flexibility in nesting allows the usage of ICON for many different use cases. Therefore the modeling framework can be used for high resolution short-term numerical weather predictions as well as for global climate analysis over decades. The many components of the ICON framework, called ICON flavors, are adapted to the different needs of global versus regional simulations, as well as climate simulations and weather forecasting (Pham et al., 2021). One of this flavors is ICON-LAM.

4.1.1.1. ICON-CLM

ICON-LAM (limited area mode) is a weather forecast model used for regional numerical weather predictions. Based on ICON-LAM a new mode called ICON-CLM (climate limited area mode) was created, which is used in this work. ICON-CLM is an adaptation of ICON-LAM for climate applications. It is used for long-term regional climate simulations and allows for high resolutions. ICON-CLM is based on the technical infrastructure of COSMO-CLM (Pham et al., 2021).
To perform regional climate simulations, boundary data has to be provided. One possibility is to provide reanalysis data. Another possibility is to use output data from previous simulations with lower resolution over a larger area (nesting) (Pham et al., 2021).

A tool to simplify the work with ICON-CLM is SPICE (Starter Package for ICON-CLM Experiments) (Geyer et al., 2025). It provides a runtime environment for ICON-CLM simulations, including the necessary pre- and postprocessing. In this work, all simulations are performed with the help of SPICE or SPICE-daily, which is an adaptation of SPICE for daily simulations.

4.1.2. ERA5 Reanalysis Data

Reanalysis data is a special form of climate and weather data over a historic period. It is gained by a process called data assimilation, where observational data is combined with data from numerical weather simulations to get a best guess of the state of the atmosphere at a certain timestep.

ERA5 is one such set of reanalysis data (C3S, 2018), which reaches from 1940 to the present. It is the fifth generation of ECMWF reanalysis data. ERA5 provides hourly data on a normal lat lon grid resolution of 0.25° x 0.25° in the atmosphere and 0.5°x0.5° for the ocean. In this work several simulations are performed with ERA5 data as boundary data for ICON-CLM.

4.1.3. AWI Climate Model

The Alfred-Wegener Institute Climate model (AWI-CM) is a global coupled climate model participating in the Coupled Model Intercomparison Project Phase 6 (CMIP6) (Semmler et al., 2020). The AWI climate model is composed of the atmospheric model ECHAM6.304p1 from the Max Planck Institute for Meteorology (Stevens et al., 2013) and the Finite Element Sea Ice-Ocean Model (FESOM) (Wang et al., 2014), representing the ocean and sea ice. The atmospheric model is a spectral model running on a horizontal resolution of approximately 100 km and 95 vertical levels up to 0.01 hPa. FESOM is based on an unstructured mesh with resolutions ranging from 8 to 80 km, with higher resolutions in important areas with small-scale dynamics.

4.2. ICON-CLM experiments

As a first step in this thesis, the representation of European windstorms in the ICON model was tested. This was achieved by using ERA5 reanalysis data as initial and boundary data for limited area ICON simulations. The ICON simulations were performed with ICON release 2024.07 with ICON-CLM and with the help of SPICE-daily version 2.2.1 (see 4.1.1). To make sure that the large-scale circulations follow the reanalysis data, additional upper boundary grid-point nudging was applied to the upper-level horizontal velocity, analogous to the method presented in Klimiuk et al. (2025). For the upper boundary nudging a sponge zone with decreasing nudging strength α_{nudge} towards lower levels is implemented

$$\alpha_{\text{nudge}} = B_0 \left(\frac{z - z_{\text{start}}}{z_{\text{top}} - z_{\text{start}}} \right)^2 \quad ,$$

with z_{top} referring to the models top height and z_{start} being the lower boundary of the nudging zone, where the nudging strength is fixed to zero. B_0 is the maximum nudging coefficient, determining $\alpha_m nudge$ at z_{top} (Reinert et al., 2024). It is set to a default value of 0.04. The nudging is applied by adding a forcing term to the prognostic equations at each fast-physics time step Δt. This yields a modified prognostic variable ψ

$$\psi(t) = \psi^* + \alpha_{\text{nudge}} N_{\text{ds}} \underbrace{(\psi_{\text{bc}}(t) - \psi^*(t))}_{\delta\psi} \quad ,$$

with ψ^* being the value before applying the nudging and ψ_{bc} the value of the reanalysis ERA5 data that is used for nudging. N_{ds} refers to the number of dynamic substeps per fast-physics step.
In this first step, the storms were simulated with a horizontal resolution of 12 km, which corresponds to R12B05 and a vertical resolution of 60 vertical levels. The chosen domain can be seen in Figure 4.1a. As a further step, only for windstorm Kyrill, a nested simulation with a horizontal resolution of 3 km (R13B07) and 65 vertical layers was performed over Germany, on the domain shown in 4.1b. For the preparation of this domain, the tool Zonda was used (Center for Climate Systems Modeling (C2SM) et al., 2025).

The ICON-CLM simulations with ERA5 boundary data will be further referred to as ERA5 simulations.

4.3. Nudged storyline simulations and downscaling

The modeling strategy for nudged storyline simulations follows the method used by Klimiuk et al. (2025). Nudged simulations with the AWI-CM1 climate model (see 4.1.3) were performed by Sánchez-Benítez et al. (2022) by forcing the upper-level winds to follow the ERA5 reanalysis data from 1979 to 2024. This was achieved by spectrally nudging the vorticity and divergence in the upper levels (only vertical levels between 700 and 100 hPa)

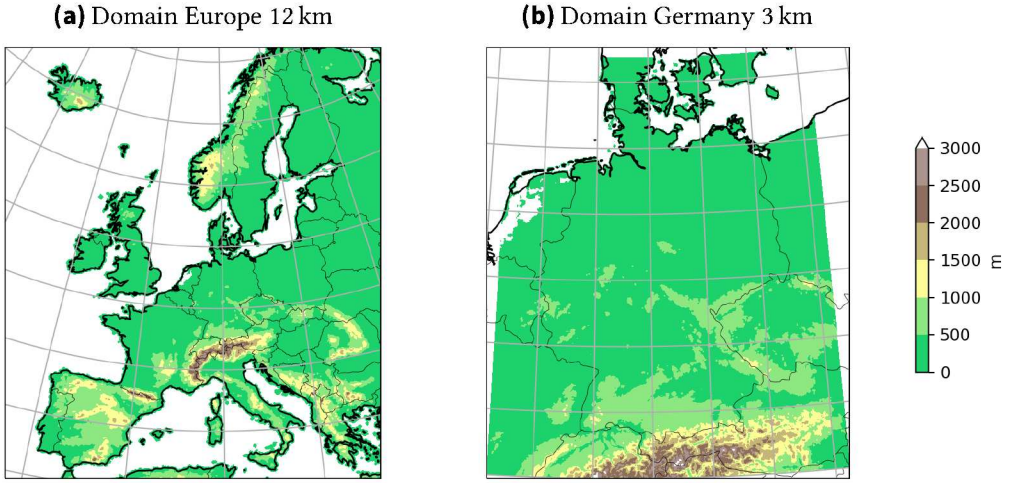

Figure 4.1.: Domain for ICON simulations, a) Europe 12 km resolution, b) Germany 3 km resolution

for wavenumbers up to 20, such that smaller scale structures can evolve freely. For the nudging strength, an e-folding time of 24 hours was used.

With this method, three simulations were conducted, starting in three different years corresponding to the present climate and the 2 and 3 K warming levels according to the SSP370 scenario. To dynamically downscale the nudged AWI simulations, ICON-CLM simulations were run with the same settings as described above, except that now the output of the AWI climate model simulations was used as boundary and initial data, as well as for the upper-level nudging. In the AWI simulation output the soil temperature is not available. Hence, the soil temperature from the ERA5 reanalysis data was used. Just as it was done for the ERA5 simulation, additional storyline simulations with a resolution of 3 km were performed for windstorm Kyrill. Therefor, the domain over Germany is extended northwards compared to that shown in 4.1b), because of a northward shift for the future storyline simulations of Kyrill.

In the following, the term storyline simulations will be used to refer to the downscaled nudged storyline simulations. Alternatively, in the sections specifically comparing the storyline simulations, the individual storyline simulations are referred to as present storyline simulation or present simulation, and 20xx simulation or x K warming level simulation for both future simulations, referring to the corresponding year of occurrence or warming level.

4.4. Storm Selection

This work presents a case study applying the nudged storyline approach to three storms. These storms were selected from many considered high impact storms between 1979 and 2022. To get an initial selection, the surface pressure charts of the AWI run in the present climate were analyzed for about 20 storms, including storms like Daria (1990), Anatol (1999),

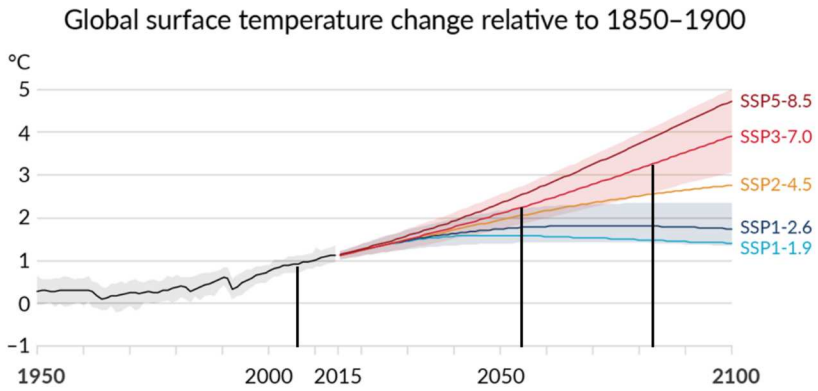

Figure 4.2.: Global surface temperature change relative to 1850-1900 for the five main SSP scenarios, with the vertical black lines indicating the years of the present, 2 and 3 K warming level simulation for windstorm Kyrill (adapted from Met Office, 2023)

Jeanett (2002) and Xynthia (2010). Several of the tested storms were reproduced poorly, either not occurring at all or with strongly deviating tracks. In a second step, seven storms that were well represented in the AWI present simulation were downscaled, using the ICON model. The three storms, for which the surface pressure charts and maximum 10 m gust footprints resembled the observations best, were chosen for this case study, namely Kyrill (2007), Christian (2013) and Thomas (2017).

As described above for these storms three simulations in different climate states were preformed, the present climate state and the 2 and 3 K warming level. For Kyrill and Christian the corresponding runs of the AWI climate model were started in 1979, 2027 and 2055. Therefore the years of the storms are, for Kyrill, 2007 in the present climate, 2055 for the 2 K and 2083 for the 3 K warming level and for Christian 2013, 2061 and 2089 respectively. In case of windstorm Thomas another set of AWI runs was used, reaching from 2017 to 2022 for the present climate and starting in 2065 and 2093 for the two warming levels. Although in Figure 4.2 it is visible that the years 2065 and 2093 correspond to a warming of approximately 2.5 and 3.5 K according to the SSP3-7.0 path, these runs will still be referred to as 2 and 3 K warming level runs, for simplicity. The timesteps for windstorm Kyrill are exemplarily sketched by the black vertical lines in Figure 4.2.

5. European Windstorms in the Present Climate

5.1. Kyrill

Kyrill was a European windstorm reaching hurricane strength that occurred in January 2007. It led to 54 fatalities and 7.6 billion euros of economic loss (Ludwig et al., 2015). On January 16th, a low pressure system developed over Newfoundland. Starting at 16.01 12 UTC, Kyrill underwent explosive cyclogenesis over the northeastern Atlantic, deepening from 998 hPa to 968 hPa in 24 hours. This was supported by the crossing of the very strong jet stream (Fink et al., 2009). The jet stream reached wind speeds of up to 370 km/h at 300 hPa. This led to the system traveling eastwards at a very high speed. In this environment, on 18th at 00 UTC, a secondary cyclogenesis started along the occluded front of the cyclone. This is a rare phenomenon, as most secondary cyclones build along the cold and warm fronts (Ludwig et al., 2015). The secondary cyclone traveled over Ireland and the North Sea, reaching its minimum core pressure of 962 hPa over the Baltic states on January 19th at 00 UTC. This strong deepening was supported by a strong upper-level divergence, caused by the vicinity of the left exit region of the upper-level jet streak (Fink et al., 2009).

During the 18th of January, the warmfront of Kyrill moved across western Germany, bringing long, intense precipitation and the first severe gusts (Wettergefahren Frühwarnung, 2007). When the coldfront moved in during the afternoon, it brought intense convective rain

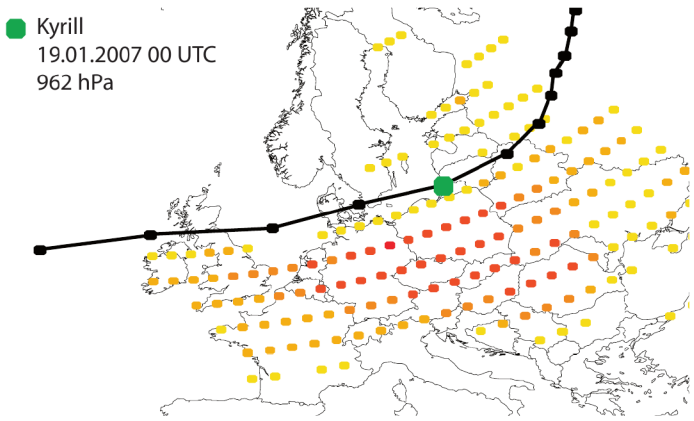

Figure 5.1.: Stormtrack of windstorm Kyrill, black dots show the 6 hourly storm location and the green dot the position of minimum core pressure (Fink et al., 2009)

along with some thunderstorms. These convective cells at the cold front caused severe gusts, reaching up to 202 km/h on the Wendelstein and 198 km/h on the Brocken (Müller-Westermeier, n.d.). In total, eight tornadoes were reported in Eastern Germany, the Czech Republic and Poland (Ludwig et al., 2015). Even in the flatlands, e.g. at Düsseldorf airport and Artern, gusts of 144 km/h were measured (Wettergefahren Frühwarnung, 2007). According to Fink et al., 2009, these strong gusts were supported by a strong pressure gradient of around 70 hPa between the low pressure center of Kyrill and the center of an anticyclone over Spain. In large areas the convective rain led to accumulated precipitation of 20-40 l/m^2 and at the Brocken up to 90 l/m^2 were reached. Accompanying the warm sector, subtropical air made its way over the Alps. This led to several temperature records in the night from 18. to 19.01, like 16°C at 22 MEZ in Mannheim (Wettergefahren Frühwarnung, 2007).

5.1.1. Kyrill in ICON-CLM simulations

The simulations of windstorm Kyrill are run as described in Section 4, with startdate 16.01.2007 00 UTC. Conducting various simulations with different initialization times, the simulation starting on the 16th at 00 UTC was closest to the observations. For Kyrill, additionally, nested simulations at 3 km resolution were performed, covering the same time period.

In Figure 5.2 the observed mean sea level pressure (MSLP) field in the DWD surface pressure charts is compared to the ERA5 and storyline simulations. In the first of the DWD surface pressure charts, at 18.01 00UTC, the secondary cyclogenesis along the occluded front is clearly visible. Twelve hours later, the low pressure system has moved over the North Sea, east of Scotland. At 19.01 00 UTC Kyrill has crossed Germany and Denmark and is located over the Baltic States. For all three timesteps the core pressure is equal to or lower than 965 hPa. In the ERA5 simulation (see Fig.5.2b) the pressure field is very similar. The storm is located at the same position with similar core pressure for all three timesteps. The core pressure at 18.01 12 UTC is slightly higher, but still below 970 hPa. Overall the storm track and core pressure are well represented in the ERA5 simulation.

In the present climate storyline simulation (Fig. 5.2c) the storm is traveling through the same area with a similar track and core pressure. But it is delayed by several hours compared to the DWD surface pressure map. In the first timestep the low is less deep with a core pressure higher than 975 hPa. Twelve hours later, when Kyrill had already passed Great Britain, the simulated system is still west of Scotland in the Atlantic, now with a core pressure below 970 hPa. Only at 19.01 00 UTC the storm is moving towards Germany, reaching a core pressure below 965 hPa, similar to the observations nine to twelve hours in advance. This delay could be related to small differences in the large scale structure, such as the jet stream. However overall the jet stream is very similar to the observations in the ERA5 and the present storyline simulations (see Appendix A.2). Although the storm in the storyline simulation is delayed by nine to twelve hours, it is still considered good enough for further analysis, as it moves along a similar track with similar core pressure.

(a) DWD Surface Pressure Charts

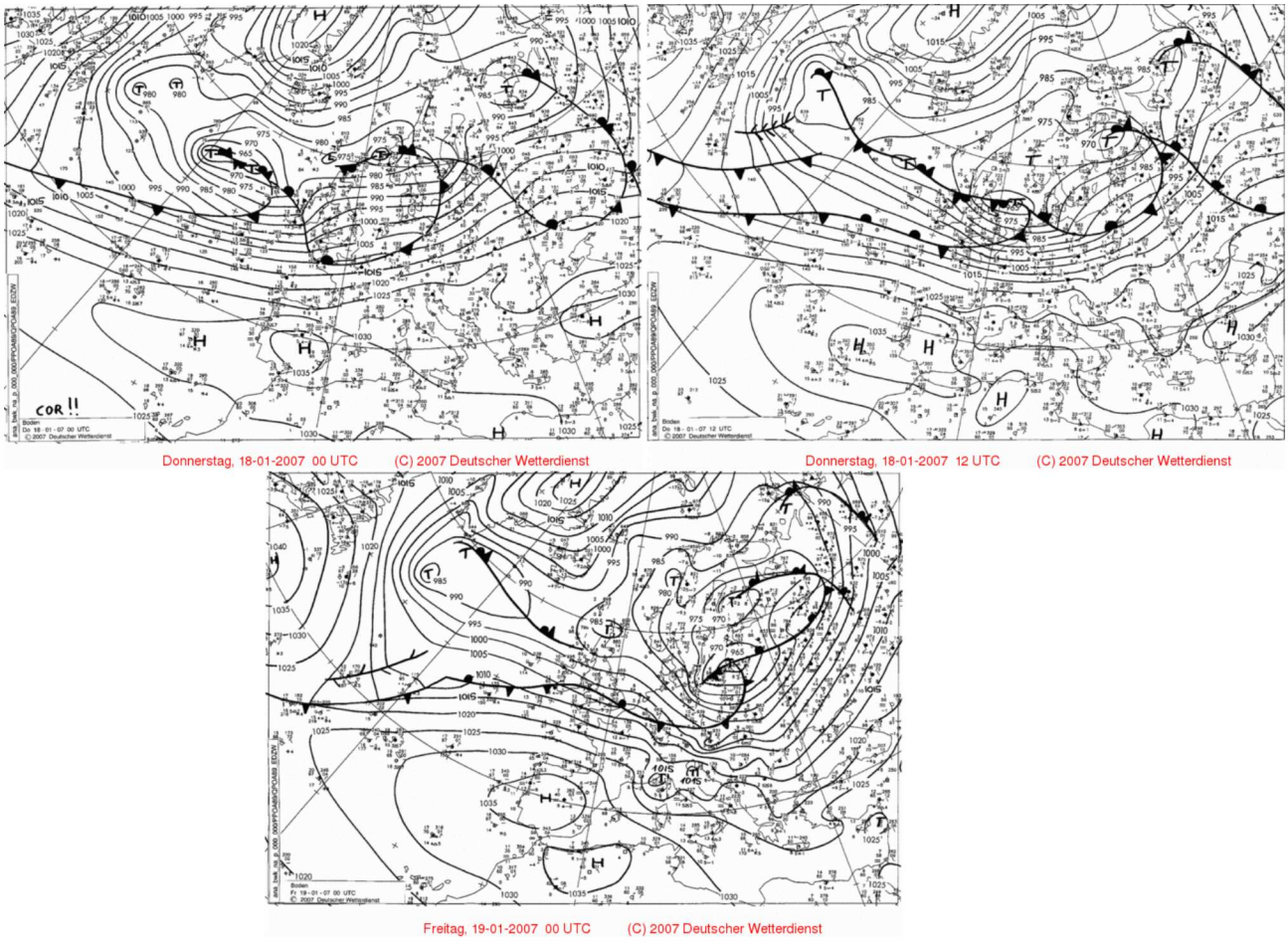

(b) ERA5 Simulation

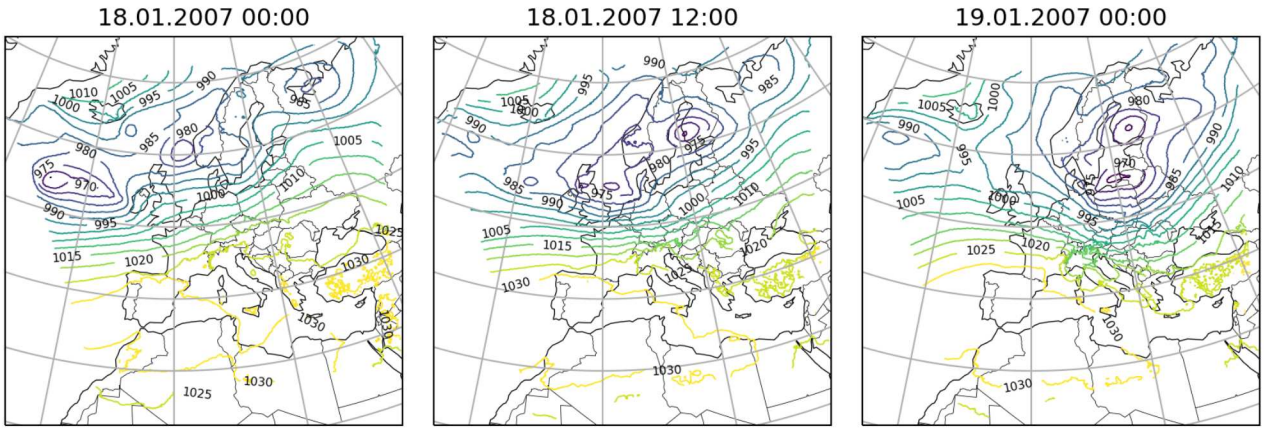

(c) Present Storyline Simulation

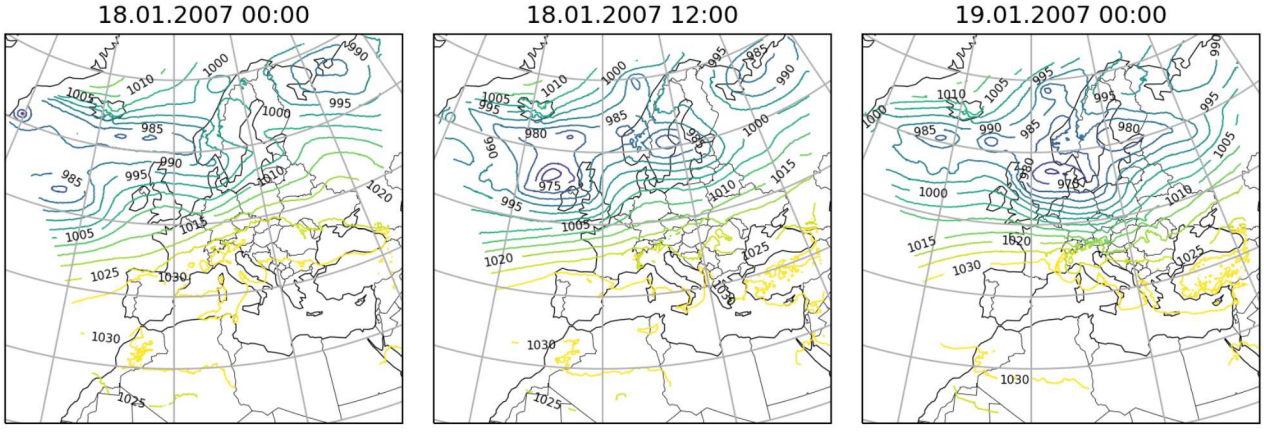

Figure 5.2.: MSLP during windstorm Kyrill from 18.01 00 in two twelve hour steps, pressure in hPa, a) DWD surface pressure charts, b) ERA5 simulation, c) present storyline simulation

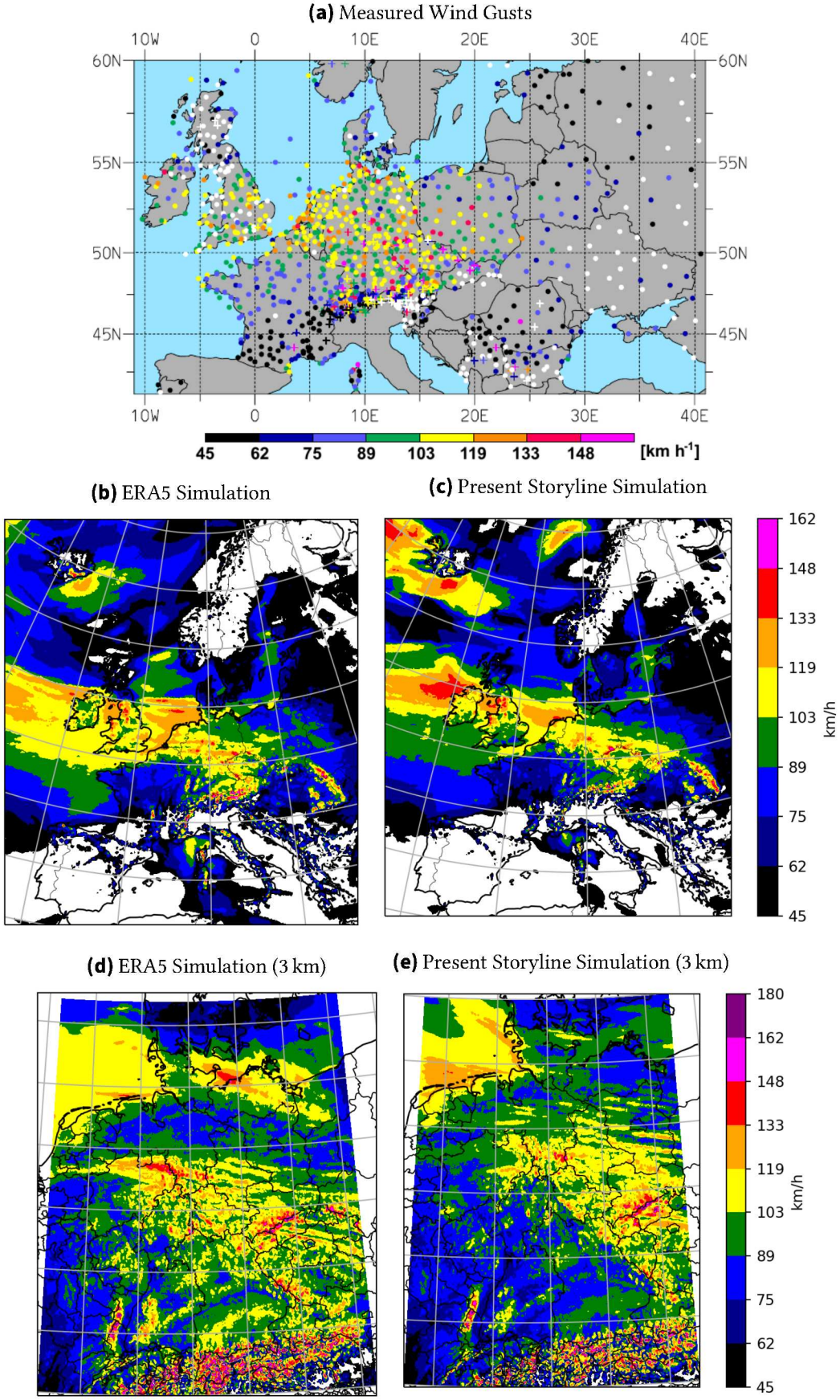

Figure 5.3.: Kyrill Maximum 10m Wind Gust, a) Maximum 10m wind gusts reported during 17.01 00 UTC - 19.01 18UTC, white symbols indicate no reported gusts, crosses indicate mountain stations (Fink et al., 2009), b)-e) Maximum simulated 10m wind gust over the time period 18.01. 00 UTC - 19.01.2007 12 UTC, resolution: mid: 12 km, bottom: 3 km, left: ERA5 simulation, left: present storyline simulation

In figure 5.3 the footprint of windstorm Kyrill is depicted. All three storms show a similar pattern with gusts > 100 km/h over large parts of England, the Netherlands, Belgium, Germany and Eastern Poland, as well as some regions with gusts exceeding 130 km/h over Germany and Poland. The ERA5 and storyline simulations agree on high gust speeds exceeding 120 km/h over the North Sea, west of Great Britain and Ireland. The high resolution simulations over Germany allow for a more detailed assessment of the high gust speeds associated with the convective cells along the cold front. In Figure 5.3d) and e) the stripes of high gust speed, produced by the convective cells along the cold front, are clearly visible. In both simulations, there are gusts exceeding 119 km/h in flat areas and >145 km/h in mountainous areas. But the very high gust speeds measured over the flatlands, such as >140 km in Düsseldorf, seem to be better represented in the ERA5 simulation.

To summarize, the analysis of the footprint and sea level pressure confirms that the ERA5 and storyline simulations are able to reproduce the historic event of windstorm Kyrill in a way that makes a comparison to the historic event appropriate.

5.2. Thomas

In February 2017 a series of several low pressure systems hit Europe. The strongest of those was windstorm Thomas (Doris in the UK) from the 21. to the 24.02.2017. The description of the development and impacts of windstorm Thomas in this paragraph follows Wettergefahren Frühwarnung (2017). Thomas formed in an environment with a strong frontal zone. Warm subtropical air had spread far north in the Atlantic. Additionally, on the 21st of February a low pressure system west of Iceland transported cold arctic air southwards. This led to further strengthening of the frontal zone and the development of a low pressure system west of Ireland on the afternoon of the 21st. The development of the system can be best described by the Shapiro-Keyser model. Starting in the morning of the 22nd of February the system underwent explosive cyclogenesis, deepening to less than 980 hPa in 24 hours. This was supported by a dry intrusion over Ireland. The dry air led to the ascent of underlying moister air. This caused the release of latent heat, which helped to further reinforce the storm. The system then traveled over the North Sea without further deepening and hit France, the Benelux states and Germany.

On the 23rd of February, severe gusts were measured in the UK, with the strongest gust reaching 153 km/h in Capel Curig (Wales). This was probably related to a sting jet, as a Shapiro-Keyser cyclone with a dry intrusion provides favorable circumstances for the development of a sting jet. The pattern of very high gust speeds in a confined region supports this consideration. In Germany, along with the cold front passage, several thunderstorms were reported, bringing severe gusts. Storm wind speed was measured in the whole area of Germany, with gusts exceeding hurricane strength in some regions. The strongest gust speed was reported at the Brocken, reaching 158 km/h. As a consequence of the strong gusts in the UK and Belgium five fatalities were attributed to the storm and the final PERILS damage report estimated insured losses of 248 million euros PERILS (2017). In Ireland damaged infrastructure left 60,000 people without electricity and during the 23rd and 24th

of February air and train traffic were interrupted in many regions. During the passage of the warm sector in southern Germany several decadal temperature records for the end of February were measured, which was supported by the foehn wind.

5.2.1. Thomas in ICON-CLM simulations

The ERA5 and storyline simulations for windstorm Thomas were conducted as described in section 4, with startdate 22.02.2017 at 12 UTC. Figure 5.4a) shows the DWD surface pressure map on 23.02.2017 at 6 and 18 UTC. In the first timestep, Thomas is located over the UK with a core pressure below 980 hPa. This configuration could be reproduced in the ERA5 simulation. Similarly at the second time step, the DWD analysis and the ERA5 simulation show the storms location over the North Sea close to the German coast with a core pressure below 980 hPa. Looking at the storyline simulation (Fig. 5.4c)) the storm is visible at the same locations, but with higher core pressure of below 990 hPa at 6 UTC and below 985 hPa at 18 UTC. Most likely, the storm simulated in the storyline simulation did not undergo explosive cyclogenesis. Unlike the observed storm it still deepens after hitting the UK. The reason for this might be the structure of the jet stream, which is depicted in Figure 5.5. In the observations and the ERA5 simulation, at 23.02 00 UTC a narrow trough west of Ireland is visible at the storms location. In the global forecast system (GFS, National Centers for Environmental Prediction, n.d.) analysis one can further see a strong upper level divergence in the exit region of this trough, which most likely supported the deepening of the storm. This trough is still visible in the storyline simulation at the same timestep, but it is much weaker. At 12 UTC the storm is surrounded by the tip of the split jet structure in the GFS analysis and the ERA5 simulation. This tip is not as developed in the storyline simulation, such that the storm is not equally surrounded by it. As described above, another factor influencing the development of the storm is the dry intrusion over Ireland. It is shown in Figure 5.6. Again, in the GFS analysis and the ERA5 simulation, the dry intrusion is visible and very similar, while in the storyline simulation the dry intrusion is present, but not as distinct as in the other two cases. This could be an additional factor leading to enhanced core pressure in the storyline simulation visible in Figure 5.4.

Emission

In Figure 5.7 the maximum gust speed of windstorm Thomas is depicted. Figure 5.7a), produced by PERILS (2017), shows the observed footprint of maximum gust speeds. The main affected regions are the UK, especially the Atlantic between England and Ireland, as well as the North Sea, the Baltic Sea and mid Germany, all with gusts of 80-100 km/h. The highest gusts are over England, Wales and North-Ireland. A very similar pattern shows for the ERA5 simulation, although over Germany and the North Sea the affected region is slightly smaller. In the present storyline simulation, the region of high gusts over the UK is missing. Additionally, the area of high gusts over Germany is smaller compared to the PERILS report. As mentioned above, there are speculations that a sting jet was responsible for these severe gusts over the UK. This could explain the absence of high gusts in the storyline simulation, as a sting jet, being a small scale event, is difficult to represent in simulations with 12 km resolution.

(a) DWD Surface Pressure Charts

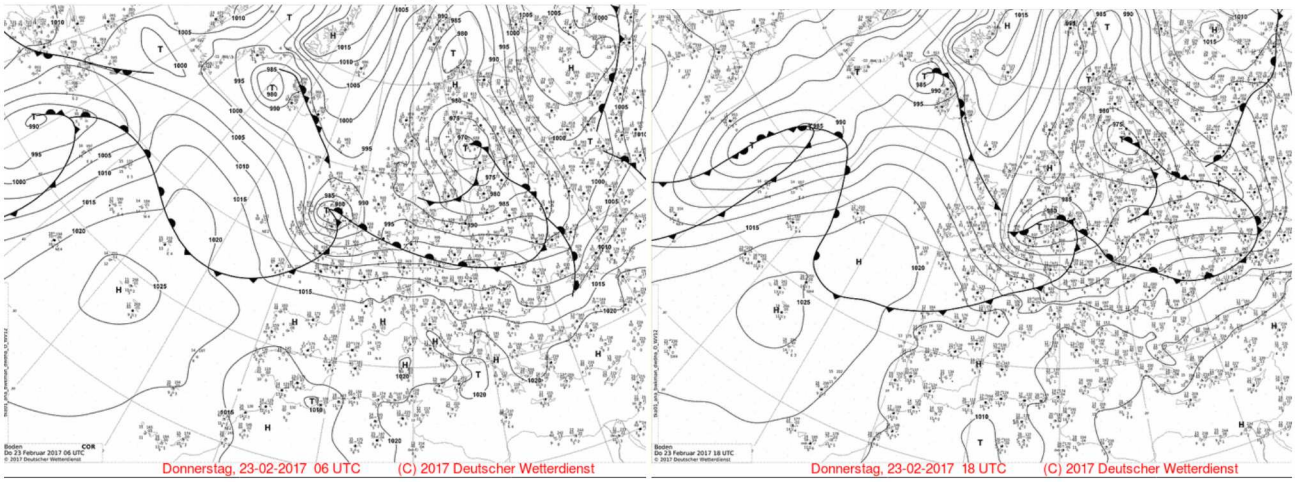

(b) ERA5 Simulation

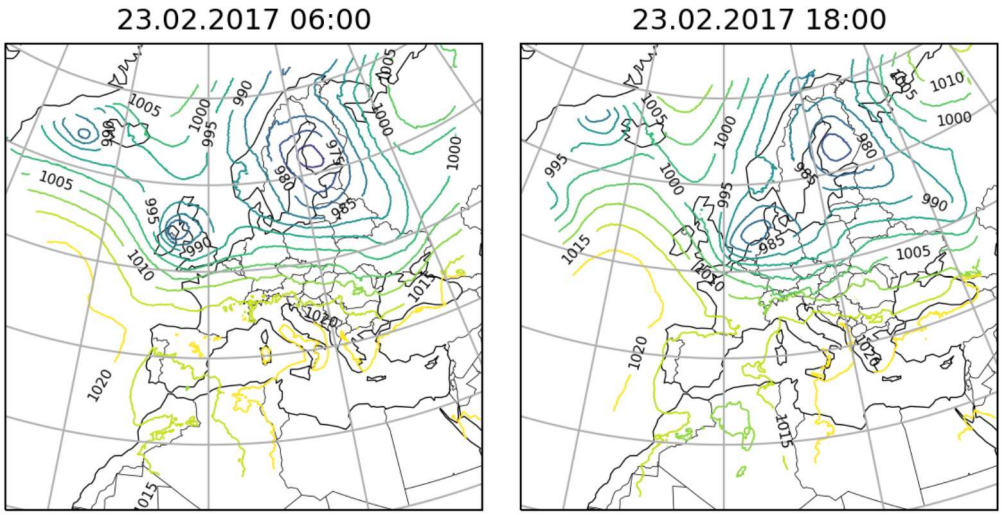

(c) Present Storyline Simulation

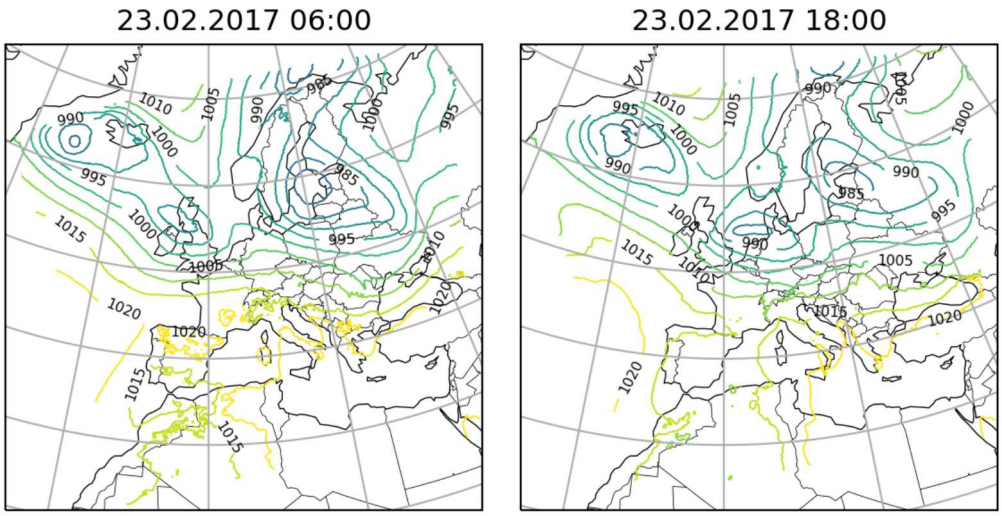

Figure 5.4.: MSLP during windstorm Thomas at 23.02.2017 06 and 18 UTC, isobars in hPa, a) DWD surface pressure charts, b) ERA5 simulation, c) present storyline simulation

(a) GFS Analysis

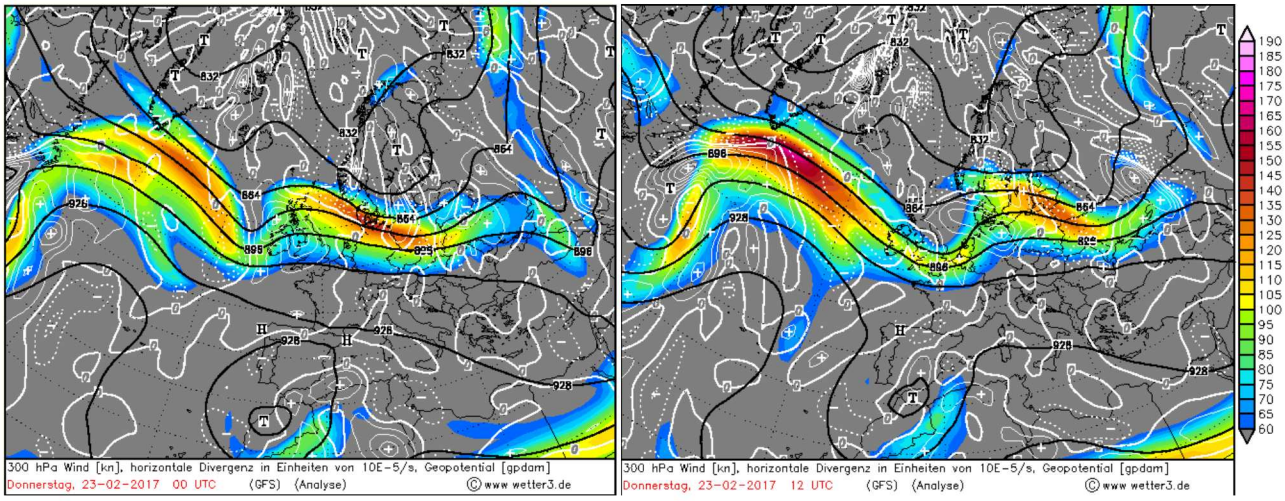

(b) ERA5 Simulation

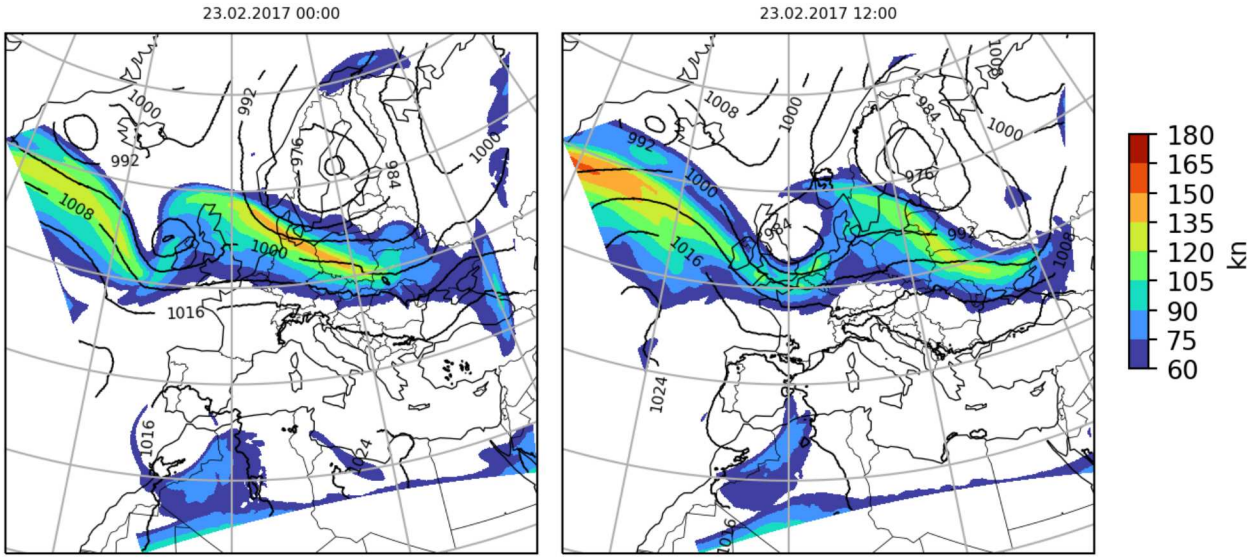

(c) Present Storyline Simulation

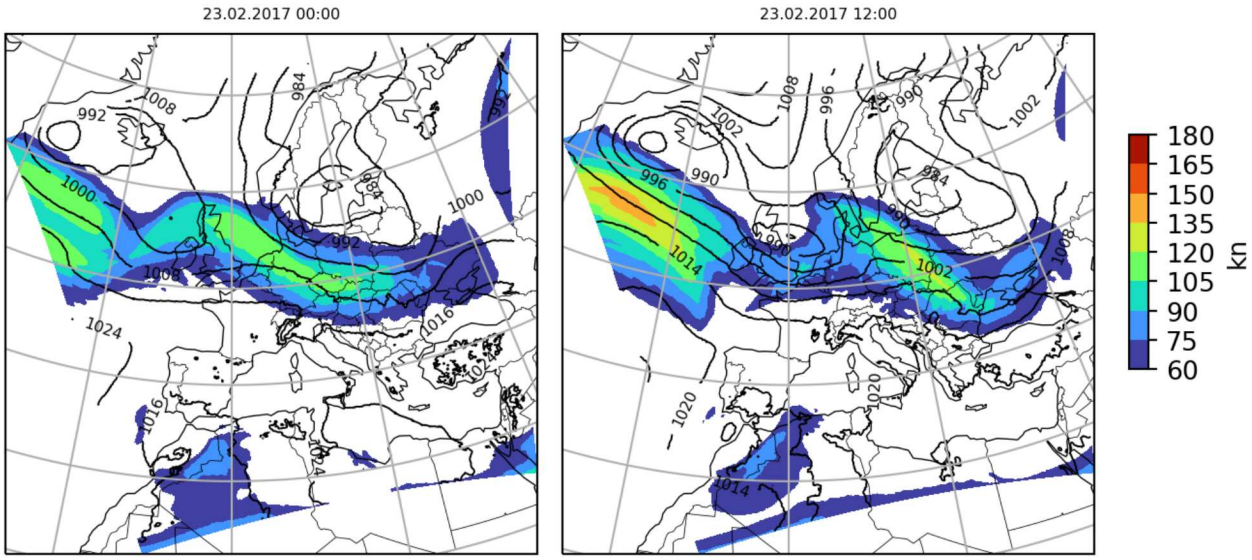

Figure 5.5.: Jet stream during windstorm Thomas at 23.02.2017 00 and 12 UTC, colored area shows the wind speed in kn in 300 hPa, a) GFS analysis, black lines show the geopotential and white lines the divergence, b) ERA5 simulation, c) present storyline simulation, black lines show MSLP in hPa

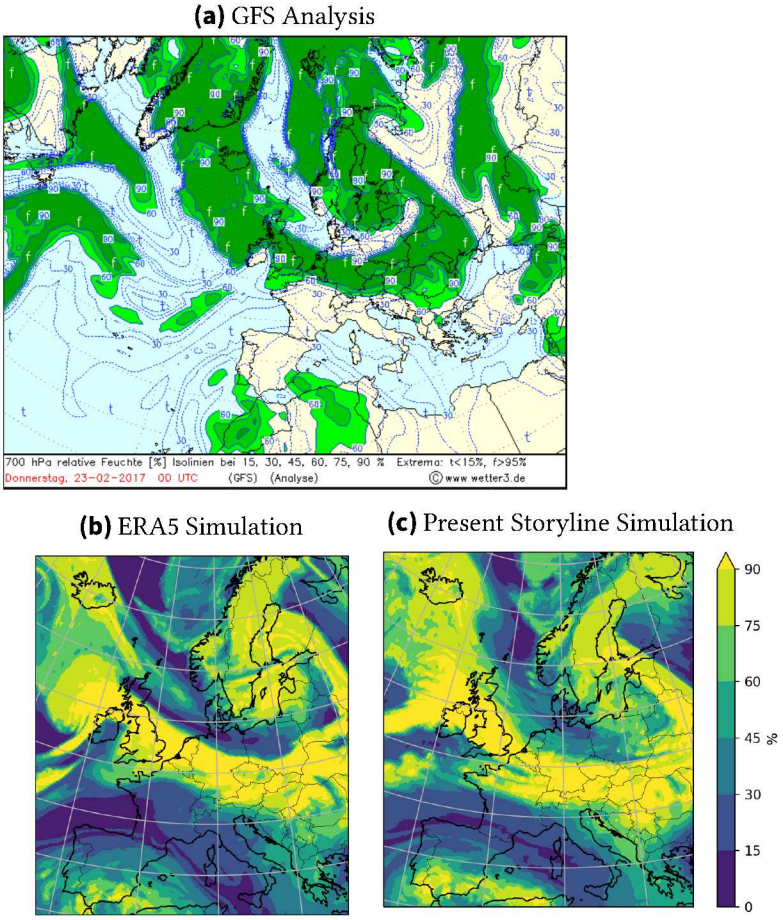

Figure 5.6.: Dry intrusion during windstorm Thomas, figures showing the relative humidity on 23.02 00 UTC at 700 hPa in %, a) GFS analysis, shaded green marks area with more than 60% of relative humidity, b) ERA5 simulation, c) present storyline simulation

To summarize, windstorm Thomas is very well represented in the ERA5 simulation, with the core pressure and footprint, as well as the structures important for the development of the storm, being very similar to the original event. In the storyline simulation, the storm is visible and following the same track, but with an increased core pressure. This is associated with differences in the jet stream and the dry intrusion that lead to a weaker development of the storm. Consequently, the footprint of the storm is smaller, with lower overall gust speeds.

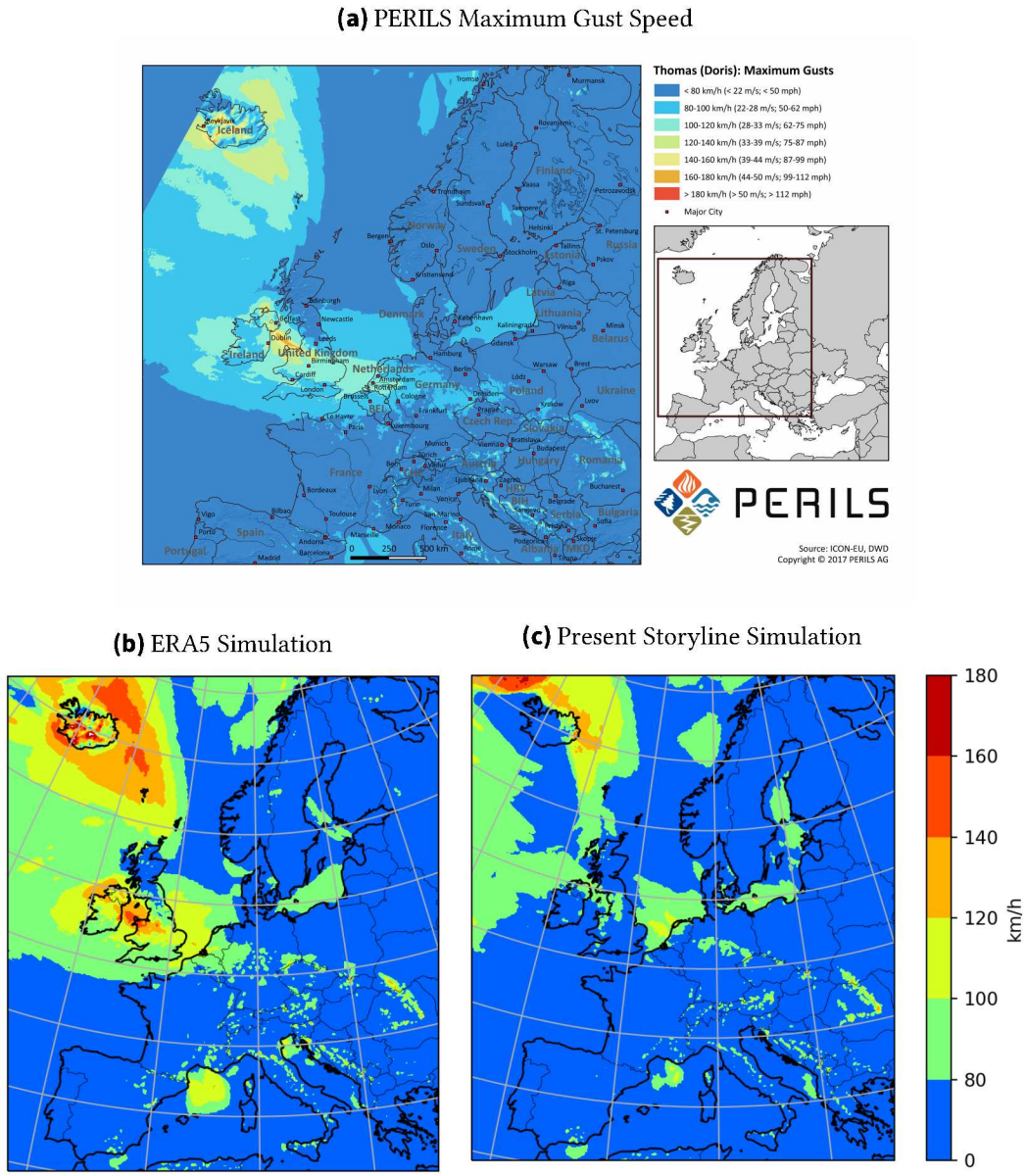

Figure 5.7.: Maximum 10 m gust speed during windstorm Thomas, a) produced by PERILS, b) and c) Maximum gust speed on 23. and 24.02 in ERA5 and storyline simulations

5.3. Christian

Windstorm Christian, called St. Jude storm in the UK, moved over Europe on the 28th of October 2013. It affected southern England, the Netherlands and Denmark, as well as the north of France, Germany and southern Sweden. Gust speeds of more than 150 km/h were reached, even in landlocked areas. The storm formed on the 26th of October southwest of Newfoundland at the edge of low pressure system Burkhard (Laps and Wagner, 2013). Due to the strong jet stream, the system traveled over the North Atlantic very fast, reaching England in the first hours of the 28th of October. The deepening of the storm was supported

by strong temperature gradients north of the Azores, due to warm subtropical air at the south and cold air from Greenland at the north side of the low pressure center. Additionally, a so called double jet configuration led to an overlap of the divergence zone of two jet streaks, which further deepened the storm (Wettergefahren Frühwarnung, 2013). Christian crossed England with a relatively southern track. During the 28th of October, Christian reached its minimum core pressure of 967 hPa over the North Sea. After crossing Denmark the system started to weaken while moving over the Baltic states towards Russia. The track of the storm is shown in Figure 5.8.

Christian was a Shapiro-Keyser cyclone. It built a dry intrusion in the morning of the 28th of October, reaching down to the lower troposphere over the Netherlands. This led to a sting jet, which was responsible for the very high gust speeds measured in the flatlands of northern Germany and Denmark. In Kegnæs (Denmark) a gust of 193 km/h was measured, which was a new all-time gust speed record in Denmark (Laps and Wagner, 2013).

Caused by the appearance of windstorm Christian early in autumn and the mild weather beforehand, many trees, still in leaf, were downed. This led to damage to buildings and infrastructure, as well as disruptions in transport. In the UK, France, the Baltic states and Germany many households were without electricity after the passage of the storm. Overall Christian caused 14 fatalities and an insured loss of 1.1 billion euros (Haesler and Lefebvre, 2013, PERILS, 2014). In England and Wales cellars were flooded due to heavy precipitation, with a maximum of 50 mm in 14 hours in Hampshire. For the North Sea and the Elbe storm surge warnings were given in advance. Afterwards no major damage was reported, although the Elbe at Husum and Eiderstedt was in flood, with more than 2 m over the mean high water and several islets reaching 1.5 m over the mean high water (Haesler and Lefebvre, 2013).

5.3.1. Christian in ICON-CLM simulations

In this section, the goal is to compare the ERA5 and the present storyline simulations to the observations. The simulations were conducted as described in section 4 starting at 27.10 00 UTC. Looking at the storm track and core pressure, in all three cases, on the 28th of October at 06 UTC, the low pressure center is located over southeast England, with a core pressure $\leq$980 hPa (see Appendix A.1). The next three 6 hourly timesteps are shown in Figure 5.9. Around 12 UTC Christian reached its minimum core pressure of 965 hPa over the North Sea. In the simulations the pressure at this timestep is higher, below 975 hPa. Both simulated storms reach their minimum core pressure of less than 970 hPa at 18 UTC, when the storm is located over northern Denmark. Following this, the observed event and the storm in the ERA5 simulation weaken. They are located over the Gulf of Bothnia at 29.10 00 UTC. The event in the storyline simulation that was already slightly further west in the earlier timesteps, is still located over the south of Sweden at 29.10 00 UTC. In contrast to the other two cases, it has deepened further, now reaching less than 965 hPa. Only at the 29th 06 UTC it has started to weaken. At this point it is located over the Gulf of Bothnia, while the observed system is already located over Russia (see Appendix A.1). This behavior could be caused by differences in the jet stream, shown in Figure 5.10. The figure

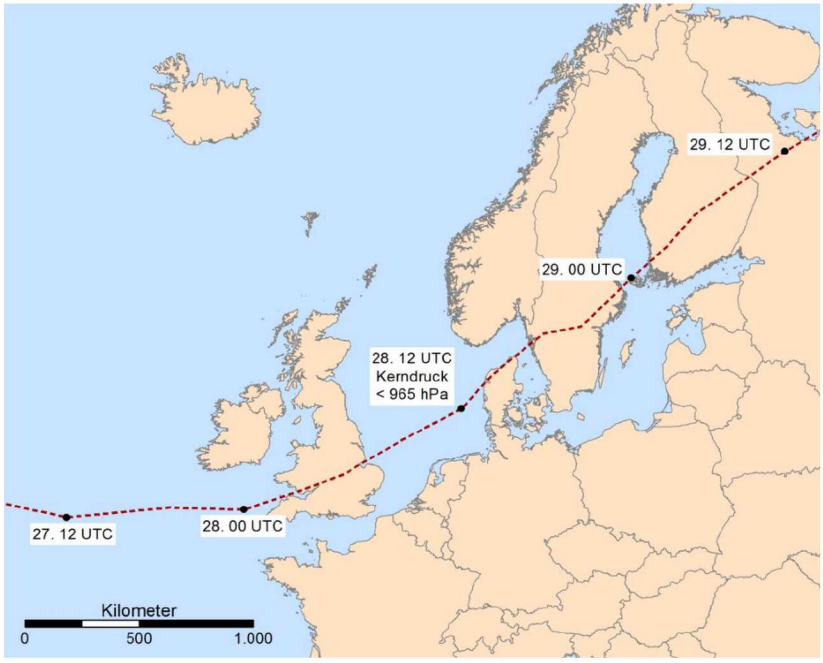

Figure 5.8.: Stormtrack of windstorm Christian on 27.-29.10.2013 (Haesler and Lefebvre, 2013)

shows the 300 hPa wind speed. For the two simulations isobars are depicted, indicating the storms location. Evidently, the pattern of the jet stream in the GFS analysis and the ERA5 simulation are very similar in the vicinity of the storm. In contrast, the jet stream in the storyline simulation shows slower wind speeds in the core, which could explain the slower movement of the storm. For the second timestep there is a split jet structure in all three cases. In the GFS analysis the splitted part of the jet stream is very narrow and considerably north of the storm center. Simultaneously a more distinct split jet structure can already be seen at 12 UTC in the storyline simulation. At 18 UTC this split jet is closer to the storm, such that it is nearly sitting in the bend. This difference in the jet stream structure is probably the cause for the extended deepening period of the storm in the storyline simulation.

As already described, similarly to windstorm Thomas, a dry intrusion occurred during windstorm Christian. This led to favorable conditions for a sting jet and supported the deepening of the storm. In the GFS analysis the dry intrusion is already visible and very distinct at 06 UTC. This not the case for the ERA5 simulation, where it is only quite weak at this time. In the storyline simulation the dry intrusion is barely visible at 06 UTC (see Figure 5.11). At the 28th of October at 12 UTC the dry intrusion over the Netherlands and western Germany is clearly visible in the observations and the ERA5 simulation, while it is not as distinct in the storyline simulation. This could partially explain the enhanced core pressure in the storyline simulation. Due to the less distinct dry intrusion, there is less latent heat available that is associated with the further deepening of a storm.

Looking at the footprint, the area affected by gusts reaching storm wind speed is quite similar in all three cases (see figure 5.12). Although both simulations lack the very high gust speeds above 140 km/h over the North Sea, the coast of the Netherlands and Germany, as well as over Denmark. Besides this, in the ERA5 simulation there are higher gust speeds

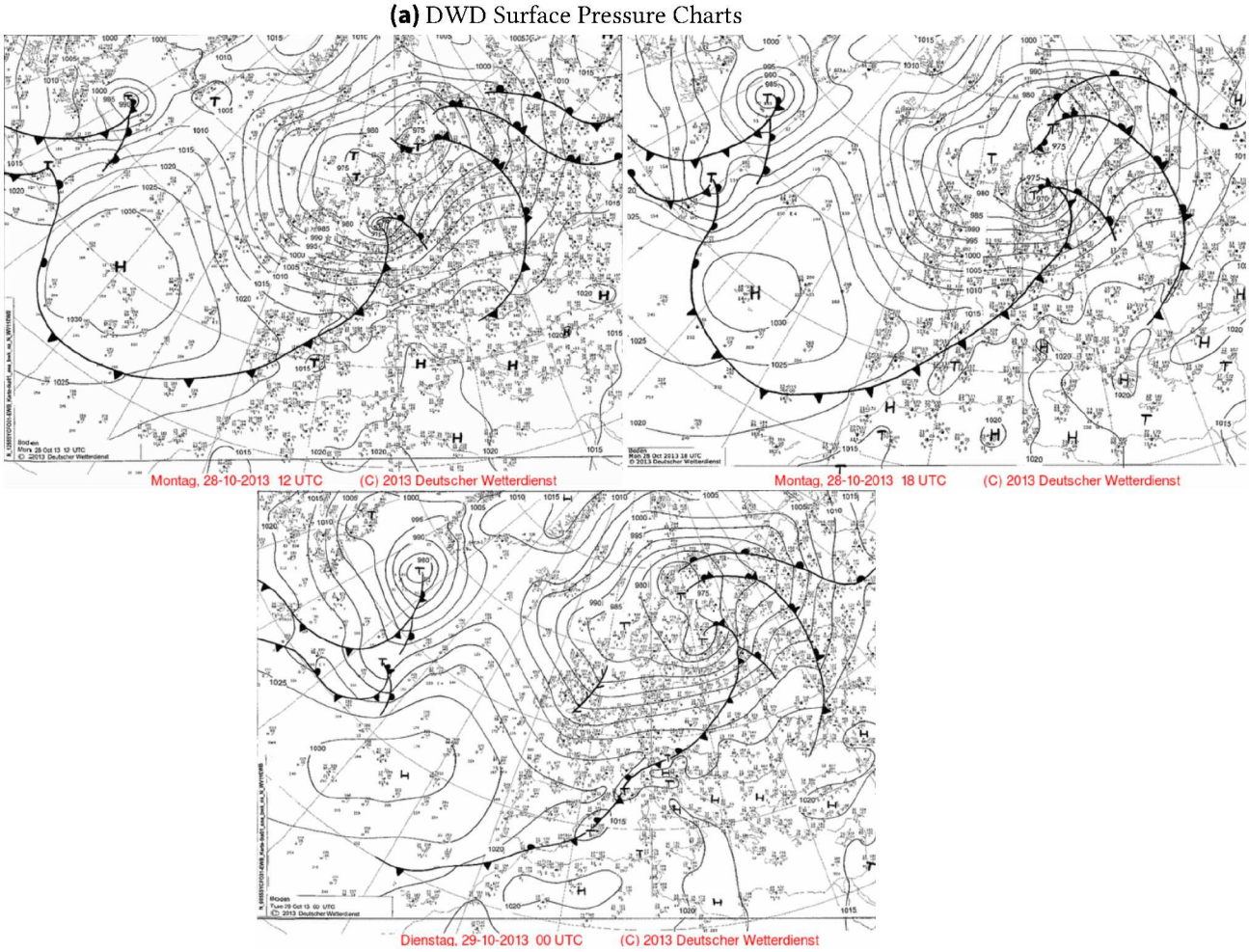

Figure 5.9.: MSLP during windstorm Christian at 28.10 12 and 18 UTC and 29.10.2013 00 UTC, pressure in hPa, a) DWD surface pressure charts, b) ERA5 simulation, c) present storyline simulation

(a) GFS Analysis

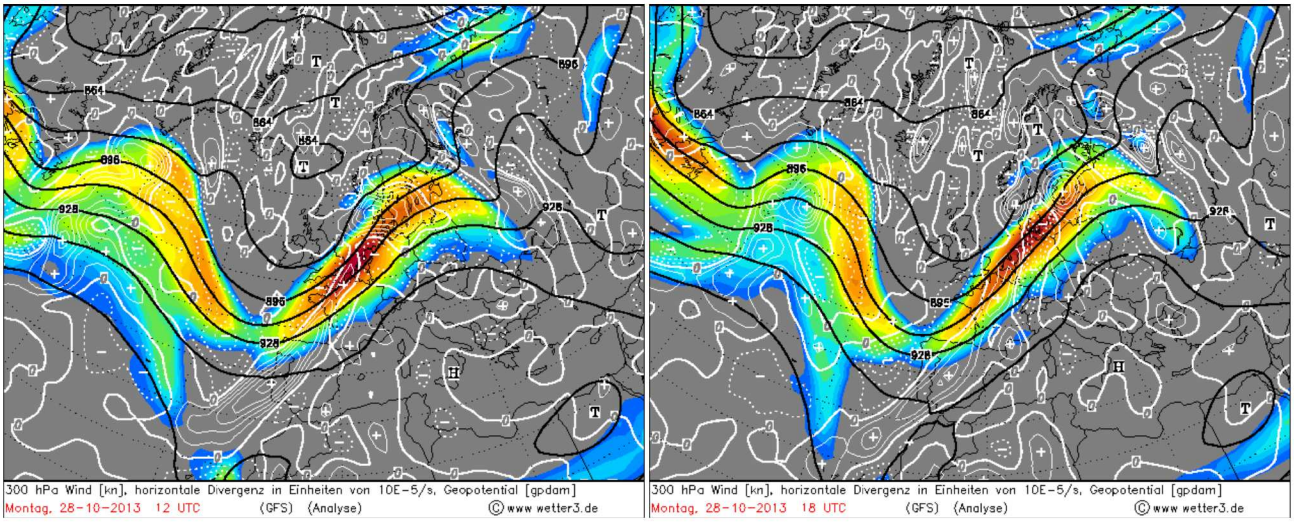

(b) ERA5 Simulation

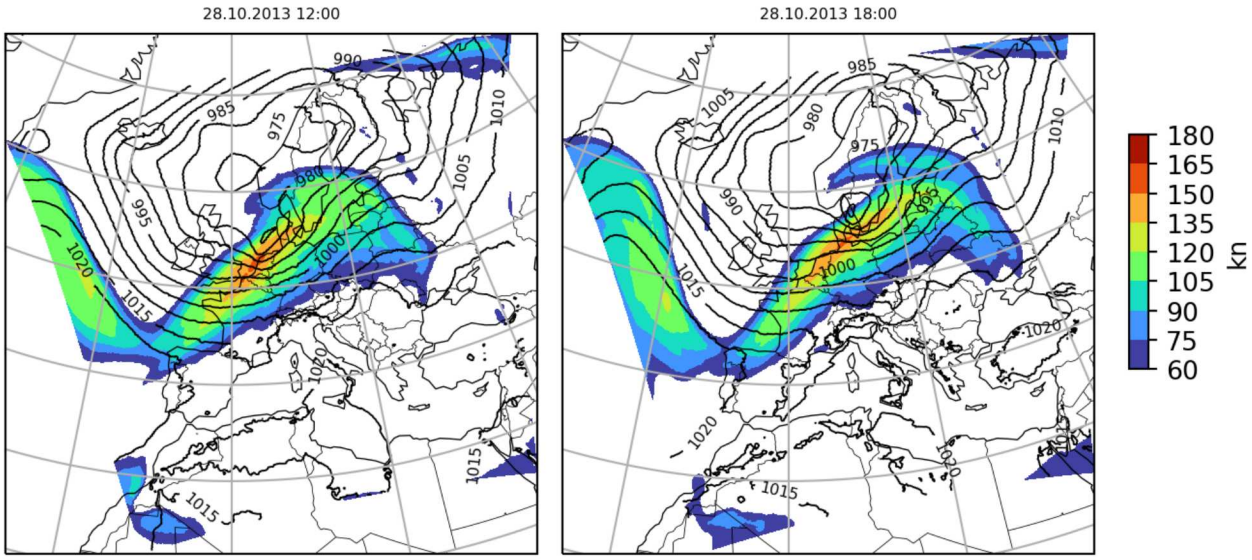

(c) Present Storyline Simulation

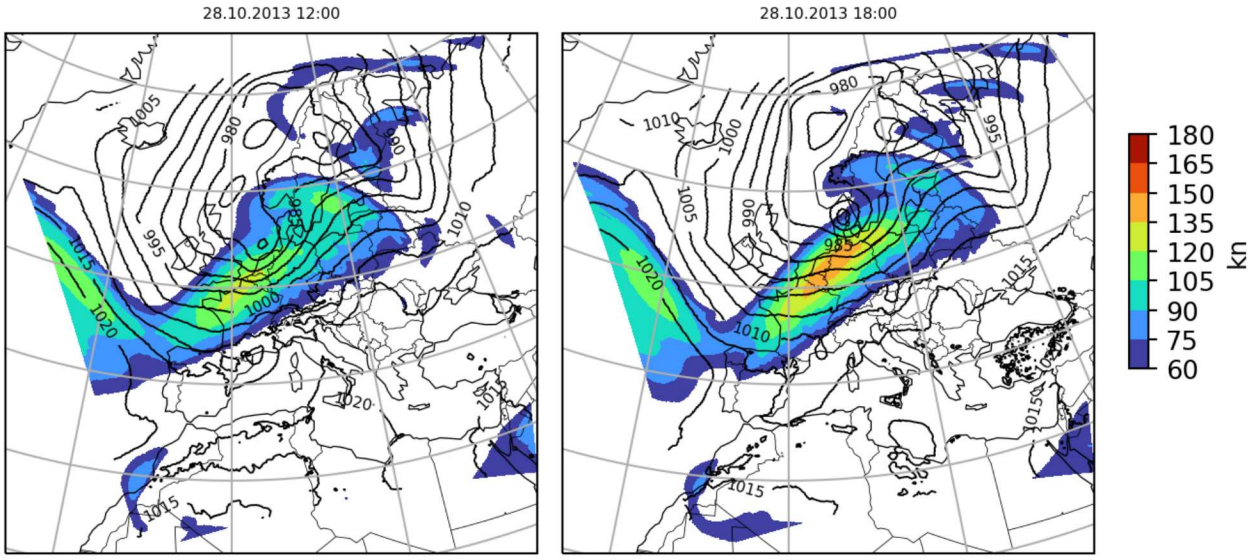

Figure 5.10.: Jet stream during windstorm Christian at 28.10.2013 12 and 18 UTC, shaded region shows the 300 hPa wind speed in kn, a) white lines and symbols indicate the divergence and black lines the geopotential, b) ERA5 simulation, c) present storyline simulation, black lines show the MSLP in hPa

(a) GFS Analysis

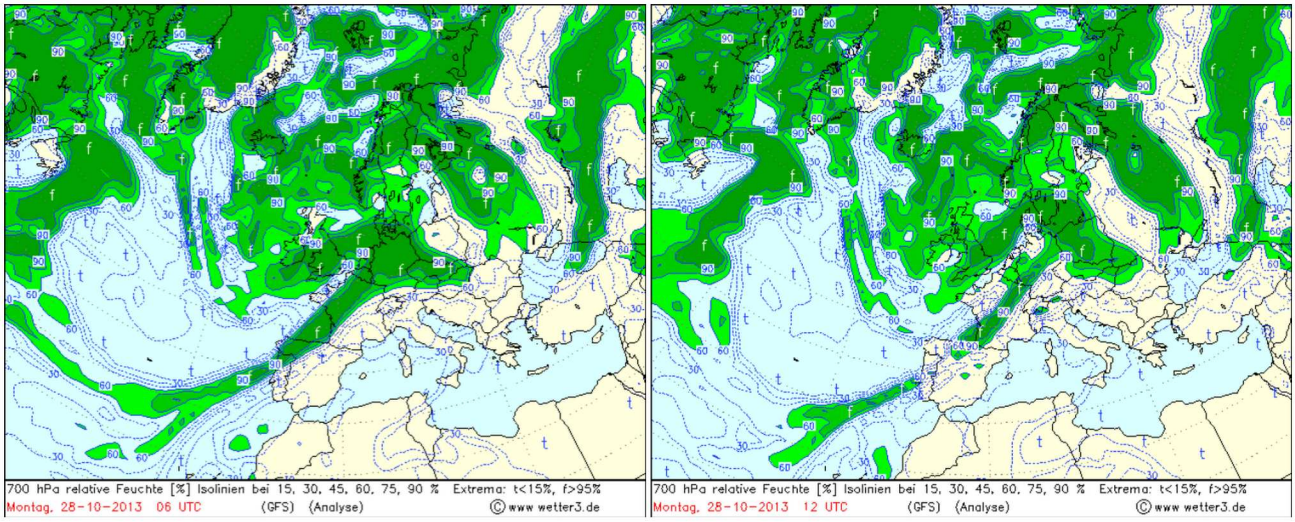

(b) ERA5 Simulation

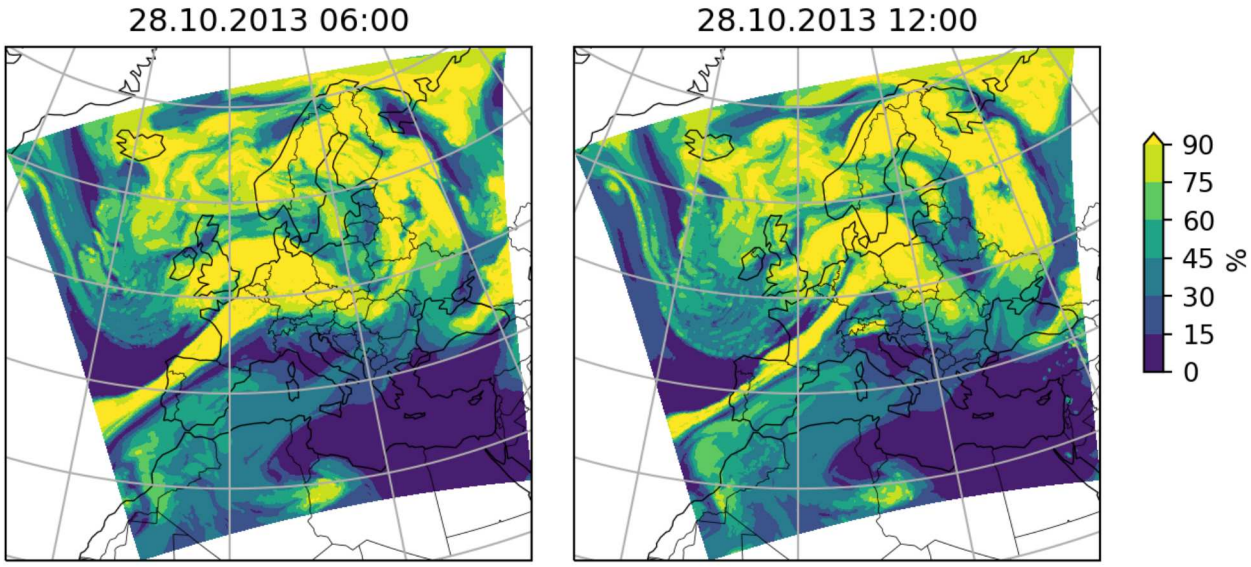

(c) Present Storyline Simulation

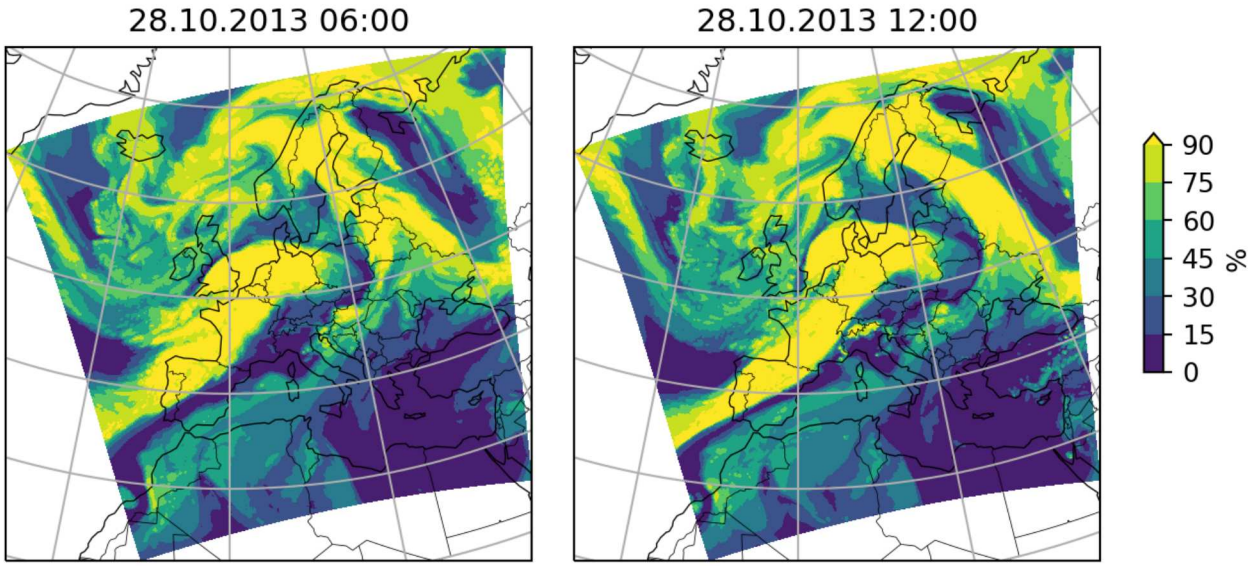

Figure 5.11.: Dry intrusion during windstorm Christian at 28.10.2013 06 and 12 UTC, shaded region shows the relative humidity at 700 hPa in %, a) GFS analysis blue lines indicate the isolines of relative humidity in 15% steps, b) ERA5 simulation, c) present storyline simulation

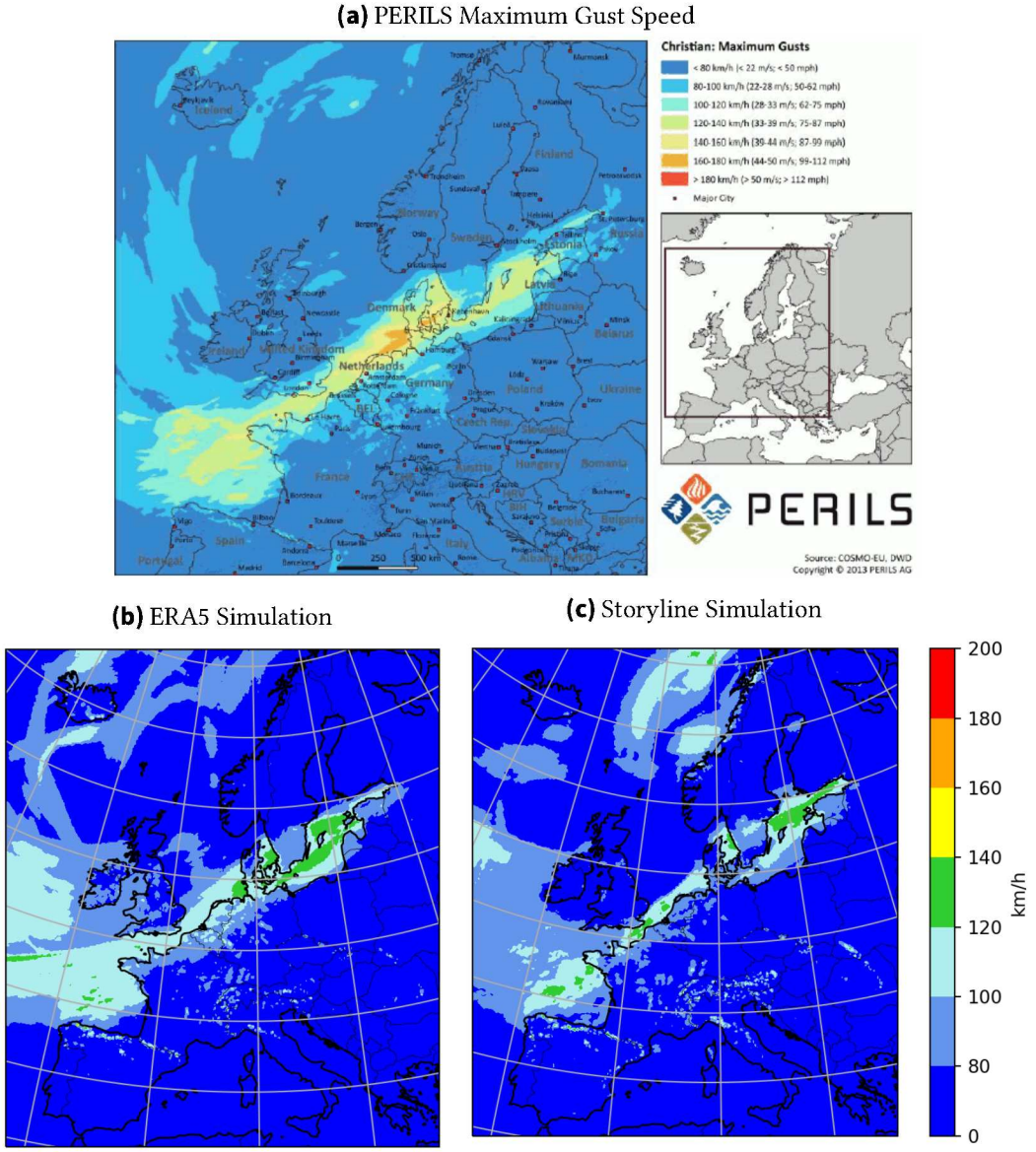

Figure 5.12.: Maximum 10 m gust speed during windstorm Christian, a) produced by PERILS, maximum gust speed from 27.10 00 to 29.10 12 UTC in b) ERA5 and c) present storyline simulation

over the Atlantic west of Ireland than in the PERILS report. For the storyline simulation, the area of gust speeds with more than 100 km/h is not extended as far northwards as observed. Simultaneously the higher gust speeds of 120-140 km/h between France and Spain and in the Channel are better represented in the storyline than in the ERA5 simulations. Overall, the footprint is quite similar in both simulations, although the very high gust speeds are missing. These very high gust speeds are most likely caused by a sting jet. Therefore, the absence of these severe gusts was to be expected.

6. European Windstorms in the Future Climate

In this chapter, the storyline simulations in the present climate will be compared to those of the higher warming levels to assess future changes in European windstorms. The simulations are conducted as described in section 4.

6.1. Kyrill

The startdate of all storyline simulations of windstorm Kyrill is the 16th of January at 00 UTC. In Figure 6.1 storm track and core pressure of all three warming levels are compared. The overall minimum core pressure for the present, 2 and 3 K warming level simulations are 964 hPa, 962 hPa and 956 hPa respectively. In Figure 5.2 the pressure change with time is depicted. Looking at the minimum core pressure at each time step on the 18th and 19th of January, the mean difference between the 2 K warming level and the present is around 3 hPa. The 3 K warming level has, on average, a 10 hPa lower core pressure. The temporal development of the core pressure is very similar for all three storms. Evidently, the storms in the future simulations are shifted northwards, with a stronger shift for the higher warming level. This matches the expected northward shift of the North Atlantic storm track (Ipcc, 2023). However, the idea of the storyline simulations is to reproduce the dynamic features of the historic event. Hence, it would be desirable to get simulations without such shifts in the stormtrack. The structure of the jet stream looks similar for all three warming levels (see Appendix A.3). Although there are some differences in the split jet structure, which could play a role in the observed northward shift.

The northward shift of the future storms is likewise visible in the footprint. Figure 6.2b) and c) show the footprints of the two warming levels. It is visible that there is a larger area of high gust speeds over the North and Baltic Sea for the 3 K warming level run. To see the changes more clearly, the differences in maximum 10 m gust speed on the 18th and 19th of January are depicted in Figure 6.2d),e). For the 2 K warming level run the main difference is a northward shift of the footprint. There is increased gust activity over the North and Baltic Sea, while Scotland, northern Germany and southern Poland are less affected. For the 3 K warming level simulation, there is increased gust speed in Scotland, the North and the Baltic Sea, while the southern regions of Germany and Poland as well as the Czech Republic face less severe gusts. Overall, the storm in the 3 K warming level simulation clearly has an increased footprint compared to the present storyline simulation. To get a closer look at the

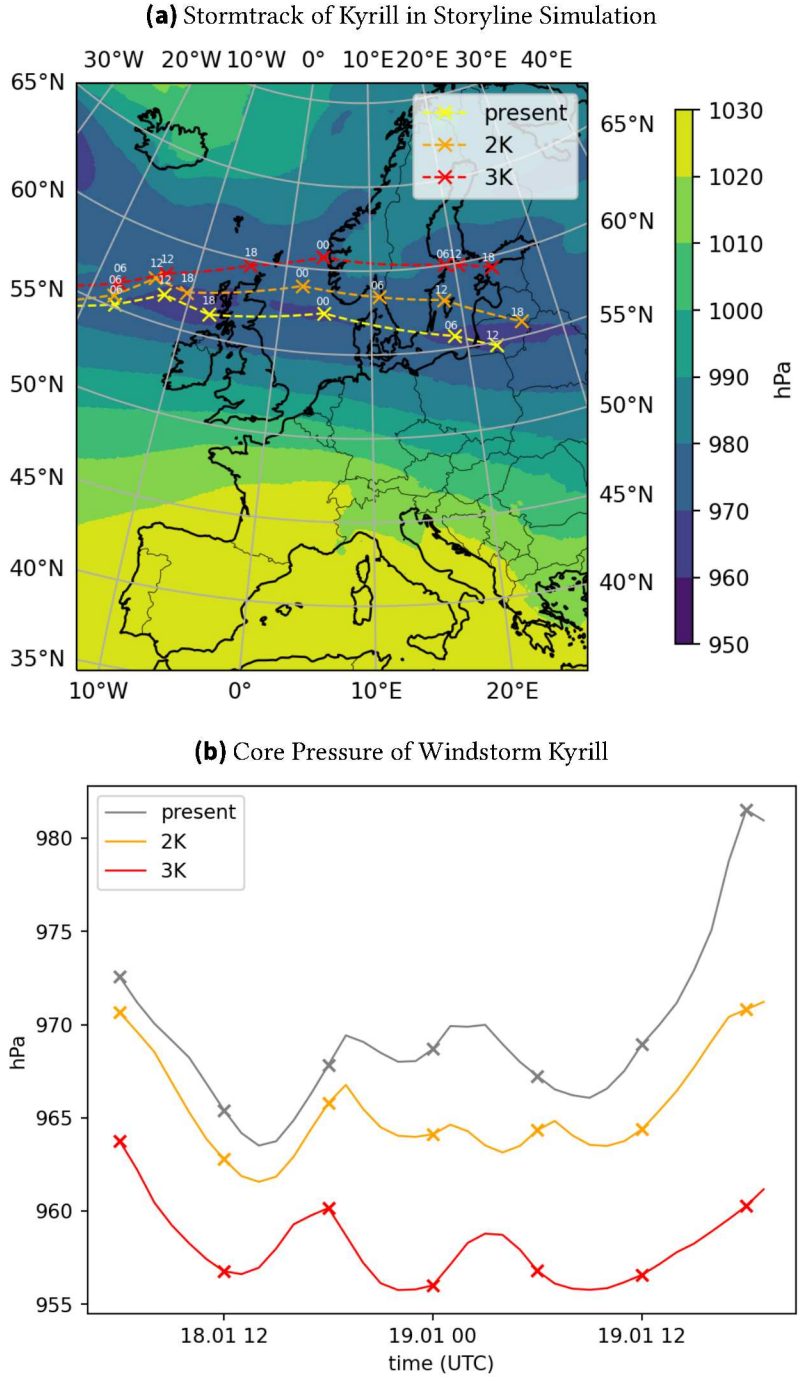

Figure 6.1.: Stormtrack and core pressure of Kyrill in storyline simulations, a) crosses indicate 6 hourly position of the storm, with the first cross showing the storm location at 18.01 06 UTC, shaded color showing the minimum pressure of the present storyline simulation, b) minimum core pressure with time, crosses at the same timesteps as above

differences in gust speed, the maximum gust values in the red box, shown in Figure 6.2a, are further analyzed. As shown in Table 6.1, the highest maximum gust speed is reached in the present run, with 44.7 m/s over the Erzgebirge. The maximum values of the future storms occurred in Great Britain and are slightly lower. The mean gust speed of all grid cells and timesteps is slightly increased for the 3 K warming level. To get a better comparison of the footprints, the number of grid cells with maximum gusts exceeding hurricane wind speed (32.7 m/s) is counted, resulting in similar values for the present and the 2 K warming level and a strong increase towards the 3 K warming level. In all three simulations most of the grid cells are affected by storm wind speed, with 90% in the 3 K warming level, 87% in the 2 K warming level and 85% in the present run. This analysis of the 10 m gust speed shows that overall the simulated event in the 3 K warming level comes with the most severe gust field, with a considerably larger area affected by hurricane wind speeds and the highest mean gust speed. No major differences are visible between the simulated event in the 2 K warming level and the present simulation. In Figure 6.3 a histogram of the gust speeds is depicted, including all gusts exceeding storm wind speed, in grid cells and timesteps in the red box in Figure 6.2a) on 18th and 19th of January. Therefore, not only the maximum temporal values of each grid cell, but the values of all timesteps are considered. It shows that the present and 2 K warming level simulation are overall very similar, except for the 2 K warming level simulation showing more gusts around 25 and 30 m/s and therefore more gusts exceeding storm wind speed. It is clearly visible that there are more severe gusts in the 3 K warming level simulation. The distribution tends stronger towards higher values, having a much higher and longer tail. In figures one finds that 27%, 32% and 36% of the total number of gridcells and timesteps are affected by storm wind speed for the storms simulated in the present, 2 and 3 K warming level respectively. Hence the increase with warming is stronger, if one considers not only the maximum temporal value, but all timesteps. This means that in a warmer climate individual grid cells are affected by storm wind speed for a longer time period during windstorm Kyrill.

The northward shift of the future simulations of windstorm Kyrill leads to difficulties in comparing the region of increased gusts relative to the storm center. Additionally, it is important to note that the differences in wind gusts are not necessarily all caused by the different warming levels. The comparison is limited by the shifted footprints of the storm. Due to the northward shift, the storm simulated in the 3 K warming level covers a lot more coastal and sea areas. These areas are generally associated with higher wind speeds. Hence, this could cause an increase in gust speed regardless of climate change.

Figure 6.4a) shows the accumulated precipitation from 18th 00 UTC to the 19th of January 12 UTC for the present storyline simulation. In large areas of the west coast of the UK, the Netherlands, Belgium, Germany and southern Poland, 20-30 l/m^2 of precipitation were simulated. In eastern France, southern and western parts of Germany and in Switzerland precipitation amounts of more than 50 l/m^2 accumulate. For both warming levels, the area affected by strong precipitation is clearly increased. Looking at the differences between the present and future simulations (see Figure 6.4d),e)), both precipitation fields show a northward shift. Mid and southern parts of France and Germany are dryer. In case of the 3 K warming level there is a strong decrease in precipitation close to the border triangle of France, Germany and Switzerland. The coasts of the North and Baltic Sea, as well as the

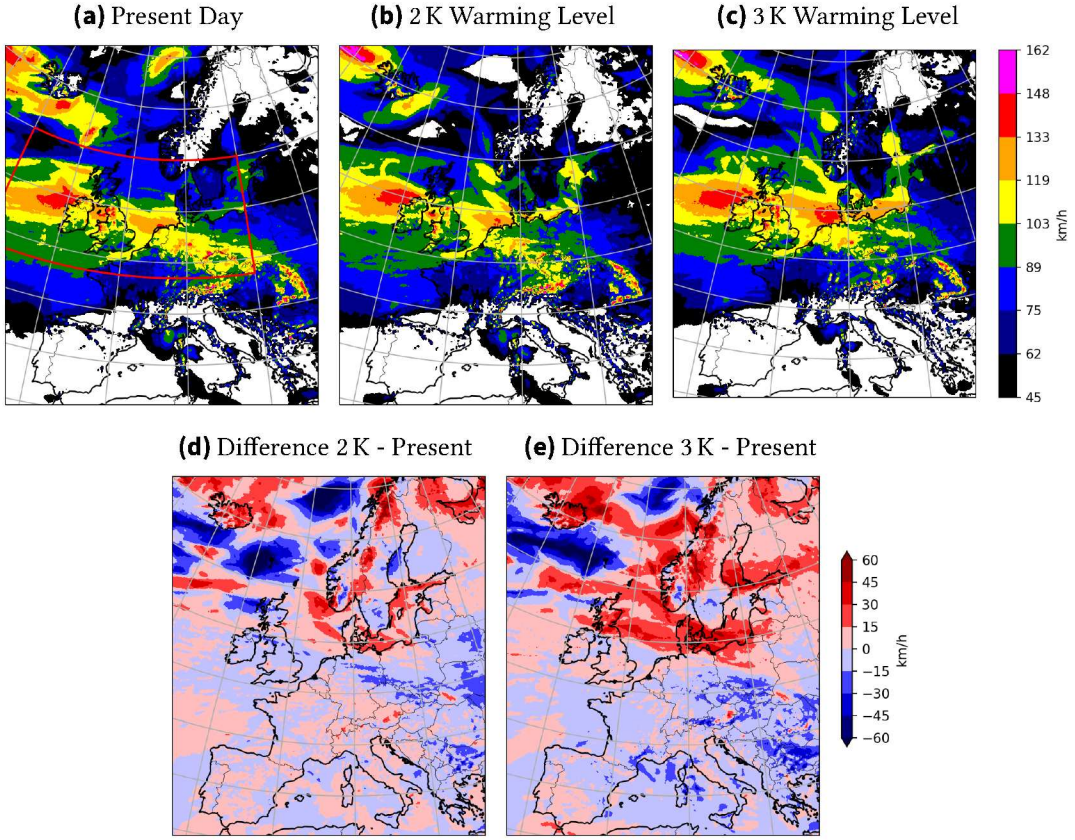

Figure 6.2.: Footprint of windstorm Kyrill on 18. and 19.01 for the storyline simulations, a) Maximum 10 m gust speed in present simulation, with the red box indicating the area considered in Table 6.1, b), c) analogue to a) but for the 2 K and 3 K warming level d) Difference of maximum 10 m gust speed v_{max} reached in the 2 K warming level vs the present storyline simulation $v_{max,2\,K} - v_{max,present}$, e) analogue to d) for 3 K warming level

Table 6.1.: Kyrill analysis of 10 m gust speed, considering all grid cells and timesteps in the area of the red box depicted in Figure 6.2a on 18. and 19.01; rows from top to bottom: global maximum 10 m gust speed, temporal and spatial mean of 10 m gust speed, percentage of grid cells with 10 m gusts reaching storm and hurricane wind speed at any timestep

	present day	2 K warming level	3 K warming level
max. gust speed in m/s	44.7 (Erzgebirge)	43.8 (UK)	43.2 (UK)
mean gust speed in m/s	16.7	17.1	18.2
gridcells with ≥ 20.8m/s	85%	87%	90%
gridcells with ≥ 32.7m/s	12%	11%	19%

UK and southern Scandinavia are affected by higher precipitation amounts. The analysis in Table 6.2 shows a similar pattern. The percentage of grid cells with more than 20 mm of total precipitation is considerably increased in the area and time frame considered (red box in Figure 6.4 from 18.01 00 UTC to 19.01 12 UTC). In fact it is more than doubled for the 2 K warming level and nearly tripled in the 3 K warming level simulation. Likewise

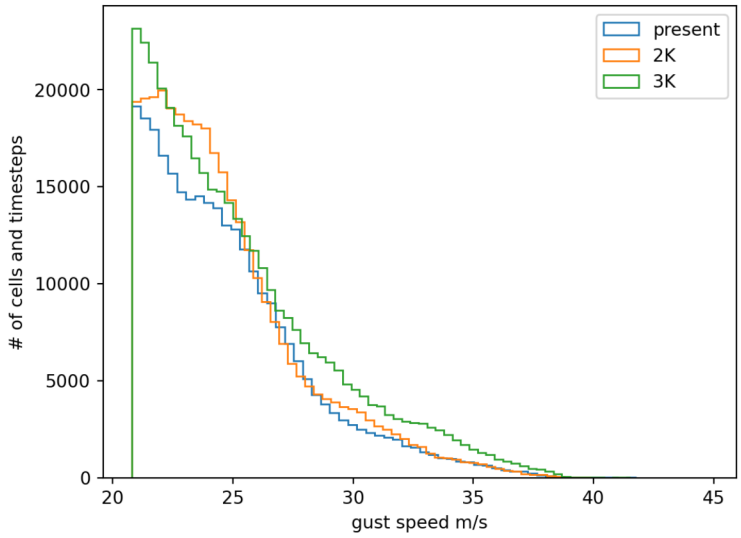

Figure 6.3.: Histogram of 10 m gusts exceeding storm windspeed during windstorm Kyrill, all grid cells and timesteps in the red box in Fig. 6.2a) on 18. and 19.01 are counted

Table 6.2.: Precipitation analysis for windstorm Kyrill, the considered values are all grid cells in the red box shown in Figure 6.4 and all timesteps between 18.01 00 UTC and 19.01 12 UTC, total precipitation (tot. prec.) refers to the precipitation amount summed over all timesteps

	present day	2 K warming level	3 K warming level
max. hourly precipitation	7.9 (Wales)	11.1 (west Poland)	12.9 (east Germany)
max tot. prec. in mm	94 (east France)	85 (east France)	68 (Wales)
mean tot. prec. in mm	11.1	14.2	14.4
% of cells with >20 mm tot. prec.	11.5	26.7	31.1

the maximum amount of precipitation simulated in a one hour time frame increases with warming. The location indicates that this is due to enhanced convective precipitation along the cold front, as the maximum values are located over western Poland and northeastern Germany for the future simulations, while in the present simulation the maximum is reached over Wales. The maximum total amount of simulated precipitation decreases with increasing warming level, with a considerably lower amount in the 3 K warming level simulation. In the histogram in Figure 6.4 the amount of precipitation summed over all timesteps for each grid cell is counted. All three distributions show a maximum for 0-1 mm and a second, local maximum, which is around 15 mm in the present warming level. For both future warming levels this local maximum is located at around 20 mm. Hence the future distributions are shifted towards higher amounts of precipitation. Additionally they are broader, meaning the span of events is larger, with higher local variability, than in the present climate.

For windstorm Kyrill high resolution storyline simulations were conducted, similar to those in the ERA5 simulation. In Figure 6.6 the maximum 10 m gust speed between 18.01 12 and 19.01 12 UTC is shown. Here, the stripes of high gust speed, coming from the convective

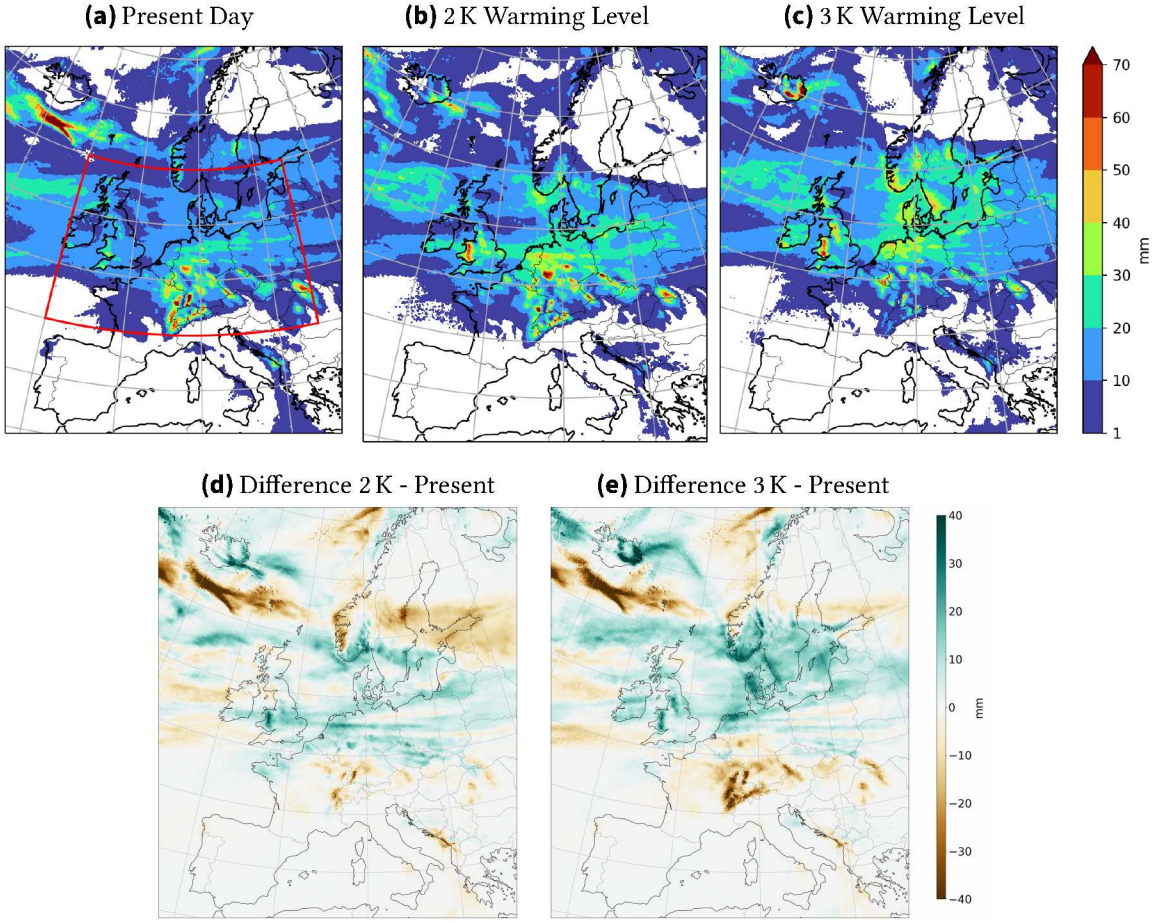

Figure 6.4.: Total Precipitation of windstorm Kyrill from 18.01 00 UTC to 19.01 12 UTC for the storyline simulations, a) Total precipitation in the present climate simulation, the red box shows the area considered for Table 6.2, b) and c) analogue to a) but for 2 and 3 K warming level, d) Difference of total precipitation in 2 K warming level vs present day simulation $\text{prec}_{2\,\text{K}} - \text{prec}_{\text{present}}$, e) analogue to d) for 3 K warming level

cells along the cold front, are clearly visible for all three simulations. Their positions are shifted for the 2 and 3 K warming level runs, matching the described northward shift. The intensity of the gusts at the cold front seems to be similar in the present and the 3 K warming level and slightly reduced in the 2 K warming level simulation. The convective cells are even better visible in the precipitation distribution. In Figure 6.7 the precipitation on 19th of January at 02:30 UTC is depicted. The strong convective precipitation is clearly visible for all three storms. The comma shape of the cold front associated with the convective cells can be clearly recognized. A difference in cold front precipitation is evident. There are higher amounts of precipitation and a larger area covered by the cold front precipitation for higher warming levels, substantiating the insights of tabular 6.2.

To summarize, in case of windstorm Kyrill, the intensity, in terms of MSLP, increases for higher warming levels, with considerably lower core pressure in the 3 K warming level run. Additionally, increased total precipitation and precipitation along the cold front were

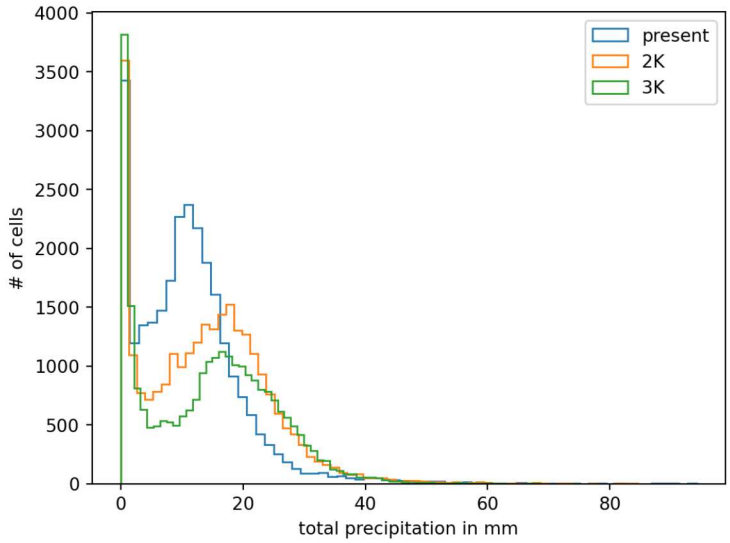

Figure 6.5.: Histogram showing the total precipitation during windstorm Kyrill from 18.01 00 UTC to 19.01 12 UTC, counting all grid cells in the red box in Fig. 6.4a)

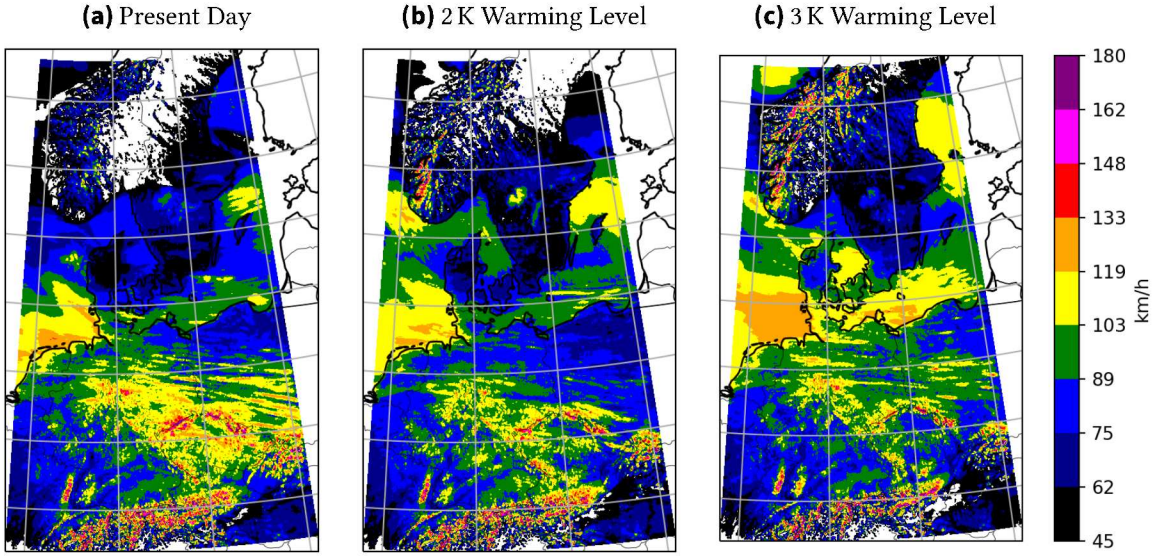

Figure 6.6.: Kyrill maximum 10 m gust speed between 18.01 12 and 19.01 12 UTC in the nested storyline simulations with a resolution of 3 km, a) present storyline simulation, b) 2 K and c) 3 K warming level

found. The distributions of the future simulations are broader, indicating stronger local variability and are shifted towards higher values. The largest increase in precipitation is found between the present and the 2 K warming level. In contrast, for the 10 m gust speed, the difference between the 2 K warming level and the present simulation is small, while there is a strong increase towards the 3 K warming level simulation. The tail of the 3 K

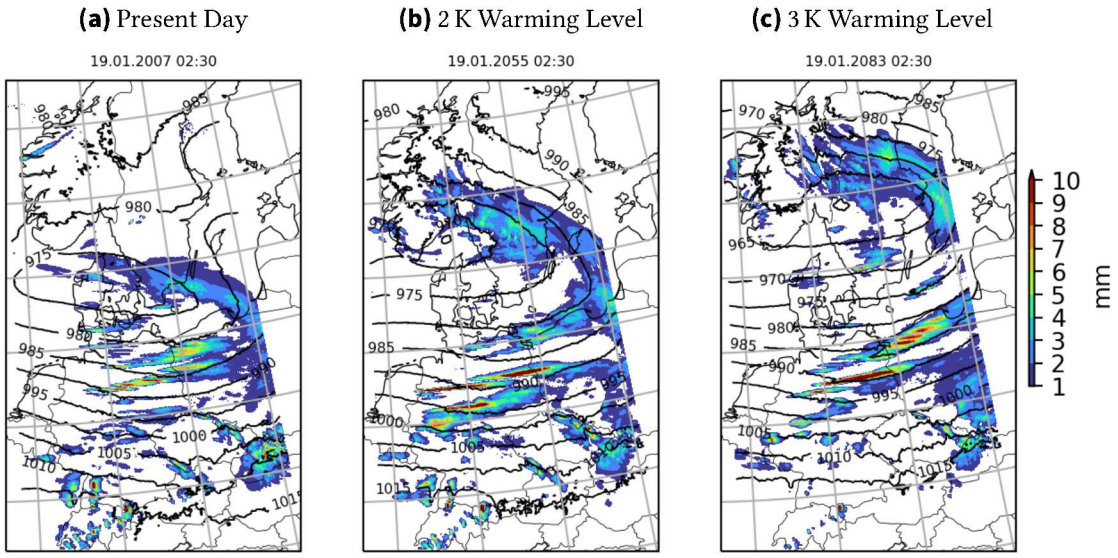

Figure 6.7.: Kyrill cold front precipitation at 19.01 2:30 UTC in storyline simulations with 3 km resolution, black lines show MSLP in hPa, a) present storyline simulation, b) 2 K and c) 3 K warming level

warming level 10 m gust distribution is much longer and higher. Despite the shift of the distributions towards higher values, the global maximum value is decreasing towards the higher warming level for both maximum 10 m gust speed and total precipitation. Regarding the results for windstorm Kyrill, one needs to be aware of the northward shift that could have caused some of these changes due to differences in topography and land versus sea mass of the affected area.

6.2. Thomas

The storm track of windstorm Thomas is shown in Figure 6.8a). Evidently, the path is very similar for all simulations. The future storms travel slower than the simulated storm in the present climate, with the 3 K warming level storm having the slowest track. This can also be seen in Figure 6.8b), where the delay of the time of the lowest core pressure is visible. All three simulated storms have similar core pressures and nearly the same overall minimum core pressure with 982 hPa for the present day and 2 K warming level simulations and 981 hPa in the 3 K warming level simulation. Additionally, the storm in the 3 K warmer world has a steeper de- and increase of core pressure than the other two storms. The structure of the jet stream looks very similar (see Appendix A.4), with higher wind speeds in the present storyline simulation, which could be responsible for the slower travel speed in the future simulations.

In Figure 6.9a) the maximum gust speed of the present storyline simulation is depicted. The strongest gusts are located in the North Sea, west of Scotland and in Northern Ireland. Additionally, in central Europe the areas affected by the strongest gusts are the coast of

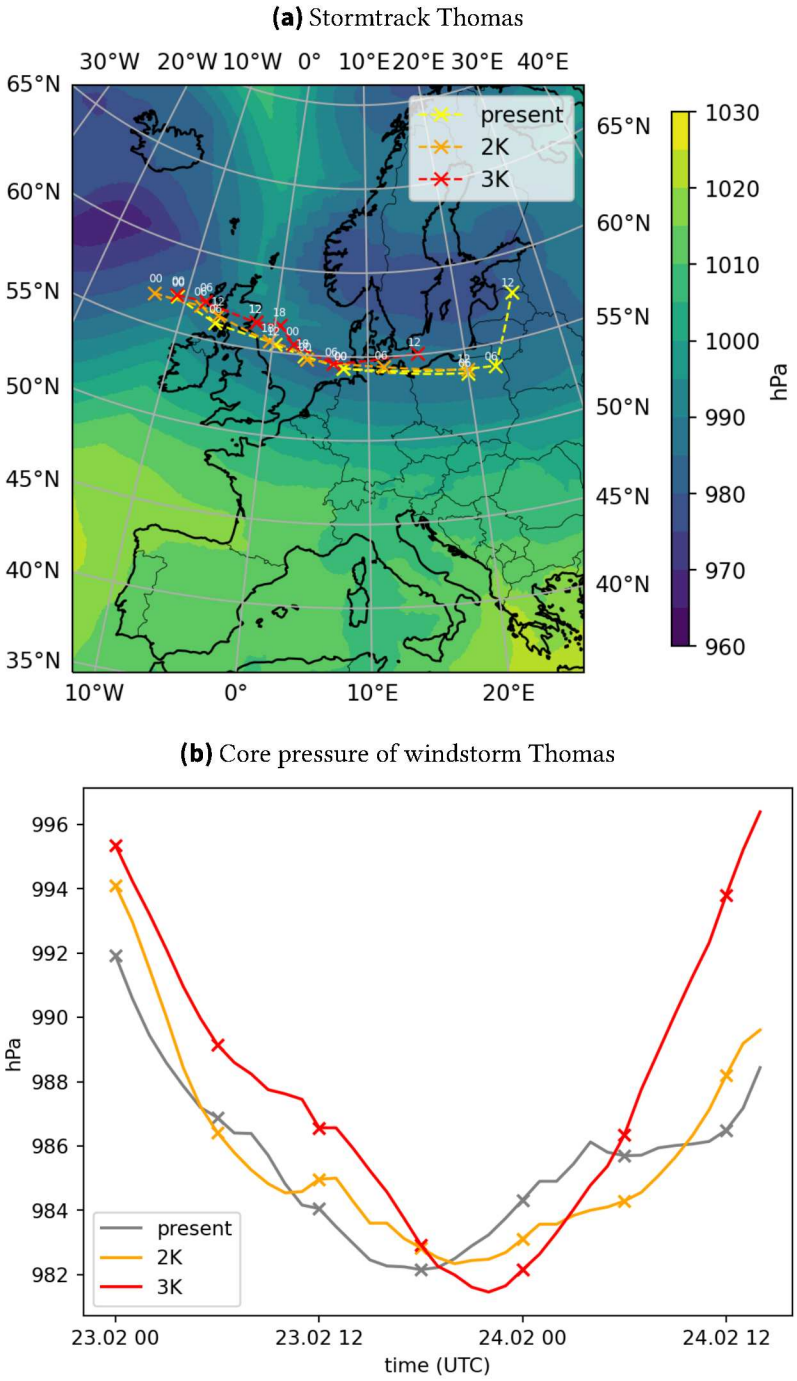

Figure 6.8.: Stormtrack and core pressure of Thomas in storyline simulations, a) crosses indicate 6 hourly position of the storm, first cross shows the storms location at 23.02 00 UTC, shaded colors show the minimum pressure of the present storyline simulation, b) minimum core pressure with time, crosses at the same timesteps as above

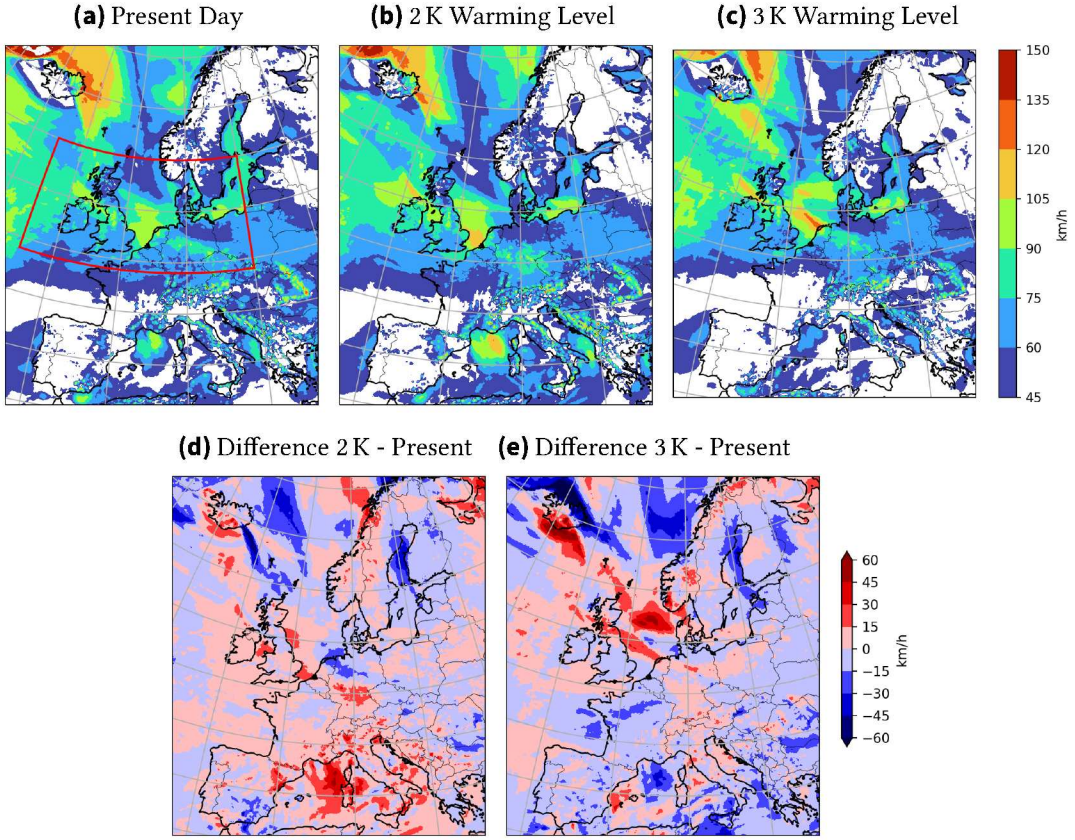

Figure 6.9.: Footprint of windstorm Thomas on 23. and 24.02 for the storyline simulations, a) Maximum 10 m gust speed in present simulation, with the red box indicating the area considered in Table 6.3, b), c) analogue to a) but for the 2 K and 3 K warming level d) Difference of maximum 10 m gust speed v_{max} reached in the 2 K warming level vs the present storyline simulation $v_{max,2\,K} - v_{max,present}$, e) analogue to d) for 3 K warming level

Belgium, the Netherlands and a band through mid Germany. Parts d) and e) of Figure 6.9 show the difference between the gust speed in the present simulation and that one in the future simulations respectively. In the 2 K warming level simulation, there are stronger gusts at the British coast and in the English Channel. Furthermore, there is kind of a shift over Germany and the Netherlands, with some northern regions being affected by less strong gusts, while there is a region of increased gust over mid and southern Germany. Part c) shows an area of higher gust speed south of Norway. This could be associated with an increase of gust speed in the cold conveyor belt. A band of increased gust speed is visible along the storm track extending from Scotland to northern Germany. This indicates an increase in gust speed close to the cyclone center. It is worth noticing the different spatial patterns of the 10 m gust speed, considering that the location of the storm tracks does not change. It would be interesting to have a small ensemble of simulations to verify whether these changes are significant or a result of the high internal variability of windstorms. If they turn out to be a clear trend, this would indicate a change in the spatial distribution of wind for future windstorms.

Table 6.3.: Thomas analysis of 10 m gust speed, considering all grid cells and timesteps in the area of the red box depicted in Figure 6.9a on 23. and 24.02; rows from top to bottom: global maximum 10 m gust speed, temporal and spatial mean of 10 m gust speed, percentage of grid cells with 10 m gusts reaching storm and hurricane wind speed at any timestep

	present day	2 K warming level	3 K warming level
max. gust speed in m/s	32.0 (Wales)	32.0 (B coast)	35.3 (NL coast)
mean gust speed in m/s	11.9	12.1	12.7
gridcells with $\geq$ 20.8m/s	35%	36%	38%
# gridcells with $\geq$ 32.7m/s	0	0	69

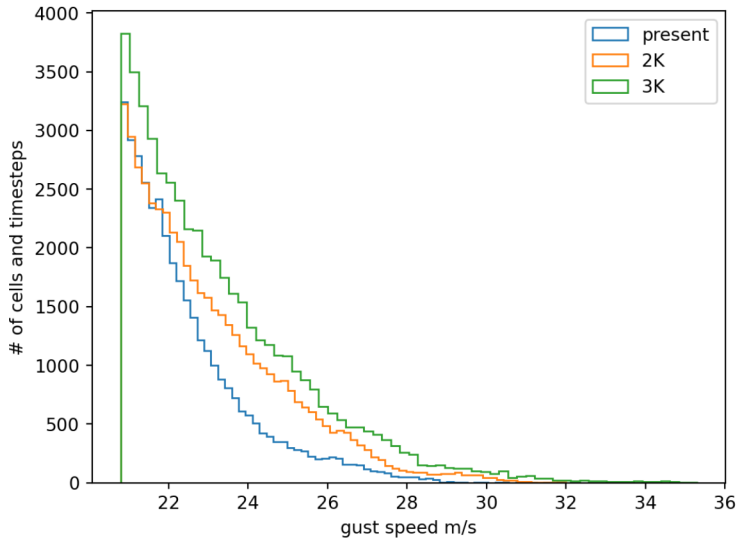

Figure 6.10.: Histogram of 10 m gusts exceeding storm windspeed during windstorm Thomas, all grid cells and timesteps in the red box in Fig.6.9a) on 23. and 24.02 are counted

Table 6.3 shows some values describing the gust speed on 23rd and 24th of February in the grid cells in the red box, shown in Figure 6.9a). The mean gust speed is calculated from all temporal and spatial data, while the other values are calculated from the maximum gust field. The gust maximum is reached in Wales for the present storyline simulation and at the coast of Belgium and the Netherlands for the 2 and 3 K warming levels. All values shown in Table 6.3 are very similar in the present and the 2 K warming level simulations, while for the 3 K warming level all of these properties are increased. The histogram in figure 6.10 shows more grid points and timesteps with storm wind speed for the future simulations. Especially the tail of the distributions is considerably longer in a 2 and even more in a 3 K warmer world. Hence, there are many more temporal and spatial points with severe gusts. Although it seems that in table 6.3 the gust speed in the present and 2 K warming level is very similar, the histogram shows that there are much more high gusts, looking at all grid cells and time steps. This indicates that individual grid cells are affected by high wind

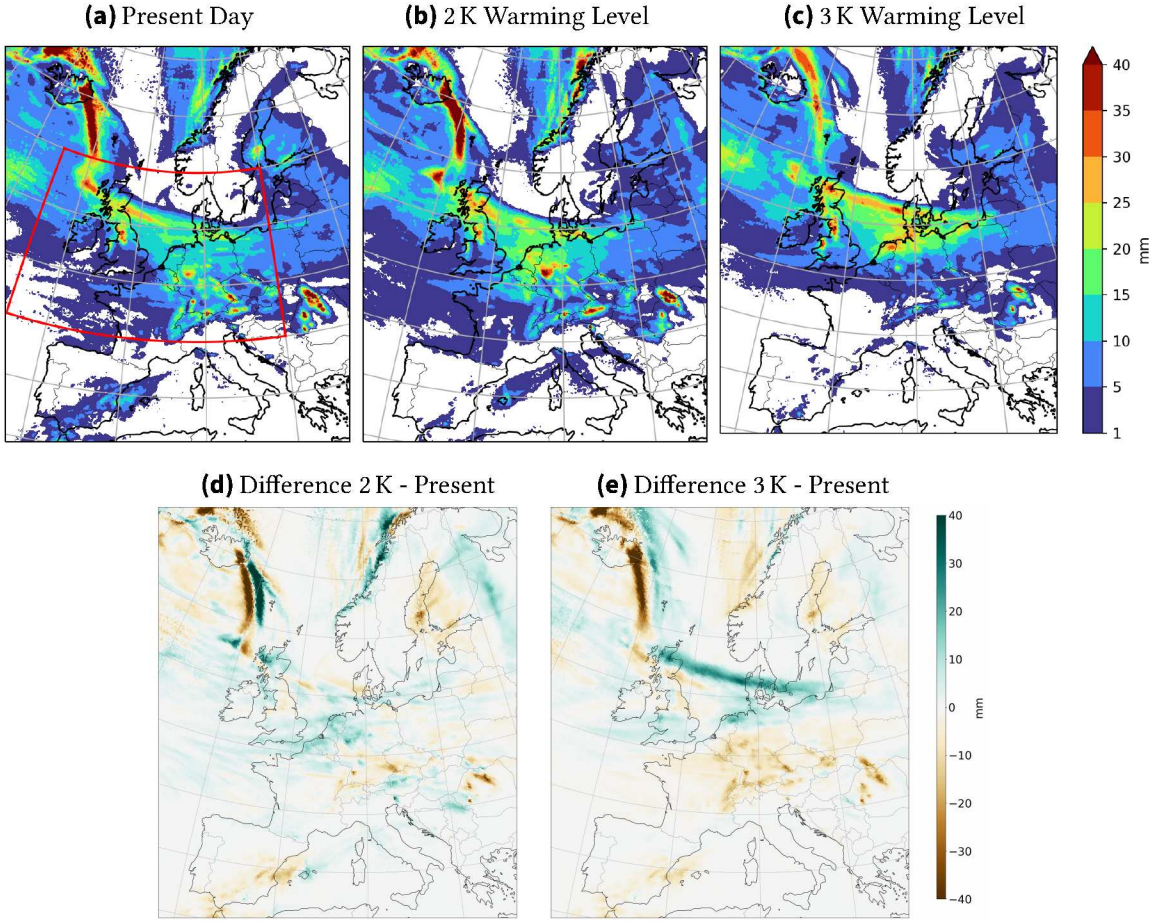

Figure 6.11.: Total Precipitation of windstorm Thomas from 23.02 00 UTC to 24.02 12 UTC for the storyline simulations, a) Total precipitation in the present climate simulation, the red box shows the area considered for Table 6.4, b) and c) analogue to a) but for 2 and 3 K warming level, d) Difference of total precipitation in 2 K warming level vs present day simulation $\text{prec}_{2\,\text{K}} - \text{prec}_{\text{present}}$, e) analogue to d) for 3 K warming level

speeds for a longer time period. This could be explained by the slower movement of the future storms.

Another property of interest for windstorm Thomas is the precipitation. In Figure 6.11, the accumulated precipitation from 23rd 00 UTC to 24th of February 12 UTC is shown. For the present day storyline simulation, there is a band of high precipitation following the storm track from the Atlantic west of Scotland extending into the North Sea. Additionally, there are areas of high precipitation in northern England and Germany, especially in mountainous regions. The maximum amount of precipitation accumulated during the considered time was reached over the Erzgebirge. The maximum hourly precipitation is simulated north of the coast of Brittany with 6.3 mm (see Table 6.4). Looking at the 2 K warming level difference plot, there is slightly increased precipitation over southern England, the Benelux states and northern Germany and a decrease over southern Germany. In the difference plot, the precipitation is considerably decreased for the 3 K warming level, over southern

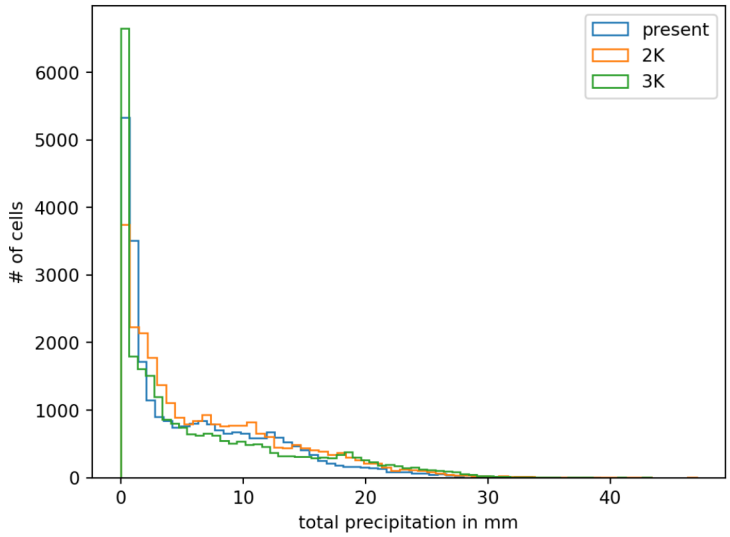

Figure 6.12.: Histogram showing the total precipitation during windstorm Thomas from 23.02 00 UTC to 24.02 12 UTC counting all grid cells in the red box in Fig.6.11a)

Table 6.4.: Precipitation analysis for windstorm Thomas, the considered values are all grid cells in the red box shown in Figure 6.11 and all timesteps between 23.02 00 UTC and 24.02 12 UTC, total precipitation (tot. prec.) refers to the precipitation summed up over all timesteps

	present day	2 K warming level	3 K warming level
max. hourly prec. (mm)	6.4 (Brittany)	10.7 (NW of Scotland)	10.8 (NW of Scotland)
max tot. prec. (mm)	45 (Erzgebirge)	47 (NRW)	43 (north England)
mean tot. prec. (mm)	4.0	5.1	3.7
cells with >20 mm tot. prec.	4.0%	5.7%	7.5%

Germany, Switzerland and France. This leads to the maximum accumulated amount of precipitation being the smallest in the 3 K warming level. Furthermore, a band of strongly increased precipitation, north of the storm track, is simulated for the 3 K warming level, which indicates increased precipitation of the cold conveyor belt. This goes along with an increased area with more than 20 mm of precipitation (7.5% of grid cells) and the highest maximum hourly precipitation of 10.8 mm. The mean total precipitation is smallest in the 3 K warming level and highest in the 2 K warming level. In the histogram in Figure 6.12 one can see that the reduced mean total precipitation for the 3 K warming level simulation is mostly due to many grid cells with little to no precipitation. Taking into account the longer and higher tail of the future distributions, together with the increased number of grid cells with nearly no precipitation, it is evident that the local variability in the 3 K warming level simulation is higher.

Altogether, in case of windstorm Thomas, the simulations show a more severe event in the future climate. Especially the gust speed in the 3 K warming level is strongly increased with higher spatial and temporal extent. The distributions for gust speeds exceeding storm wind

speed tend more towards high values for both simulated future storms. This is likewise the case for the precipitation distributions. Overall, the area affected by strong precipitation and the maximum hourly precipitation increase with increasing warming levels, while the maximum accumulated precipitation and mean total precipitation peak in the 2 K warming level simulation, with the lowest values for the 3 K warming level.

6.3. Christian

In figure 6.13 the surface level isobars are shown at three different timesteps for all three storyline simulations. At 27th of October at 18 UTC the storm is located west of France in all three simulations, with under 1000 hPa for the present and 3 K warming level simulation and under 1005 hPa for the 2 K warming level run. For both future storms the low pressure system is located slightly more south compared to the present storyline simulation. In the second timestep 12 hours later, all three storms are located in southern England with around 980 hPa, 995 hPa and 990 hPa for the present, 2 and 3 K warming level simulation respectively. On 28th of Octobre at 18 UTC the storm in the present climate simulation has deepened considerably to less than 970 hPa. It is now located over Denmark. The storm in the 3 K warming level is similarly located over Denmark, but has only deepened to less than 980 hPa. Meanwhile in the 2 K warming level simulation, there is still no closed isobar curve. It is only a kink visible in the 990 hPa isobar. Even six hours later, when the other two simulated storms have further deepened (see Appendix A.5), there is only a kink visible in the 2 K warming level simulation. Evidently, the storm in the 2 K warming level simulation never really develops, while the one in the 3 K warming level simulation develops, but is much weaker than in the present simulation. To find the reason for this behavior, one can look at the jet stream differences, which are most likely partially responsible for the absence of the storm in the 2 K warmer climate. In Figure 6.14 the 300 hPa windspeed at 28.10 12 and 18 UTC is shown for all three storyline simulations. As already mentioned in section 5.3.1, there is a split jet structure visible close to the storm at both timesteps in the present simulation. At 18 UTC the storm is located directly in the bow of the two parts of the jet stream. This structure can be found similarly, but weaker, in 6.14c) for the 3 K warming level simulation. The split jet structure is present, but at 18 UTC the northern part of the jet stream is located further east, such that the storm is not located directly in the bend. For the 2 K warming level simulation, there is no split jet structure visible at all. It is not meaningful to use windstorm Christian for the analysis of changes in European windstorms with climate change. Most of the changes might be attributed to the different large scale structure and the corresponding lack of further storm development in the 2 K warming level.

The reduced development of the future storms is also noticeable in the footprints of the simulated storms. For both future storms the 10 m maximum gust speed is considerably reduced throughout the entire storm track (see Figure 6.15).

Interestingly, a different pattern is observed for the precipitation. In the present storyline simulation there is heavy precipitation over the Atlantic west of France, along the west

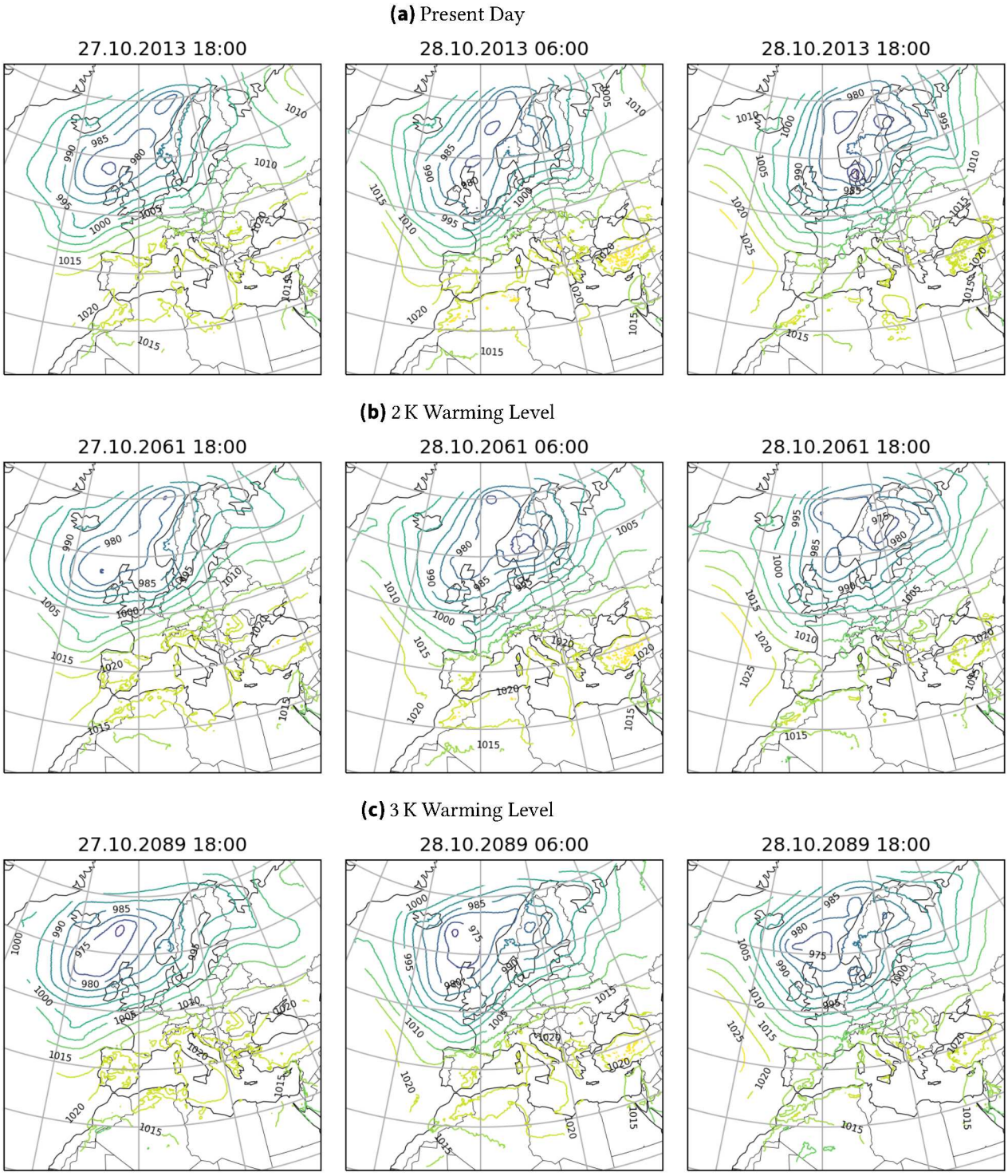

Figure 6.13.: MSLP in storyline simulations for windstorm Christian at 27.10 18 and 28.10 06 and 18 UTC, pressure in hPa, a) present storyline simulation, b) 2 K and c) 3 K warming level simulation

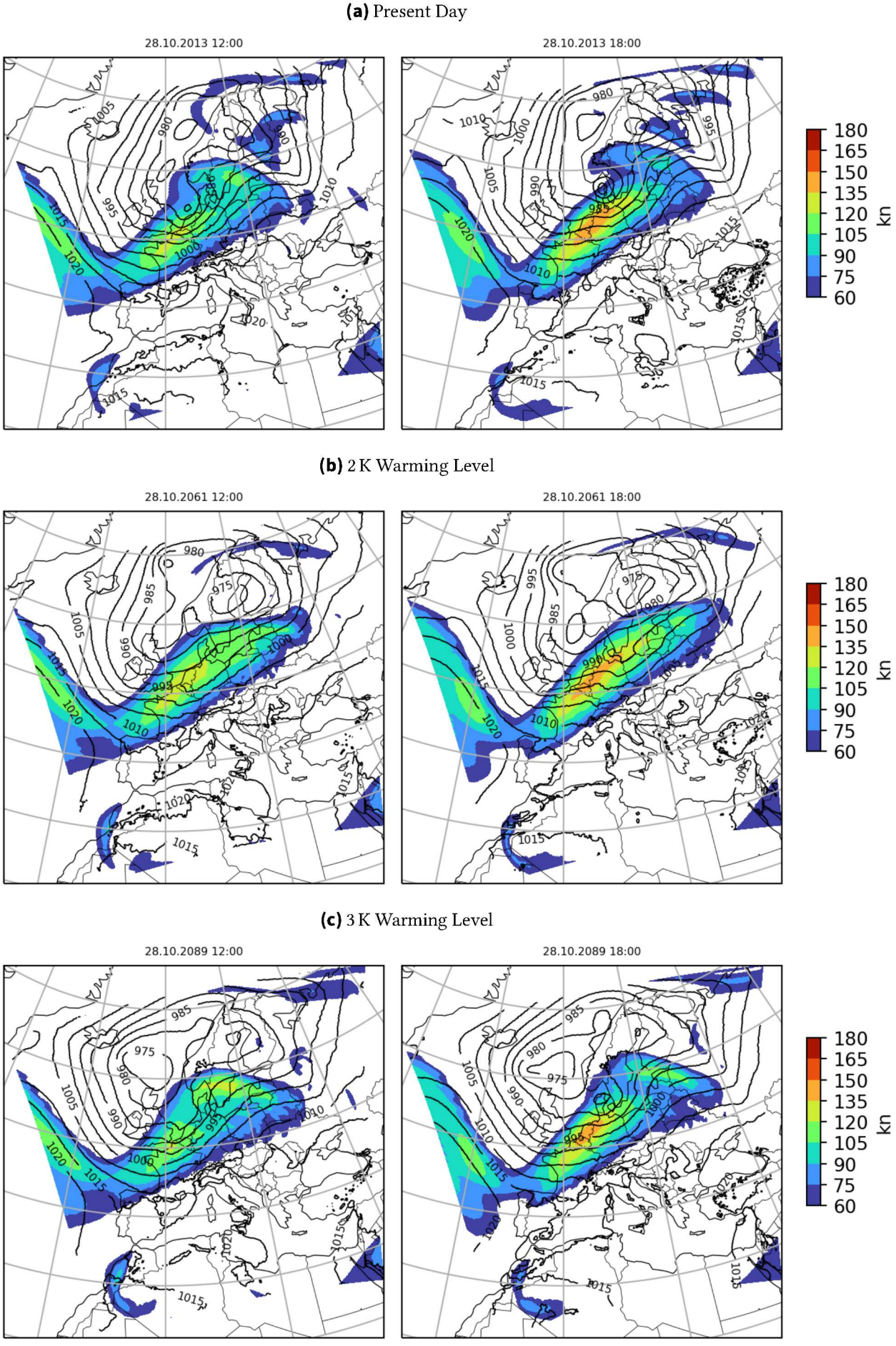

Figure 6.14.: Jet stream during windstorm Christian in storyline simulations at 28.10 12 and 18 UTC, color shaded areas show the windspeed in 300 hPa height, black lines show the isobars in hPa, a) present storyline simulation, b) 2 K and c) 3 K warming level simulation

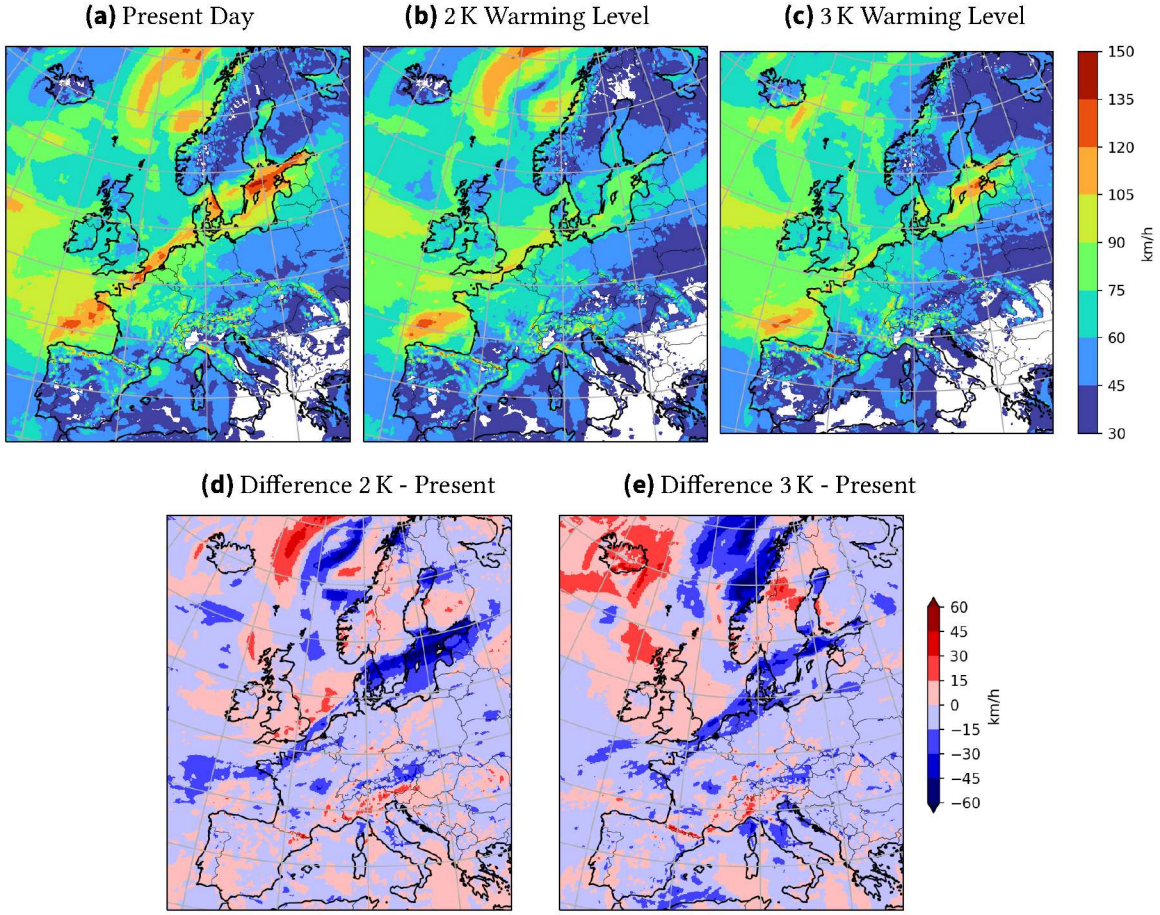

Figure 6.15.: Footprint of windstorm Christian on 27 12 UTC - 29.10 00 UTC for the storyline simulations, a) Maximum 10 m gust speed in present simulation, b), c) analogue to a) but for the 2 K and 3 K warming level d) Difference of maximum 10 m gust speed v_{max} reached in the 2 K warming level vs the present storyline simulation $v_{max,2\,K} - v_{max,present}$, e) analogue to d) for 3 K warming level

coast of Spain, at the Channel, in the North Sea, on the eastern border of France and in southern Germany (see Figure 6.16). In both future simulations strong precipitation is visible in the Channel and northern France. Figure 6.16d) and e) show the difference in total precipitation between the future and present storyline simulations. There is a southward shift of precipitation along two distinct bands for both future storms. One of them is located over the Atlantic and a second one over Spain and France. Matching this pattern, the maximum hourly precipitation and the maximum total precipitation are both located at the east coast of Spain for the present storyline simulation, while they are located at the Normandy and in eastern France for the future simulations (see Tabular 6.5). This southward shift is related to the small southward shift in the storm track. The highest maximum total precipitation is reached in the 2 K, followed by the present and then the 3 K warming level simulation. The other three properties, shown in Table 6.5, are highest for the present storyline simulation, but the differences are not very strong. It is remarkable that the amount of precipitation is quite comparable for all three simulations, considering

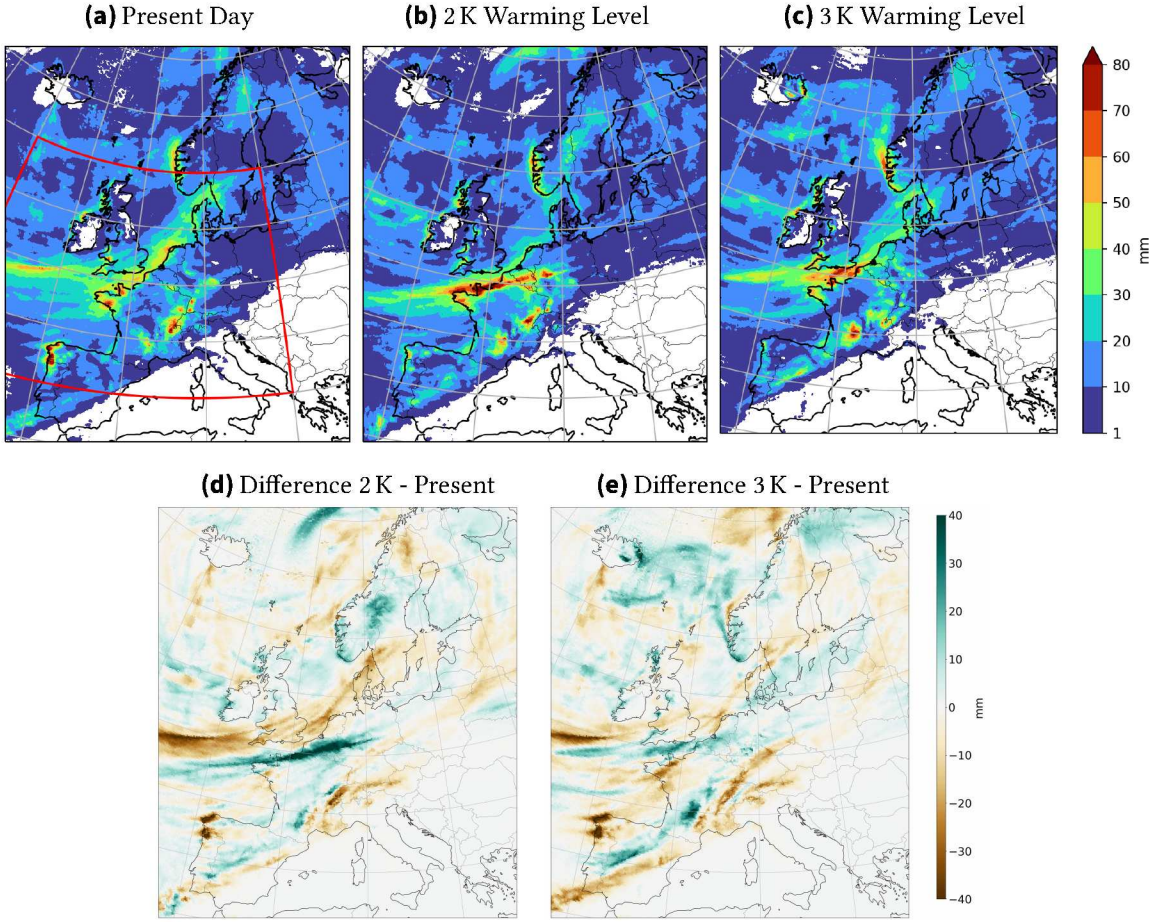

Figure 6.16.: Total Precipitation of windstorm Christian from 27 12 UTC to 29.10 00 UTC for the storyline simulations, a) Total precipitation in the present climate simulation, the red box shows the area considered for Table 6.5, b) and c) analogue to a) but for 2 and 3 K warming level, d) Difference of total precipitation in 2 K warming level vs present day simulation $\text{prec}_{2\,\text{K}} - \text{prec}_{\text{present}}$, e) analogue to d) for 3 K warming level

Table 6.5.: Precipitation analysis for windstorm Christian, the considered values are all grid cells in the red box shown in Figure 6.16 and all timesteps between 27.10 12 UTC to 29.10 00 UTC, total precipitation (tot. prec.) refers to precipitation amount summed up over all timesteps

	present day	2 K warming level	3 K warming level
max. hourly prec. (mm)	25.4 (Spain eastcoast)	15.3 (Normandy)	20.4 (east France)
max tot. prec. (mm)	92 (Spain eastcoast)	100 (Normandy)	87 (Normandy)
mean tot. prec. (mm)	12.8	12.0	11.8
cells with >20 mm tot. prec.	21.7%	18.2%	20.0%

that the future storms, especially the one simulated at the 2 K warming level, are much weaker.

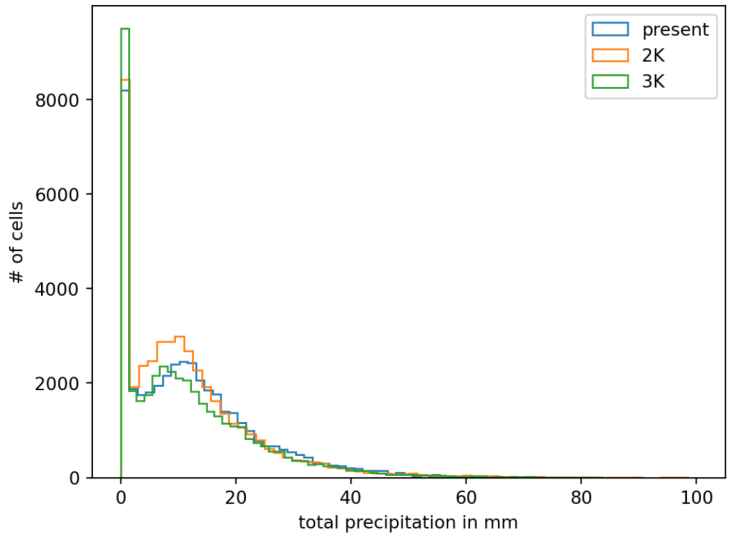

Figure 6.17.: Histogram showing the total precipitation during windstorm Christian from 27.10 12 UTC and 29.10 00 UTC in the grid cells in the red box in Fig. 6.16a)

Overall, windstorm Christian is poorly represented in the future storyline simulations, especially in the 2 K warming level, where it is nearly not visible. This is partially caused by the different structure of the jet stream, namely the missing split jet structure. Therefore, the gust speed is considerably reduced along the whole storm track for both future simulations. Despite this, the amount and extent of precipitation are quite similar for all three storyline simulations with a slight southward shift for both future simulations.

7. Discussion and Conclusion

In this chapter, the main findings of the thesis will be discussed by summarizing the results of the two chapters on European windstorms in the present and future climate.

7.1. European windstorms in the present climate

This section summarizes the findings of Chapter 5, which aims to answer the question, whether European windstorms can be reproduced with the nudged storyline approach. By conducting the ERA5 simulations, it is ensured that ICON is able to simulate the windstorms close to the real, observed events. This is the case for all three considered storms: The sea level pressure maps, as well as the development of the large scale structures show only small deviations from the observations. Additionally, the footprint of the storms was considered, because it is the main indication of the damage from a windstorm. For windstorm Kyrill and Thomas, the simulated footprint of the ERA5 simulations matches the observed one quite well. In case of windstorm Kyrill the higher resolution simulations could even reproduce the high gust speeds associated with the convective cells at the cold front. Only for windstorm Christian the footprints differ considerably. Especially the highest gust speeds in the North Sea, northern Germany and Denmark could not be well reproduced. This is most likely due to the model's inability to reproduce the sting jet, which caused these high gust speeds.

Unlike the ERA5 simulations, the present storyline simulations exhibit differences from the observations in several aspects. For windstorm Kyrill, its passage is delayed by nine to twelve hours. In the case of Thomas, the core pressure is higher compared to the observations and Christian undergoes an extended deepening phase after the observed storm has already started to weaken. These differences are directly connected to variations in the large scale structures. For windstorm Thomas and Christian, it can be shown that the dry intrusion is weaker in the storyline simulations compared to ERA5. Additionally, there are differences in the jet stream structure, especially in split jet structures, that can be associated with these changes. Nevertheless, all three considered storms move along the same track, with MSLP comparable to that of the historic storms.

Looking at the footprint, the present storyline simulation of windstorm Kyrill reproduces the observations very well. In the simulation with 3 km resolution even the high gust speeds along the convective cells at the cold front could be simulated, although the very high gust speeds in the flat areas of North-Rhine-Westphalia are better represented in the ERA5 simulations. For Thomas and Christian, there are stronger differences. In both cases, the areas of the strongest gust speeds could not be reproduced, as it was already the case for

Christian in the ERA5 simulations due to the sting jet. It is unclear whether the severe gust speeds over the UK during windstorm Thomas were caused by a sting jet as well.

In a 12 km resolution simulation, small scale events like sting jets and convective processes can only be calculated via parametrization, which leads to them being either poorly represented or not represented at all. Hence, such processes cannot be considered in the comparison of the storylines and their future changes cannot be assessed in a 12 km resolution storyline simulation. This is especially problematic for sting jets, as they are known for often causing the highest wind gusts and, according to Catto et al. (2019), their frequency might increase with climate change. Therefore, it could be interesting for future studies to further investigate high resolution simulations. Here, high resolution simulations were only conducted for windstorm Kyrill. In this case, the higher resolutions led to an improvement in the representation of smaller scale features, like the convective cells.

Overall, despite the differences, the storyline simulations were considered realistic because they follow a similar track with core pressures similar to the observed events, such that a comparison to the historic events is meaningful. Nevertheless, it is important to keep the differences from the historic events in mind when comparing the present and future storyline simulations. This is especially important as being accessible to the public, by referring to events that people have experienced, is one of the key advantages of the nudged storyline approach. A result like enhanced gust speed over the UK during windstorm Thomas could, when remembering the real event, easily be misinterpreted as enhanced gust speed compared to the real event with gusts exceeding 150 km/h, while actually it refers to enhanced gust speed over the UK compared to the present storyline simulation, which only shows gust speeds of 80-100 km/h over the UK.

As the ERA5 simulations are very similar to the observations, the problem lies in the nudging of the AWI climate model, not in the ICON-CLM downscaling simulations. As described in chapter 4, the method of conducting the storyline simulations followed the method used by Klimiuk et al. (2025). This paper analyzes heatwaves, for which the nudging strength is considered to be optimal. Unlike European windstorms, the blocking associated with heatwaves is a very stable large scale process. European windstorms, which are shorter-lived and smaller scale events, can be considerably changed by small variations in the large scale structures. Therefore, the described problem could be reduced by implementing stronger nudging in the AWI climate model, to ensure that there are only minor differences in the large scale structures. But even with stronger nudging, differences like the absence of high gusts from a sting jet would still require caution, when comparing the results of the nudged storyline approach to the real event.

Additionally, the three storms considered are the ones for which the present storyline simulations turned out to be the most comparable to the observations among many tested storms. Other well known storms, such as Xynthia (2010), Klaus (2009), Daria (1990) or Anatol (1999), showed strong deviations from the observed storm tracks or were not represented at all in the AWI simulations. Therefore, stronger nudging would also lead to a broader selection of storms. This would allow for the assessment of storms with different characteristics; for example, by making use of the categories brought together by Catto (2016). Additionally, more storms that are better known to the public would be available.

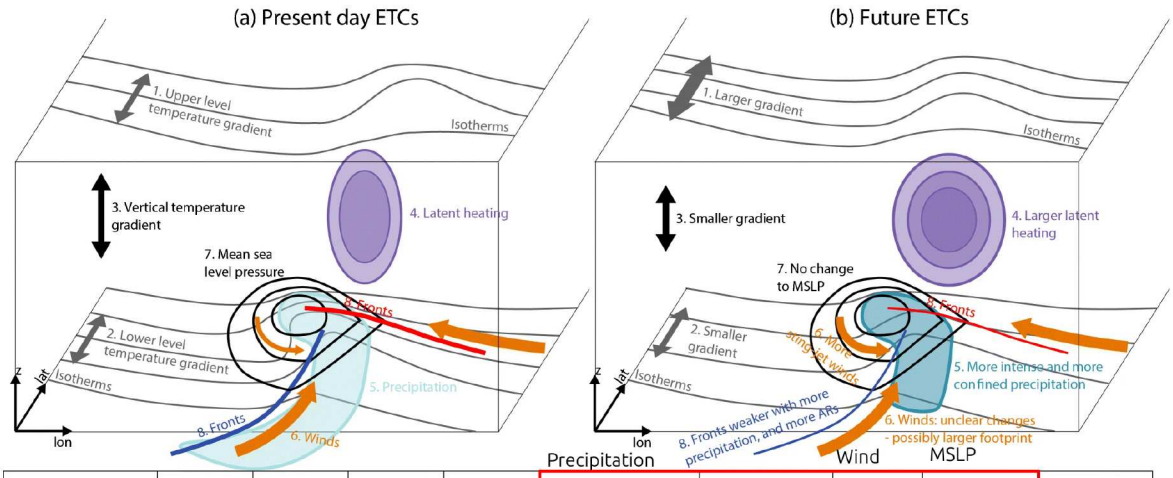

Feature	1	2	3	4	5 (intensity)	5 (extent)	6	7	8
Confidence	High	High	High	High	High	Low	Low	Medium	Low

Figure 7.1.: Schematic diagram summarizing the future changes of ETCs found by Catto et al. (2019) in their review paper, focusing on the changes of eight key features, the confidence of the changes found is indicated in the table, the red box shows the features assessed in this thesis (adapted from Catto et al., 2019)

7.2. European windstorms in the future climate

Part two of the second research question is, how the analyzed storms change in the future climate. This is assessed in chapter 6 by comparing the three storyline simulations at the different warming levels for each storm. In the following, these results are brought together to identify common trends and differences and are compared to the findings of Catto et al. (2019) shown in Figure 7.1. Windstorm Christian is an example for which the method of nudged storyline simulations reaches its limitations. Consequently, it will not be directly included in the comparison of changes in the key features.

7.2.1. Stormtrack and core pressure

The best representation of the future storms in terms of their tracks is found for Thomas, with very similar tracks for all three simulations, although the passage of the future storms is delayed. Kyrill shows a northward shift for both future storms. This makes the comparison harder, as the covered area is different for each warming level, with different topographic features that influence the key properties analyzed, such as gust speed and precipitation. The goal of storyline simulations is to reproduce historic events in a different climate state. For Thomas and Kyrill, both future storms are represented with similar movement speed and pressure sequences and are considered to fulfill this definition. Hence, they can provide meaningful insights into future changes. This is different in case of windstorm Christian, for which, in the 2 K warming level simulation, no storm evolves and the storm in the 3 K warming level is much weaker, with considerably higher core pressure. Hence, the

representation of Christian in the future storyline simulations cannot provide meaningful results regarding future changes. This could have been prevented by applying stronger nudging to the AWI climate model. It could be shown that one factor leading to the misrepresentation of both future storms of windstorm Christian is the difference in the jetstream, especially the split jet structure. Stronger nudging of the large scale structures or nudging up to higher wavenumbers, to force the upper level structures down to smaller scales, would lead to a more similar jet structure, even for smaller features like split jet structures. This stronger nudging could also help to avoid the northward shift for windstorm Kyrill, leading to better comparability of the storyline simulations.

The core pressure values of windstorm Kyrill show a strong decrease. For Thomas a small decrease is found. So, based on the storms analyzed, the core pressure of windstorms decreases in a warmer climate indicating increased storm intensity. This points in a different direction than the findings of Catto et al. (2019), who found no change in MSLP with medium confidence.

7.2.2. Wind

In the difference plots (Figure 6.2, 6.9) it is difficult to see whether there is only a shift or additionally an increase or decrease in the footprint for the 2 K warming level. Similarly, in tables 6.3 and 6.1, only small increases for the 2 K warming level are found. In the histograms (Figure 6.3, 6.10) stronger changes can be found, as they additionally consider the timesteps and not only the maximum gust speed reached in each grid cell. This indicates that individual grid cells are affected by strong gust speeds for a longer time period in case of the future storms. Looking at the 3 K warming level, both Thomas and Kyrill show a distribution that is considerably shifted towards higher gust speeds, with a longer and higher tail. Matching this, there is a larger area affected by storm and hurricane wind speeds and higher mean gusts. In the 3 K warming level simulation of windstorm Thomas, an enhanced increase in gust speed close to the cyclone center is found, as well as an increase north of the center in the area of the cold conveyor belt. Remarkably, the overall increase in gusts from the 2 to the 3 K warming level does not go linearly, but rather with a disproportionately higher increase towards the higher warming level for both storms, especially considering the number of grid cells affected by hurricane wind speed. This, in general, does not match the findings of studies doing CMIP5 simulations that generally simulate a reduction in ETC winds (Catto et al., 2019). Catto et al. (2019) additionally state with low confidence that the wind footprint might be larger for future ETCs, which can be seen in the analysis presented here, especially for the 3 K warming level. According to Li et al. (2014) increasing maximum wind speed is expected over the North Sea and the British Isles, which is supported by the changes seen in the 3 K warming level simulations of both storms. Looking at the lifetime gust speed peak, the storyline simulations of Thomas show an increase for the 3 K warming level, while there is a decrease towards higher warming levels in the simulations of windstorm Kyrill. This shows that statements on the changes in gust speed, solely based on the lifetime peak, provide limited information, as they consider

only one value and for example for the 3 K simulation of Kyrill it would indicate a reduction in gust speed, which is definitely not the case.

Both storms show an increase in gust speed in terms of extent and intensity, as well as an increase in duration for the future climate, with a clearer trend for the 3 K warming level. In their review paper Catto et al. (2019) concluded that "wind strength projections are uncertain". The clear trends observed in this thesis show the potential of the method. By applying it to further storms and using ensembles, it could provide new insights into the still very uncertain future change of winds in ETCs.

The future storyline simulations of windstorm Christian show a strong decrease in severe gusts, matching the considerably reduced storm intensity.

7.2.3. Precipitation

To analyze the precipitation during European windstorms Catto et al. (2019) distinguish intensity and extent, finding increased intensity and decreased extent. For windstorm Kyrill in both warming levels and for windstorm Thomas in the 2 K warming level an increase in precipitation intensity was found, with higher mean precipitation and higher maximum hourly precipitation (see Table 6.2, 6.4). For the 3 K warming level of windstorm Thomas it is not clear whether there is an increased or decreased intensity, based on the values in table 6.4. The main change is a higher local variability, with more grid cells showing nearly no precipitation and simultaneously more grid cells with very high amounts of precipitation. This increase in local variability can also be found for Kyrill. Similarly to the gust speed, the precipitation distributions of the future simulations have a higher tail (see Figures 6.5, 6.12). This matches the strong increase in grid cells with an accumulated amount of precipitation of more than 20 mm. Additionally, for all four future simulations, the maximum hourly precipitation is strongly increased. In case of Kyrill it could be shown that this is due to stronger precipitation of the convective cells at the cold front. For the 3 K warming level of windstorm Thomas, the strongest increase is north of the storm track in the cold conveyor belt area, with a small decrease in the precipitation associated with the cold front. Interestingly, the maximum total precipitation decreases for the 3 K warming level for both storms.

As visible in Table 7.1 there is a clear trend in the future storyline simulations towards an increase in precipitation intensity and extent. The first one matches the findings of Catto et al. (2019), who found increased precipitation intensity with high confidence. Furthermore, the review stated with low confidence that the area affected by precipitation will be more confined. This could not be supported by the storms analyzed in this case study.

Despite their considerably reduced intensity, the future simulations of windstorm Christian show amounts of precipitation very similar to the present storyline simulation.

Table 7.1.: Summary table of the changes with warming found for the analyzed storms compared to the findings of Catto et al. (2019); the top row shows the findings of Catto et al. (2019) for changes in future ETCs in general, with the confidence indicated in brackets, the further rows show the changes found for the respective future storyline simulation when compared to the according present storyline simulation, symbols: ↗ increase, ↘ decrease, - no change, ? unknown change

	5 prec (intensity)	5 prec (extent)	6 wind	7 MSLP
Catto et al. (2019) (Confidence)	↗ (High)	↘ (Low)	? (Low)	- (Medium)
Kyrill (2 K)	↗	↗	↗	↘
Kyrill (3 K)	↗	↗	↗	↘
Thomas (2 K)	↗	↗	↗	-
Thomas (3 K)	–	↗	↗	↘

7.2.4. Summary

A summary of the changes in the properties considered can be found in the table 7.1. In this table the arrows indicate the direction of change for each feature when comparing the respective future with the according present storyline simulation. It can be seen that there are clear trends even for properties for which Catto et al. (2019) have only low confidence. Naturally, the analysis here is is based on three case studies, but this indicates that one might be able to find statements with higher confidence using the method applied here.

The changes found in this case study show different trends than Catto et al. (2019) found, except for the increase in precipitation intensity that was stated with high confidence in the review paper. Hence, it would be interesting to further look into these properties, using the nudged storyline approach to see if studies considering more storyline simulations yield the same results.

As suggested by Catto et al. (2019) for the precipitation and 10 m gust speed, not only the mean or maximum values but the whole distribution was considered in this work. It was found that for Kyrill and Thomas the distributions of the future simulations are shifted towards higher values compared to the present simulations. Especially for the 3 K warming level, the 10 m gust speed distribution has a much longer and higher tail. Additionally, the precipitation distributions show increased local variability with more values with very weak and very strong precipitation for both 3 K warming level simulations. Therefore, the arrows in table 7.1 are a strong simplification of the overall changes and can only give an overview.

The analysis in this thesis focuses on a small sample of three selected case studies. It should be kept in mind that some of the changes might result from the high sensitivity of windstorms to small variations in the large scale circulation. Consequently, it is recommended to make use of small ensembles as a further step. As the simulation of European windstorms is a numerical weather prediction problem, small variations in the large scale dynamics lead to strong differences in storm development. Therefore, ensembles are necessary to ensure that the changes are a product of clear trends.

7.3. Method

The main question of this work was to assess the feasibility of the method of nudged storylines for the analysis of future characteristics and their changes in European windstorms. This approach was already used for the investigation of heatwaves, which are large scale events and therefore less sensitive to small changes (Klimiuk et al., 2025, Sánchez-Benítez et al., 2022). As shown in chapter 5, the present AWI storyline simulations are able to reproduce the storms for the three considered cases. For windstorm Kyrill and Thomas in the 2 and 3 K warming level storyline simulations, events similar to the present ones were obtained. The comparison to the present storyline simulations showed clear trends shared by both storms. This indicates that this approach has a huge potential to further assess the changes in variables for which Catto et al. (2019) could only make statements with low confidence. It might therefore help to close the gap between idealized simulations and the statistical approach of global climate model ensembles that Catto et al. (2019) found. To obtain reliable results, a further step would be to conduct small ensembles of nudged storyline simulations for certain events.

With windstorm Christian, we presented an example, where the method reaches its limitations. The storm could not be simulated properly in the future climate storyline simulations due to too strong deviations in the large scale structures. It is therefore proposed that further studies should use stronger nudging to have more storms available. By doing this, other well known or particularly damaging storms could be assessed. Additionally, it would be interesting to assess more different storms to obtain insights into the different changes of storms in the categories identified by Catto (2016). Furthermore, simulations with higher resolutions have the potential to better represent small scale features, like sting jets or convective cells, as it was shown exemplarily for windstorm Kyrill. Therefore, it is suggested to perform more high resolution simulations to look more closely into these processes.

While these are quite interesting pathways for future research, it is still necessary to approach the problem from the perspective of traditional climate modeling. The demonstrated approach is unable to provide any statements on the likelihood of the appearance of the simulated storms. There are several indications of frequency changes for ETCs (Catto et al., 2019). Additionally, Michaelis et al. (2017) performed high resolution pseudo global warming simulations for the North Atlantic stormtrack and found "a lack of correspondence between the strongest events in the current and future simulations, indicating the future simulations produced a different population of storms". This change in frequency or population would not be seen in the storyline simulations and cannot be assessed with this approach. So, this limitation has to be kept in mind and it has to be ensured that there is no mismatch between the storms analyzed with storyline simulations and the storms expected to occur in a future climate. Thus, a combination with other methods, e.g. using analogues for CMIP6 ensemble simulations, as done for the 2018 heatwave by León-FonFay et al. (2025), could be an interesting perspective to address this caveat.

Bibliography

Brasseur, G., Jacob, D., & Schuck-Zöller, S. (Eds.). (2023). *Klimawandel in Deutschland: Entwicklung, Folgen, Risiken und Perspektiven* (2., überarbeitete und erweiterte Auflage). Springer Spektrum. https://doi.org/https://doi.org/10.1007/978-3-662-66696-8

Brogli, R., Heim, C., Mensch, J., Sørland, S. L., & Schär, C. (2023). The pseudo-global-warming (PGW) approach: Methodology, software package PGW4ERA5 v1.1, validation, and sensitivity analyses. *Geoscientific Model Development*, *16*(3), 907–926. https://doi.org/10.5194/gmd-16-907-2023

Browning, K. A. (2004). The sting at the end of the tail: Damaging winds associated with extratropical cyclones. *Quarterly Journal of the Royal Meteorological Society*, *130*(597), 375–399. https://doi.org/10.1256/qj.02.143

C3S. (2018). ERA5 hourly data on single levels from 1940 to present. https://doi.org/10.24381/CDS.ADBB2D47

Catto, J. L. (2016). Extratropical cyclone classification and its use in climate studies. *Reviews of Geophysics*, *54*(2), 486–520. https://doi.org/10.1002/2016RG000519

Catto, J. L., Nicholls, N., Jakob, C., & Shelton, K. L. (2014). Atmospheric fronts in current and future climates. *Geophysical Research Letters*, *41*(21), 7642–7650. https://doi.org/10.1002/2014GL061943

Catto, J. L., Ackerley, D., Booth, J. F., Champion, A. J., Colle, B. A., Pfahl, S., Pinto, J. G., Quinting, J. F., & Seiler, C. (2019). The Future of Midlatitude Cyclones. *Current Climate Change Reports*, *5*(4), 407–420. https://doi.org/10.1007/s40641-019-00149-4

Center for Climate Systems Modeling (C2SM), ETH Zurich, MeteoSwiss, & Deutscher Wetterdienst (DWD). (2025). Zonda [last accessed: 30. January 2026]. https://zonda.ethz.ch/

Chen, T.-C., Braun, C., Voigt, A., & Pinto, J. G. (2024). Changes of Intense Extratropical Cyclone Deepening Mechanisms in a Warmer Climate in Idealized Simulations. *Journal of Climate*, *37*(18), 4703–4722. https://doi.org/10.1175/JCLI-D-23-0605.1

Cusack, S. (2022, December). Decadal variations of European windstorms: Linking research to insurance applications. https://doi.org/10.5194/nhess-2022-268

Eady, E. T. (1949). Long Waves and Cyclone Waves. *Tellus*, *1*(3), 33–52. https://doi.org/10.1111/j.2153-3490.1949.tb01265.x

Eisenstein, L., Schulz, B., Qadir, G. A., Pinto, J. G., & Knippertz, P. (2022). Identification of high-wind features within extratropical cyclones using a probabilistic random forest – Part 1: Method and case studies. *Weather and Climate Dynamics*, *3*(4), 1157–1182. https://doi.org/10.5194/wcd-3-1157-2022

European Commission. Joint Research Centre. (2020). *Global warming and windstorm impacts in the EU: JRC PESETA IV project : Task 13.* Publications Office. Retrieved January 31, 2026, from https://data.europa.eu/doi/10.2760/039014

Fink, A. H., Brücher, T., Ermert, V., Krüger, A., & Pinto, J. G. (2009). The European storm Kyrill in January 2007: Synoptic evolution, meteorological impacts and some considerations with respect to climate change. *Natural Hazards and Earth System Sciences*, *9*(2), 405–423. https://doi.org/10.5194/nhess-9-405-2009

Fink, A. H., Pohle, S., Pinto, J. G., & Knippertz, P. (2012). Diagnosing the influence of diabatic processes on the explosive deepening of extratropical cyclones. *Geophysical Research Letters*, *39*(7), 2012GL051025. https://doi.org/10.1029/2012GL051025

Gardiner, B. (2013). *Living with storm damage to forests*. European Forestry Institute. https://efi.int/sites/default/files/files/publication-bank/2018/efi_wsctu3_2013.pdf

Geyer, B., Churiulin, E., Jähn, M., Brienen, S., Truhetz, H., Poll, S., & Rockel, B. (2025, February). SPICE (Starter Package for ICON-CLM Experiments). https://doi.org/10.5281/ZENODO.10047046

Giorgi, F. (2019). Thirty Years of Regional Climate Modeling: Where Are We and Where Are We Going next? *Journal of Geophysical Research: Atmospheres*, *124*(11), 5696–5723. https://doi.org/10.1029/2018JD030094

H. Lennon & L. Piper. (2025). Disruption to continue after Storm Eowyn causes 'unprecedented' damage to railway [last accessed: 30. January 2026]. https://news.stv.tv/scotland/disruption-to-continue-after-storm-eowyn-causes-unprecedented-damage-to-railway

Haesler, S., & Lefebvre, C. (2013). Orkantief Christian am 28. Oktober 2013 [last accessed 30. January 2026]. https://www.dwd.de/DE/presse/hintergrundberichte/2013/Orkantief_Christian_PDF.pdf?__blob=publicationFile&v=3

Harris, C. R., Millman, K. J., van der Walt, S. J., Gommers, R., Virtanen, P., Cournapeau, D., Wieser, E., Taylor, J., Berg, S., Smith, N. J., Kern, R., Picus, M., Hoyer, S., van Kerkwijk, M. H., Brett, M., Haldane, A., del Río, J. F., Wiebe, M., Peterson, P., … Oliphant, T. E. (2020). Array programming with NumPy. *Nature*, *585*(7825), 357–362. https://doi.org/10.1038/s41586-020-2649-2

Henry, A. J. (1922). J. BJERKNES AND H. SOLBERG ON THE LIFE CYCLE OF CYCLONES AND THE POLAR FRONT THEORY OF ATMOSPHERIC CIRCULATION[1]. *Monthly Weather Review*, *50*(9), 468–473. https://doi.org/10.1175/1520-0493(1922)50<468:JBAHSO>2.0.CO;2

Hewson, T. D., & Neu, U. (2015). Cyclones, windstorms and the IMILAST project. *Tellus A: Dynamic Meteorology and Oceanography*, *67*(1), 27128. https://doi.org/10.3402/tellusa.v67.27128

Hoskins, B. J., & Valdes, P. J. (1990). On the Existence of Storm-Tracks. *Journal of the Atmospheric Sciences*, *47*(15), 1854–1864. https://doi.org/10.1175/1520-0469(1990)047<1854:OTEOST>2.0.CO;2

Huang, Z., Zhong, L., Ma, Y., & Fu, Y. (2021). Development and evaluation of spectral nudging strategy for the simulation of summer precipitation over the Tibetan Plateau using WRF (v4.0). *Geoscientific Model Development*, *14*(5), 2827–2841. https://doi.org/10.5194/gmd-14-2827-2021

Hunter, J. D. (2007). Matplotlib: A 2d graphics environment. *Computing in Science & Engineering*, *9*(3), 90–95. https://doi.org/10.1109/MCSE.2007.55

Intergovernmental Panel On Climate Change. (2023, July). *Climate Change 2021 – The Physical Science Basis: Working Group I Contribution to the Sixth Assessment Report*

of the Intergovernmental Panel on Climate Change (1st ed.). Cambridge University Press. https://doi.org/10.1017/9781009157896

Kahneman, D. (2024). *Thinking, fast and slow* (Reissued). Penguin Books.

Klimiuk, T., Ludwig, P., Sanchez-Benitez, A., Goessling, H. F., Braesicke, P., & Pinto, J. G. (2025). The European summer heatwave of 2019 – a regional storyline perspective. *Earth System Dynamics*, *16*(1), 239–255. https://doi.org/10.5194/esd-16-239-2025

Korosec, M. (2024, October). What is a Sting Jet? [last accessed: 30. January 2026]. https://www.severe-weather.eu/learnweather/severe-weather-theory/what-is-a-sting-jet-mk/

Laps, S., & Wagner, A. (2013). Orkantief CHRISTIAN – Der schwerste Sturm für den äußersten Nordwesten und Norden Deutschlands seit mindestens 1999. [last accessed: 30. January 2026]. https://www.unwetterzentrale.de/uwz/915.html

León-FonFay, D., Lemburg, A., Fink, A. H., Pinto, J. G., & Feser, F. (2025, October). A combined storyline-statistical approach for conditional extreme event attribution. https://doi.org/10.5194/egusphere-2025-4976

Li, M., Woollings, T., Hodges, K., & Masato, G. (2014). Extratropical cyclones in a warmer, moister climate: A recent Atlantic analogue. *Geophysical Research Letters*, *41*(23), 8594–8601. https://doi.org/10.1002/2014GL062186

Ludwig, P., Pinto, J. G., Hoepp, S. A., Fink, A. H., & Gray, S. L. (2015). Secondary Cyclogenesis along an Occluded Front Leading to Damaging Wind Gusts: Windstorm Kyrill, January 2007. *Monthly Weather Review*, *143*(4), 1417–1437. https://doi.org/10.1175/MWR-D-14-00304.1

Ludwig, P., Pinto, J. G., Reyers, M., & Gray, S. L. (2014). The role of anomalous SST and surface fluxes over the southeastern North Atlantic in the explosive development of windstorm Xynthia. *Quarterly Journal of the Royal Meteorological Society*, *140*(682), 1729–1741. https://doi.org/10.1002/qj.2253

Martínez-Alvarado, O., Gray, S. L., Hart, N. C. G., Clark, P. A., Hodges, K., & Roberts, M. J. (2018). Increased wind risk from sting-jet windstorms with climate change. *Environmental Research Letters*, *13*(4), 044002. https://doi.org/10.1088/1748-9326/aaae3a

Met Office. (2023, November). Making sense of climate change projections [last accessed: 30. January 2026]. https://www.metoffice.gov.uk/blog/2023/making-sense-of-climate-change-projections

Met Office. (2010 - 2015). *Cartopy: A cartographic Python library with a Matplotlib interface*. Exeter, Devon. https://doi.org/https://doi.org/10.5281/zenodo.1182735

Michaelis, A. C., Willison, J., Lackmann, G. M., & Robinson, W. A. (2017). Changes in Winter North Atlantic Extratropical Cyclones in High-Resolution Regional Pseudo–Global Warming Simulations. *Journal of Climate*, *30*(17), 6905–6925. https://doi.org/10.1175/JCLI-D-16-0697.1

Moemken, J., Messori, G., & Pinto, J. G. (2024). Windstorm losses in Europe – What to gain from damage datasets. *Weather and Climate Extremes*, *44*, 100661. https://doi.org/10.1016/j.wace.2024.100661

Mölders, N., & Kramm, G. (2014). *Lectures in Meteorology*. Springer International Publishing. https://doi.org/10.1007/978-3-319-02144-7

Müller-Westermeier, G. (n.d.). Beschreibung und klimatologische Bewertung des Orkantiefs „Kyrill“ [last accessed: 30. January 2026]. https://dwdbib.dwd.de/retrosammlung/download/pdf/695564

National Centers for Environmental Prediction. (n.d.). Global Forecast System (GFS) [last accessed: 30. January 2026]. https://www.emc.ncep.noaa.gov/emc/pages/numerical_forecast_systems/gfs.php

O’Neill, B. C., Kriegler, E., Riahi, K., Ebi, K. L., Hallegatte, S., Carter, T. R., Mathur, R., & Van Vuuren, D. P. (2014). A new scenario framework for climate change research: The concept of shared socioeconomic pathways. *Climatic Change*, *122*(3), 387–400. https://doi.org/10.1007/s10584-013-0905-2

Parker, W. S. (2010). Predicting weather and climate: Uncertainty, ensembles and probability. *Studies in History and Philosophy of Science Part B: Studies in History and Philosophy of Modern Physics*, *41*(3), 263–272. https://doi.org/10.1016/j.shpsb.2010.07.006

PERILS. (2014, October). PERILS discloses fourth and final loss estimate for windstorm Christian of EUR 1’144m [last accessed: 30. January 2026]. https://www.perils.org/news/perils-discloses-fourth-and-final-loss-estimate-for-windstorm-christian-of-eur-1144m

PERILS. (2017, May). PERILS discloses second loss estimate for extratropical cyclone Thomas of EUR 249m. https://www.perils.org/api/news/perils-discloses-second-loss-estimate-for-extratropical-cyclone-thomas-of-eur-249m

PERILS. (2026). https://www.perils.org/losses?year=&classification=1012&status=2#event-losses

Pfahl, S., O’Gorman, P. A., & Singh, M. S. (2015). Extratropical Cyclones in Idealized Simulations of Changed Climates. *Journal of Climate*, *28*(23), 9373–9392. https://doi.org/10.1175/JCLI-D-14-00816.1

Pham, T. V., Steger, C., Rockel, B., Keuler, K., Kirchner, I., Mertens, M., Rieger, D., Zängl, G., & Früh, B. (2021). ICON in Climate Limited-Area Mode (ICON release version 2.6.1): A new regional climate model. *Geoscientific Model Development*, *14*(2), 985–1005. https://doi.org/10.5194/gmd-14-985-2021

Ranson, M., Kousky, C., Ruth, M., Jantarasami, L., Crimmins, A., & Tarquinio, L. (2014). Tropical and extratropical cyclone damages under climate change. *Climatic Change*, *127*(2), 227–241. https://doi.org/10.1007/s10584-014-1255-4

Reed, K. A., Medeiros, B., Jablonowski, C., Simpson, I. R., Voigt, A., & Wing, A. A. (2025). Why Idealized Models Are More Important Than Ever in Earth System Science. *AGU Advances*, *6*(4), e2025AV001716. https://doi.org/10.1029/2025AV001716

Reinert, D., Rieger, D., & Prill, F. (2024). ICON Tutorial 2024: Working with the ICON Model [Publisher: German Meteorological Service]. https://doi.org/10.5676/DWD_PUB/NWV/ICON_TUTORIAL2024

Sánchez-Benítez, A., Goessling, H., Pithan, F., Semmler, T., & Jung, T. (2022). The July 2019 European Heat Wave in a Warmer Climate: Storyline Scenarios with a Coupled Model Using Spectral Nudging. https://doi.org/10.1175/JCLI-D-21-0573.1

Schär, C., Frei, C., Lüthi, D., & Davies, H. C. (1996). Surrogate climate-change scenarios for regional climate models. *Geophysical Research Letters*, *23*(6), 669–672. https://doi.org/10.1029/96GL00265

Schemm, S., Sprenger, M., Martius, O., Wernli, H., & Zimmer, M. (2017). Increase in the number of extremely strong fronts over Europe? A study based on ERA-Interim reanalysis (1979–2014). *Geophysical Research Letters*, *44*(1), 553–561. https://doi.org/10.1002/2016GL071451

Schultz, D. M., & Browning, K. A. (2017). What is a sting jet? *Weather*, *72*(3), 63–66. https://doi.org/10.1002/wea.2795

Semmler, T., Danilov, S., Gierz, P., Goessling, H. F., Hegewald, J., Hinrichs, C., Koldunov, N., Khosravi, N., Mu, L., Rackow, T., Sein, D. V., Sidorenko, D., Wang, Q., & Jung, T. (2020). Simulations for CMIP6 With the AWI Climate Model AWI-CM-1-1. *Journal of Advances in Modeling Earth Systems*, *12*(9), e2019MS002009. https://doi.org/10.1029/2019MS002009

Shapiro, M. A., & Keyser, D. (1990). Fronts, Jet Streams and the Tropopause. In C. W. Newton & E. O. Holopainen (Eds.), *Extratropical Cyclones* (pp. 167–191). American Meteorological Society. https://doi.org/10.1007/978-1-944970-33-8_10

Shepherd, T. G. (2014). Atmospheric circulation as a source of uncertainty in climate change projections. *Nature Geoscience*, *7*(10), 703–708. https://doi.org/10.1038/ngeo2253

Shepherd, T. G., Boyd, E., Calel, R. A., Chapman, S. C., Dessai, S., Dima-West, I. M., Fowler, H. J., James, R., Maraun, D., Martius, O., Senior, C. A., Sobel, A. H., Stainforth, D. A., Tett, S. F. B., Trenberth, K. E., Van Den Hurk, B. J. J. M., Watkins, N. W., Wilby, R. L., & Zenghelis, D. A. (2018). Storylines: An alternative approach to representing uncertainty in physical aspects of climate change. *Climatic Change*, *151*(3-4), 555–571. https://doi.org/10.1007/s10584-018-2317-9

Stevens, B., Giorgetta, M., Esch, M., Mauritsen, T., Crueger, T., Rast, S., Salzmann, M., Schmidt, H., Bader, J., Block, K., Brokopf, R., Fast, I., Kinne, S., Kornblueh, L., Lohmann, U., Pincus, R., Reichler, T., & Roeckner, E. (2013). Atmospheric component of the MPI-M Earth System Model: ECHAM6. *Journal of Advances in Modeling Earth Systems*, *5*(2), 146–172. https://doi.org/10.1002/jame.20015

the Oyster, F. (2014, September). Jetstream - Rossby Waves - N hemisphere [last accessed: 30. January 2026]. https://commons.wikimedia.org/w/index.php?curid=35217748

Tierney, G., Posselt, D. J., & Booth, J. F. (2018). An examination of extratropical cyclone response to changes in baroclinicity and temperature in an idealized environment. *Climate Dynamics*, *51*(9-10), 3829–3846. https://doi.org/10.1007/s00382-018-4115-5

Ulbrich, U., Fink, A. H., Klawa, M., & Pinto, J. G. (2001). Three extreme storms over Europe in December 1999. *Weather*, *56*(3), 70–80. https://doi.org/10.1002/j.1477-8696.2001.tb06540.x

Ulbrich, U., Leckebusch, G. C., & Pinto, J. G. (2009). Extra-tropical cyclones in the present and future climate: A review. *Theoretical and Applied Climatology*, *96*(1-2), 117–131. https://doi.org/10.1007/s00704-008-0083-8

Wald und Holz NRW. (2021). Orkan Kyrill und seine Folgen in Nordrhein-Westfalen [last accessed: 30. January 2026]. https://www.wald-und-holz.nrw.de/en/wald-in-nrw/wald-und-klima/kyrill-und-seine-folgen-in-nrw

Wang, Q., Danilov, S., Sidorenko, D., Timmermann, R., Wekerle, C., Wang, X., Jung, T., & Schröter, J. (2014). The Finite Element Sea Ice-Ocean Model (FESOM) v.1.4: Formulation of an ocean general circulation model. *Geoscientific Model Development*, *7*(2), 663–693. https://doi.org/10.5194/gmd-7-663-2014

Wettergefahren Frühwarnung. (2007). Orkantief Kyrill [last accessed: 30. January 2026]. https://www.wettergefahren-fruehwarnung.de/Ereignis/20070117_e.html

Wettergefahren Frühwarnung. (2013, October). Orkantief Christian [last accessed: 30. January 2026]. https://www.wettergefahren-fruehwarnung.de/Ereignis/20131031_e.html

Wettergefahren Frühwarnung. (2017). Orkantief Thomas [last accessed: 30. January 2026]. https://www.wettergefahren-fruehwarnung.de/Ereignis/20170224_e.html

Zängl, G., Reinert, D., Rípodas, P., & Baldauf, M. (2015). The icon (icosahedral nonhydrostatic) modelling framework of dwd and mpi-m: Description of the nonhydrostatic dynamical core. *Quarterly Journal of the Royal Meteorological Society*, *141*. https://doi.org/10.1002/qj.2378

A. Appendix

(a) DWD Surface Pressure Charts

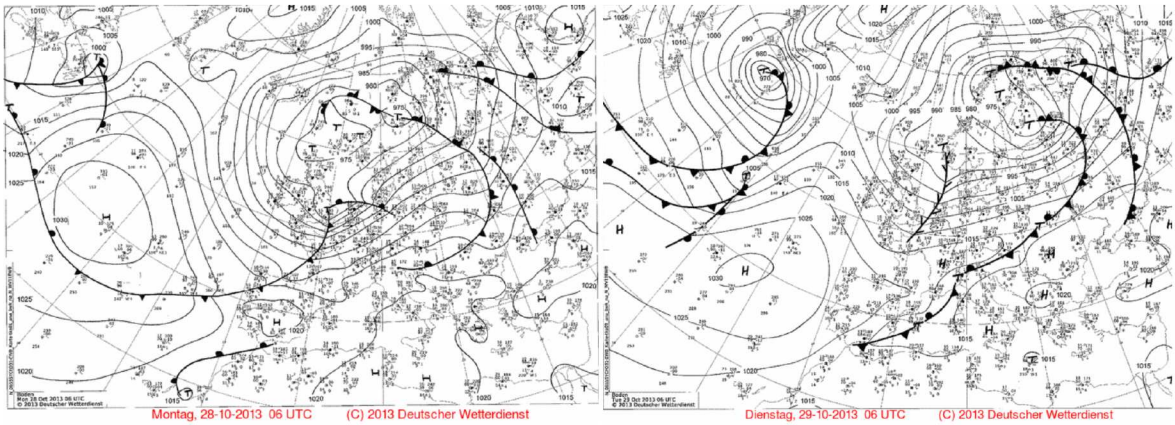

(b) ERA5 Simulation

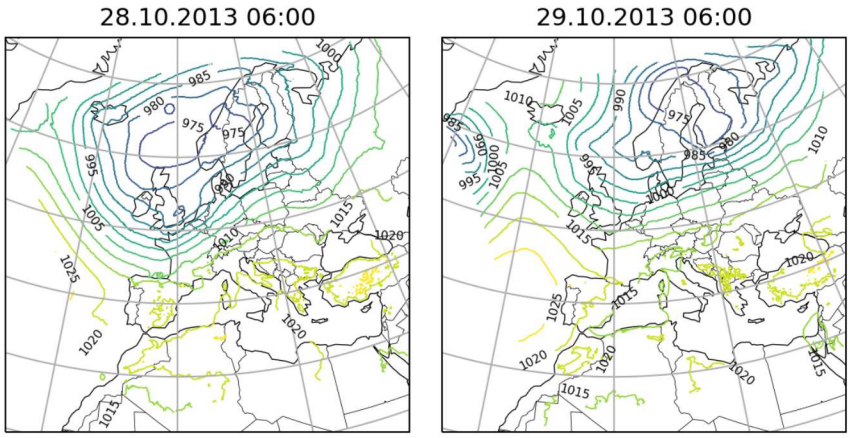

(c) Present Storyline Simulation

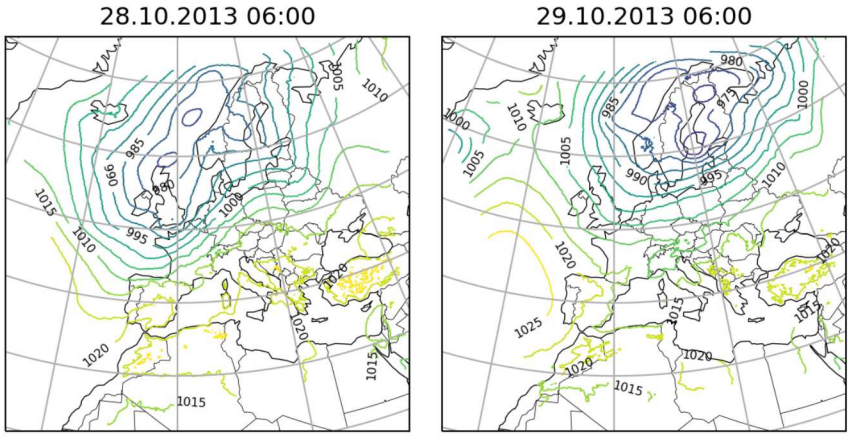

Figure A.1.: MSLP during windstorm Christian at 28.10 06 and 29.10 06 UTC, pressure in hPa, a) DWD surface pressure charts, b) ERA5 simulation, c) present day storyline simulation

(a) GFS analysis

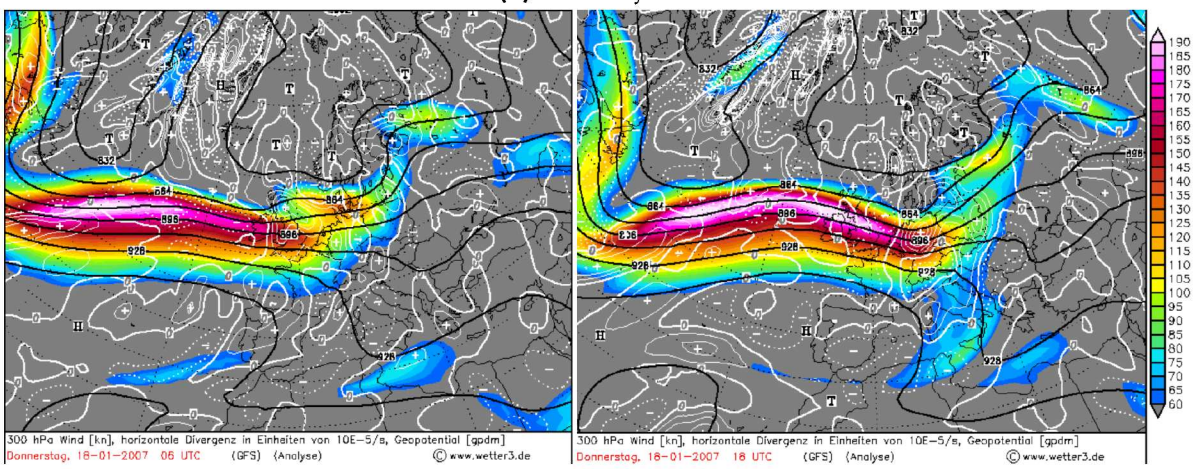

(b) ERA5 Simulation

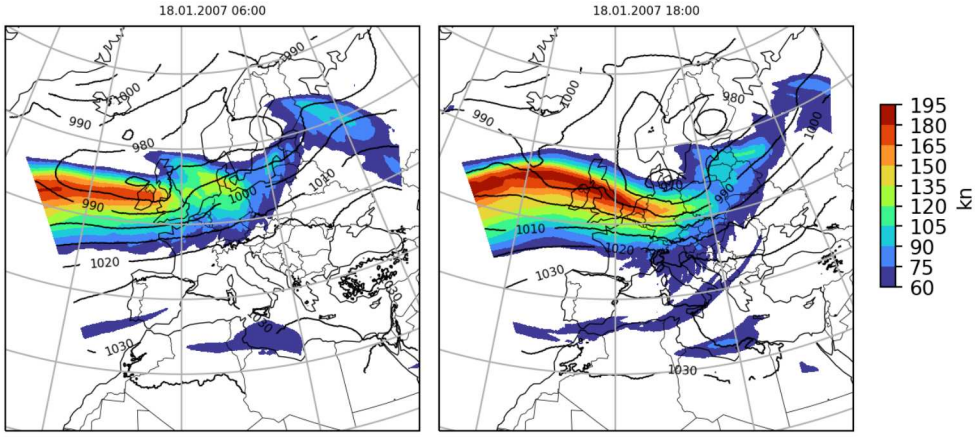

(c) Present Storyline Simulation

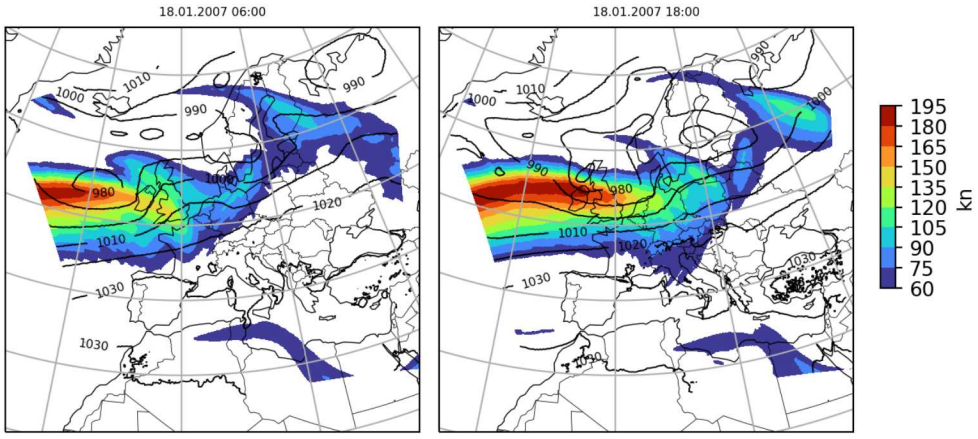

Figure A.2.: Comparison of Jetstream for windstorm Kyrill at 18.01 06 UTC and 18 UTC, the color shaded areas show the 300 hPa wind in kn, a) white lines show the horizontal divergence and black lines the geopotential, b) ERA5 simulation and c) Present storyline simulation, black lines MSLP in hPa

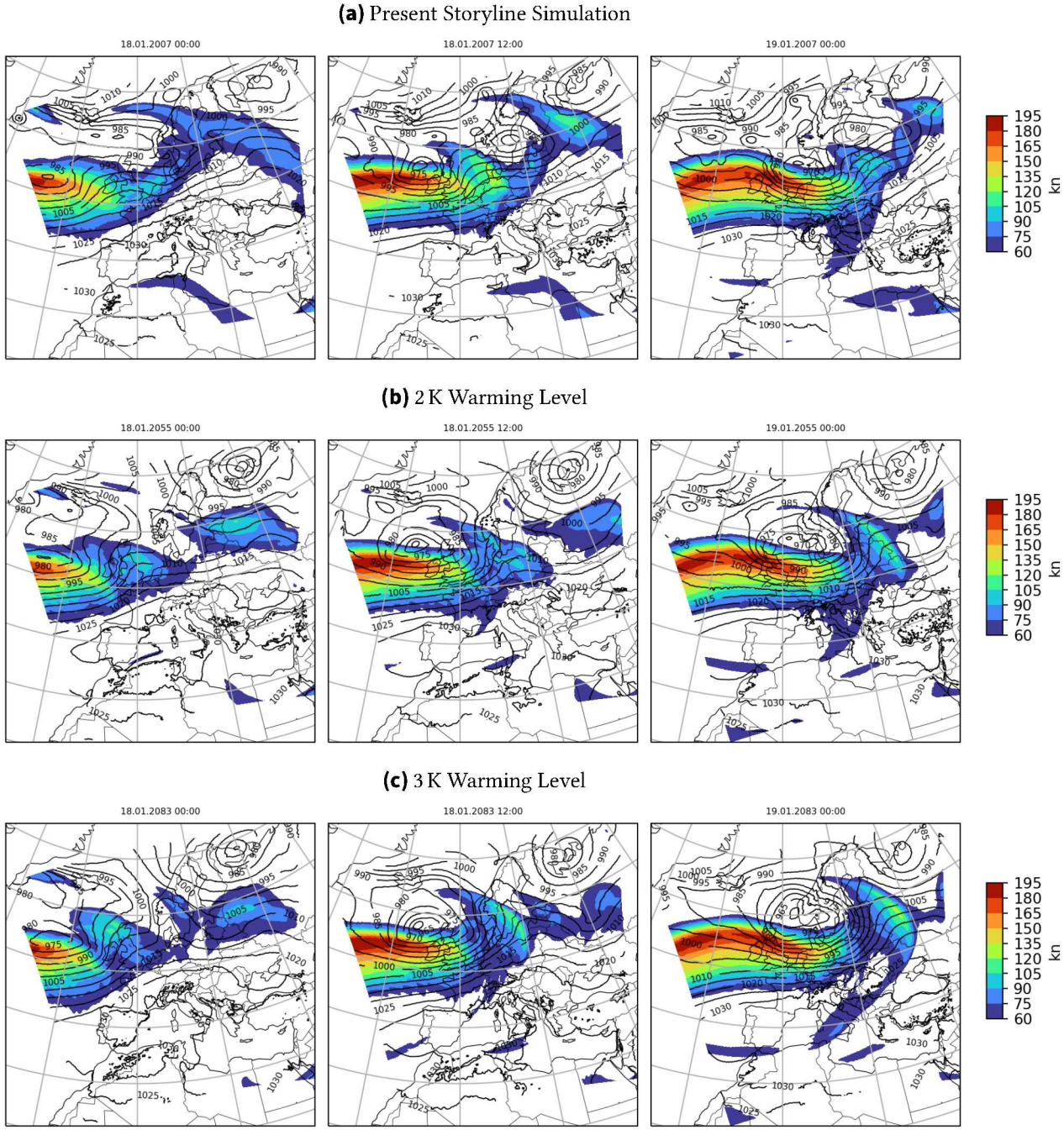

Figure A.3.: Jet stream for the storyline simulations of Kyrill at 18.01 00 UTC, 12 UTC and 19.01 00 UTC, the color shaded areas show the 300 hPa wind in kn, a) present storyline simulation, b) 2 K warming level, c) 3 K warming level

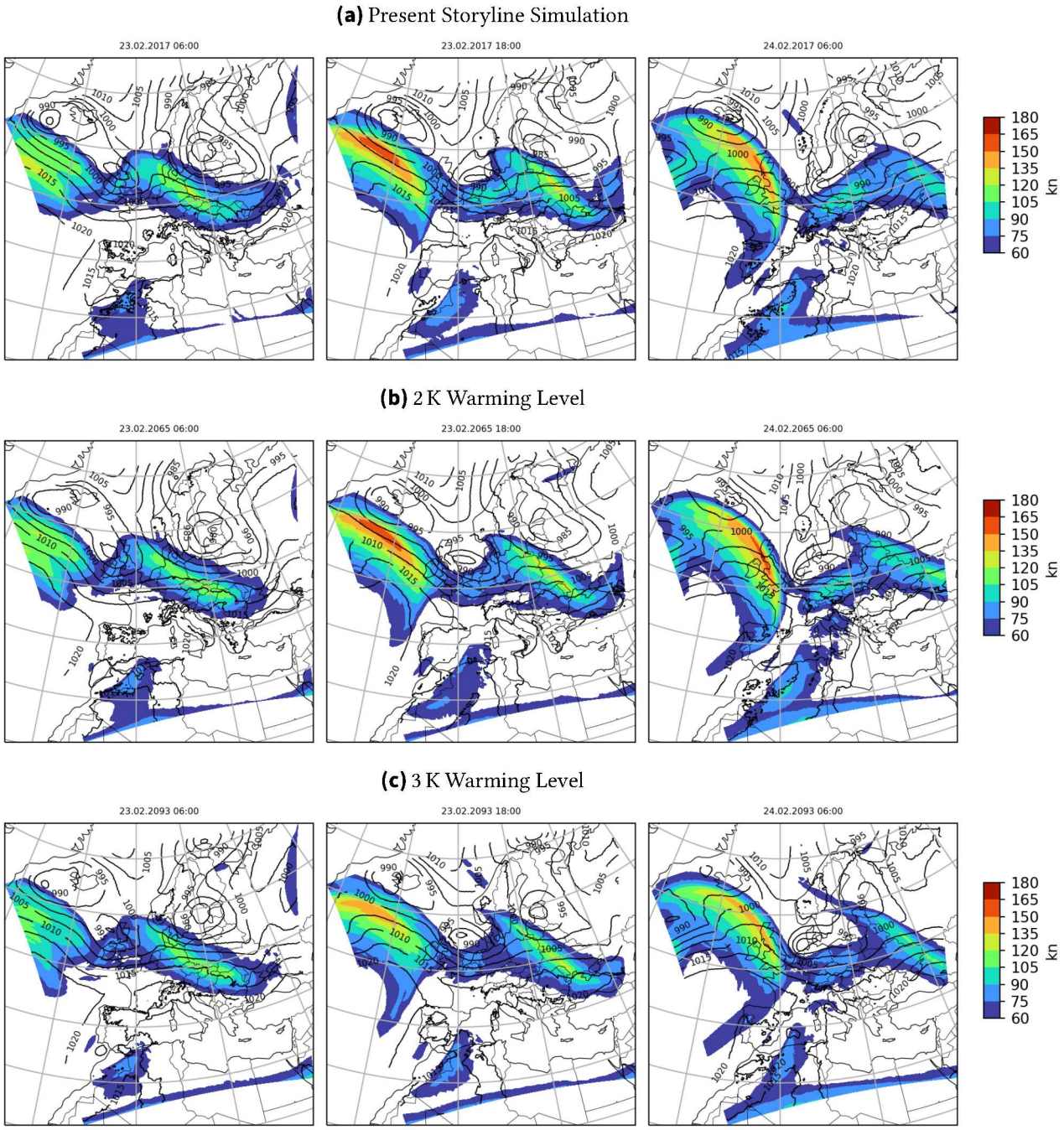

Figure A.4.: Jet stream for the storyline simulations of Thomas at 23.02 06 UTC, 18 UTC and 24.02 06 UTC, the color shaded areas show the 300 hPa wind in kn, a) present storyline simulation, b) 2 K warming level, c) 3 K warming level

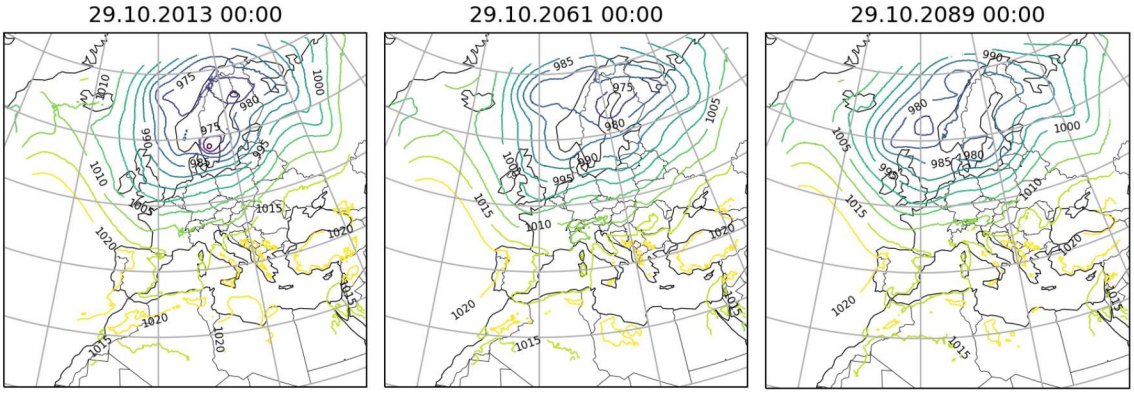

Figure A.5.: Sea level pressure of windstorm Christian on 29.10 00 UTC in storyline simulations, left: present day, mid: 2 K warming level, right: 3 K warming level

Acknowledgments

First of all, I want to thank Dr. Patrick Ludwig for his supervision. I always felt comfortable asking any question. Thank you for always answering all of them patiently and for consistently encouraging and reassuring me when I felt insecure about what I was doing or whether I was doing enough. I further appreciate that you paused my HiWi tasks during the final phase of my thesis.

Many thanks to Prof. Dr. Joaquim Pinto for his advice and feedback, especially after my try-out talk for the TRO-Seminar presentation.

Thanks to Svenja Christ for sharing her insights with me regarding which storms could serve as good examples for this thesis.

I want to thank Anika Corban for proofreading my thesis. Especially your feedback on incomprehensible sentences and inconsistencies was very valuable to me.

Special thanks to Alexander Hornig for always being there for me with a loving hug and comforting me, whenever I felt stressed out or insecure. Thank you for helping me on my way of finding out who I am and what I need. Furthermore, I want to thank you for continuously helping me improve my programming skills, such that this felt like the easy part during this thesis. Thank you for helping me with your skills whenever I got stuck with programming issues anyway.

At last, I want to thank my family; my parents for always encouraging me and Linda for our long phone calls.

Standard software tools were used for this thesis. GPT and Writefull's model, as implemented in overleaf (www.overleaf.com), were used for grammar correction and language improvement. The Abstract was translated with the help of DeepL (deepl.com). For the data analysis Python with standard packages, such as NumPy (Harris et al., 2020), matplotlib (Hunter, 2007) and Cartopy (Met Office, 2010 - 2015) were used.

Thanks to Deutsches Klimarechenzentrum (DKRZ), granted by its Scientific Steering Committee (WLA), for providing computing and storage resources under the project number 105 and the ERA5 reanalysis datasets via the DKRZ data pool.

Thanks to the Helmholtz research field "Earth & Environment" for the Innovation Pool project SCENIC ACTUATE, who supported the generation of the AWI data, that were used in this thesis.